Selection and characterization of Amyloid-$\beta_{1\text{-}42}$ binding D-enantiomeric peptides for potential therapeutic intervention of Alzheimer´s disease

Inaugural-Dissertation

zur

Erlangung des Doktorgrades

der Mathematisch-Naturwissenschaftlichen Fakultät

der Heinrich-Heine-Universität Düsseldorf

vorgelegt von

Stephan Rudolph

aus Dessau

Düsseldorf, April 2015

Gedruckt mit der Genehmigung der Mathematisch-Naturwissenschaftlichen Fakultät der Heinrich-Heine-Universität Düsseldorf

Referent: Prof. Dr. Dieter Willbold
Koreferent: Prof. Dr. Georg Groth

Tag der mündlichen Prüfung:

„Die Dummheiten wechseln, und die Dummheit bleibt.“

(Erich Kästner)

„Die dunkelste Stunde ist die vor Sonnenaufgang.“

(chinesisches Sprichwort)

Für Tante Elli

Index

1. Introduction

1.1 Alzheimer´s disease (AD) – an overview

1.1.1 General information

In 2012 the World Health Organization (WHO) and the Alzheimer´s Disease International (ADI) published an impressive yet alarming report on dementia. According to this document, dementia counts for more than 35 million patients worldwide already today, thus making dementia one of the most frequent disease patterns [1]. More than half of the autopsies and clinical studies of dementia patients confirmed the diagnosis Alzheimer´s disease (AD). Therefore, AD contributes largely to dementia [2]. The estimated number of unreported cases might be even higher since not all patients with dementia are examined *post mortem*, thus AD could not be identified with certainty. According to the WHO report, in Western Europe seven million people suffer from dementia, 1.5 million of them in Germany. Also in the South and East Asian area ten million people have dementia and in the northern part of America more than four million people are affected.

The major risk factor for AD is age. A considerable increase of AD cases can be expected in the South Asian and Western Pacific area, due to the population growth in these regions. The rate of AD patients will also increase in the leading industrial countries because of the demographic change towards a senescent society. According to several studies, the number of affected people worldwide will double every 20 years, leading to approximately 115 million people suffering from dementia in 2050 [1, 3].

AD is a progressive type of dementia. The damaged nerve tissue cannot be replaced, thereby the disease proceeds irresistibly. After diagnosis, the estimated life span is three to nine years. Typical symptoms of AD are apathy, depression, anxiety, oblivion, disorientation, hallucinations but also changes in behavior and personality.

The later etiopathology is characterized by an impairment in the ability to speak or think logically [2, 4, 5]. Pathological hallmarks are amyloid plaques, also called neuritic plaques, and neurofibrillary tangles (NFTs) consisting of aggregated tau protein [6-10].

Only 5 % of all AD cases are genetically inherited and are likely to have an early onset. This version of the disease is described as familial autosomal dominant AD (FAD). Three genes are relevant for most of the cases, notably the amyloid precursor protein (*APP*) and the presenilins *PSEN1* and *PSEN2*, which are all linked to the processing of amyloid beta (Aβ) by γ-secretase complexes. *PSEN1* for instance encodes for the catalytic subunit of the γ-secretase. Mutations in the *PSEN1* genome sequence change the balance between harmless and toxic forms of Aβ peptides [11].

The remaining 95 % of AD cases are sporadic and have a later onset (> 65 years). Even though age and probably environmental risk factors seem to be the major cause, mutations in several genes involved in Aβ clearance are discussed as well [12, 13]. One possible candidate is the *APOE4* gene, encoding for the apolipoprotein E4, which is important for the binding and transport of lipids. It might be involved in $A\beta_{1\text{-}42}$ clearance and degradation. The effect is dose-dependent, since individuals with two copies have a much higher chance to develop AD than those with only one copy [14, 15].

Until now, AD can only be treated palliatively or symptomatically, although with limited success. Hence, the symptoms lead necessarily to the need for nursing care. In Germany, more than 40 % of all places in nursing homes are occupied by dementia patients [16]. Especially in countries with years of low birth rates, like Germany, the ratio will shift from working people to elderly people within the next few years. Because of this shift, more old people with dementia will exceed the available nursing staff. Consequently, the national health care and welfare systems will be challenged [17]. Also the burden for relatives of dementia patients should not be neglected.

1.1.2 History and pathology of AD

Alzheimer´s disease was named after Alois Alzheimer (1866 – 1915), a German physician who firstly described the extracellular protein deposits called plaques and the intracellular neurofibrillary tangles (NFTs) in histopathological brain slices of his patient Auguste Deter in 1906 (Figure 1). He was the first one who connected the behavioral changes of AD with pathological changes in the brain and was able to distinguish between AD and other types of dementia [18, 19].
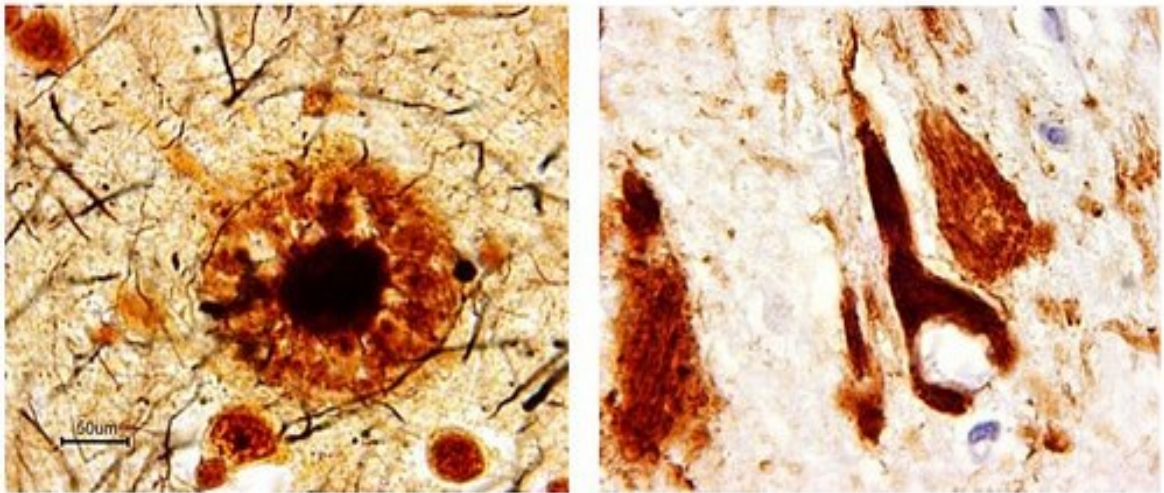
Figure 1: Stained plaques and neurofibrillary tangles in brain slices of a dementia patient.

An intercellular neuritic plaque consisting of a dense center and diffuse surroundings is shown in the left panel. Intracellular neurofibrillary tangles are shown in the right panel.

(taken from: http://dementiasos.files.wordpress.com/2011/12/dem-plaque-tangle.jpg)

Typical behavioral hallmarks of AD are listed in the latter chapter. Molecular hallmarks are a decrease in synaptic density, synaptic loss, atrophy of nerve cells in the brain, inflammation and reduced acetylcholine transferase activity [2, 5, 20, 21]. The brain shrivels, mainly because of neuron loss (Figure 2). The neocortex and hippocampus are particularly affected, followed by the striatum and the cholinergic nuclei of the basal forebrain and further also the cerebellum [21].
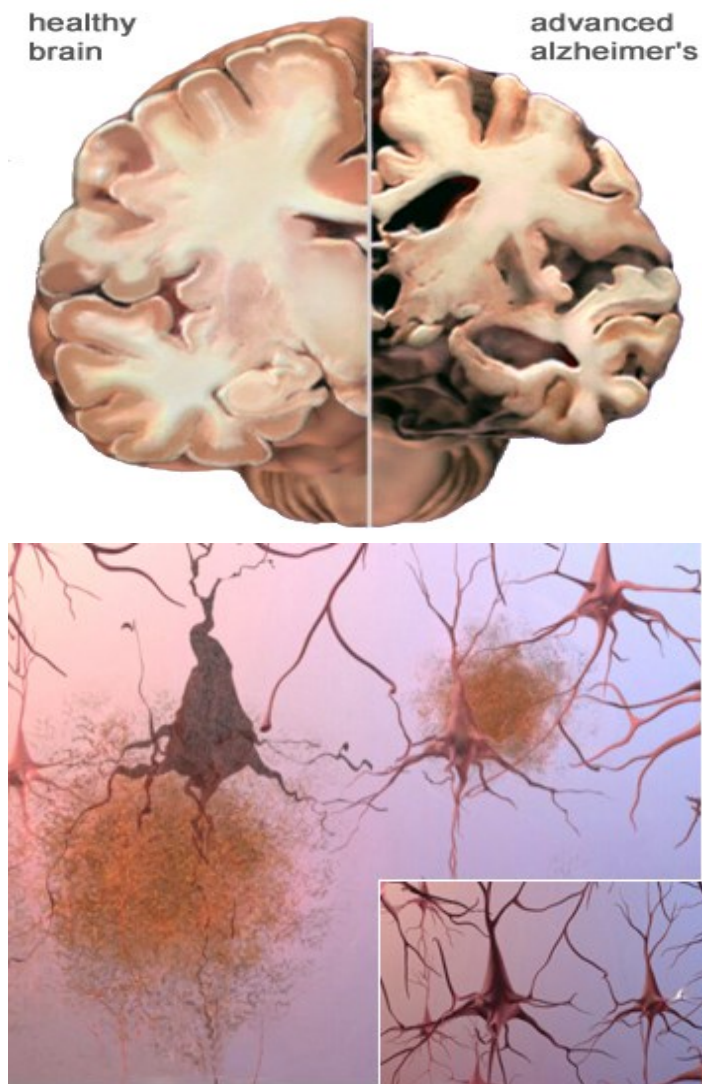
Figure 2: Comparison of a healthy and an AD affected brain and synapses.

Due to neuron loss and cell atrophy, the mass and volume of the brain decreases in AD as shown in the upper panel. The intercellular amyloid plaques destroy neuronal cell contacts and subsequently neurons as shown in the left part of the bottom picture. The right part shows healthy neurons.

(modified according to from: www.alz.org/braintour/images/alzheimer_brain.jpg &

www.alz.org/braintour/images/plaques_tangles.jpg)

1.1.3 The amyloid precursor protein (APP)

One pathological hallmark of AD are neuritic plaques consisting of neurites and predominantly Aβ peptide [6, 7]. The peptide is cleaved proteolytically from the amyloid precursor protein (APP), an integral type I transmembrane glycoprotein

localized on the human chromosome 21 (Figure 3). APP is expressed over the whole life span, primarily in neuronal cells but also in other tissue. Its molecular weight is between 110 and 135 kDa [22, 23].
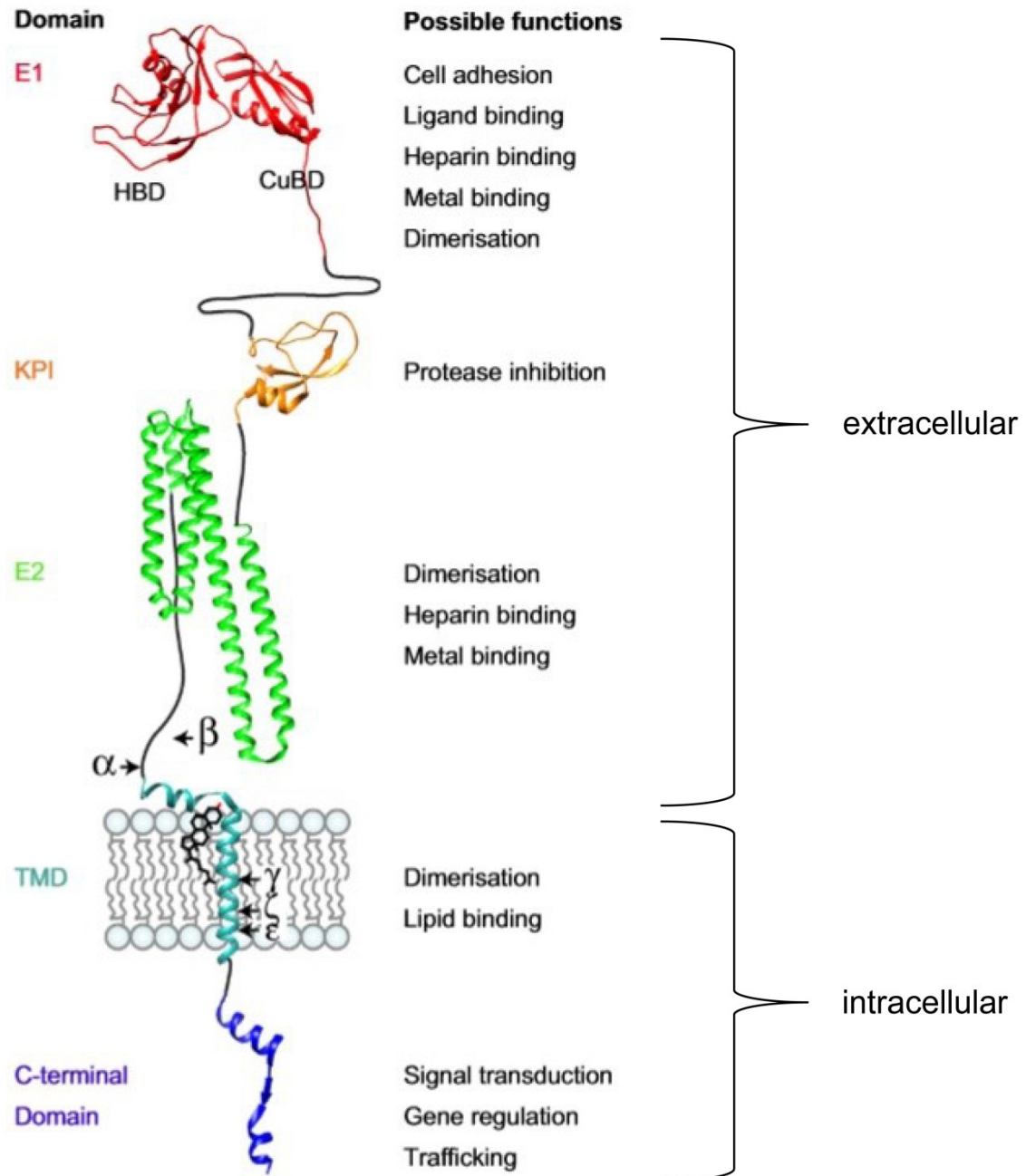
Figure 3: Hypothetical 3D structure of amyloid precursor protein (APP) and possible physiological functions.

The hypothetical 3D structure of APP and its potential functions are shown. The cleavage sites for α-, β- and γ-secretases and the localization of APP with respect to the cell membrane are marked. (modified according to: Dawkins, E & Small, DH; J Neurochem; 2014.)

Several potential functions of APP are discussed, but a clearly defined APP function is lacking until now (Figure 3). The *APP* promoter sequence is similar to promoters of housekeeping genes, indicating that *APP* itself could belong to this group. Moreover, binding sites for cell growth- and maturation-associated transcription factors were identified within the *APP* gene sequence [24, 25]. APP mRNA is spliced in different variants which appear in varying amounts in different types of tissue, indicating a broad impact. APP695 is the most prominent isoform in neuronal cells [24].

Although APP is widely expressed, knock out experiments in mice and *D. melanogaster* turned out to be not lethal, indicating a non-essential role of APP in development. However, impaired neuronal functions and behavioral defects were reported [26, 27]. Evidence from structural analysis suggest, that APP may act as a cell-surface receptor or as a growth factor [22, 28, 29]. Several studies report an influence on proliferation, differentiation and adhesion of cells and neurite outgrowth. In particular, the extracellular region of APP seems to be involved in these trophic funtions [24, 30].

Another option is that APP regulates stem cell proliferation and differentiation, since it is expressed in neural stem- and progenitor cells, neuroblasts and neurons during their differentiation and proliferation [24, 31-33]. Furthermore, APP binds to collagen type I , laminin and heparan sulphate, which can influence neurite outgrowth. Additionally, it can form trans-dimers to establish cell-to-cell contacts, eventually to stabilize synapses [34-38].

Yet another possible function of APP is the regulation of synaptogenesis, since APP is highly expressed during development at both sides of the synaptic cleft [30, 38, 39]. Also synaptic plasticity, learning and memory might be regulated by APP, since it is able to alter the expression of receptors which play a significant role in regulation of synaptic calcium permeability [40-42].

Nevertheless, the mechanisms behind these potential physiological features of APP are still unproven. Most modes of action could be explained with its role as a receptor. However, a physiological ligand that activates APP is not found [24]. Possible ligands could be G-proteins. The C-terminal domain of APP serves as a binding site for G-proteins. Subsequently, this interaction can lead to intracellular signal transduction mechanisms and neuronal migration [43, 44].

Another option is that APP induces effects via its secreted fragments, like the APP soluble fragments α (APPsα) or β (APPsβ). These fragments could activate specific signal transduction pathways by interaction with a high-affinity receptor [45].

The cleavage of the Aβ fragment from APP might represent a normal physiological function, even though it has neither a defined primary structure nor is it produced in every pathway of APP processing. However, several functions for Aβ have been proposed. Examples are the connection to the cholesterol transport and cell adhesion. The identification of physiological functions of Aβ is extremely important, because many treatment strategies for AD aim to prevent its production or increase its clearance from the brain [24].

1.1.4 From APP to Aβ

The Aβ peptide is assumed to play a major role in AD development and progression. It is cleaved from APP by γ- and β-secretases. APP can be processed in two distinct pathways one leading to non-amyloidogenic products and the other leading to the aggregation prone Aβ (Figure 4).

The non-amyloidogenic pathway starts with the cleavage by α-secretases leading to soluble APPα (APPsα) and the C-terminal fragment α (CTFα) [46]. Both fragments have regulating activities in neural activity and plasticity [47]. CTFα is subsequently cleaved by a γ-secretase to the peptide p3 and the amyloid intracellular domain (AICD).

AICD is controversially discussed in the literature. Even though the fragment seems to be degraded fast, it might have an impact on different cellular pathways including gene transcription, apoptosis and cytoskeletal dynamics. However, it is also suspected to play a role in AD [48]. The p3 fragment is considered to be part of the Aβ peptide family and was found in diffuse plaques in AD brains even though it only contributes in very low amounts. Until now, very little is known about its toxicity and actual influence on AD [49].
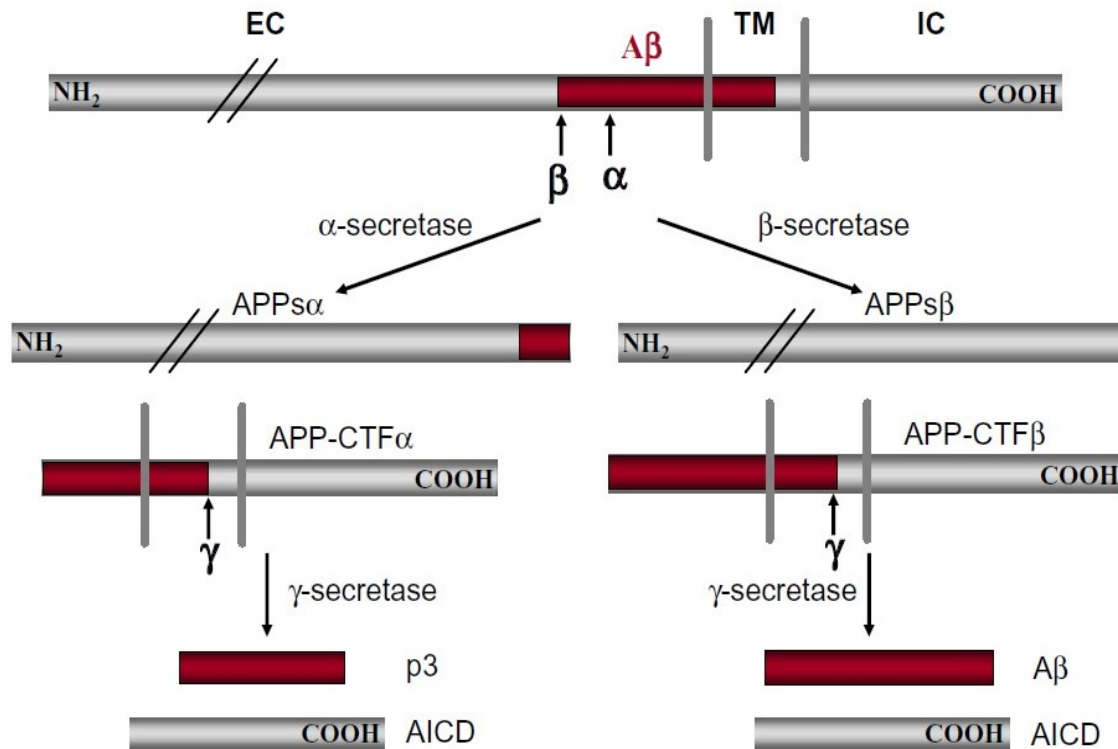
Figure 4: Schematic overview of APP processing.

APP consists of a large (~ 600 amino acids) extracellular (EC) domain, a small (~ 20 amino acids) transmembrane part (TM) and a cytosolic domain (intracellular (IC), ~ 45 amino acids) at its C-terminus. Two cleavage pathways are known which lead to different products. The non-amyloidogenic pathway starts with the processing by an α-secretase leading to two smaller protein fragments called soluble APPα (APPsα) and the C-terminal fragment α (APP-CTFα), which is later on cleaved by a γ-secretase to p3 and the amyloid intracellular domain (AICD). The pathway leading to amyloidogenic products starts with the cleavage of APP by a β-secretase leading to two fragments called soluble APPβ (APPsβ) and the C-terminal fragment β (APP-CTFβ). APP-CTFβ is subsequently processed to Aβ and AICD.
(taken from: Zheng, H & Koo, EH; Mol Neurodegener; 2006.)

Within the amyloidogenic pathway the first cleavage is catalyzed by β-secretases, mainly BACE1 (beta-site APP cleaving enzyme 1). BACE1 tends to oligomerize in the presence of Cu^{+1} [50]. The cleavage products are soluble APPβ (APPsβ) and the C-terminal fragment β (CTFβ). Even though APPsβ lacks only 16 amino acids compared to APPsα, it seems to have less influence on physiological mechanisms [51]. The CTFβ fragment is further cleaved to AICD and Aβ by γ-secretase. The first cut position of the γ-secretase within the transmembrane domain is not precise. Thus, processing of CTFβ results in the generation of Aβ peptides of different length (51 to 30 residues). $Aβ_{40}$ is the most frequent peptide fragment,

whereas $A\beta_{42}$ is the most interesting one for AD research. $A\beta_{42}$ is aggregation prone, neurotoxic and occurs as a main species in neuritic plaques in brains of AD patients [52].

Several genes involved in the processing and clearance of Aβ can be altered, leading to elevated risk or even familiar early onset AD. As an example, the *APP* gene is localized on chromosome 21, which is existent in triplicate in trisomy 21 (Down syndrome) patients, who therefore show pathological signs of AD [53]. Other mutations in the *APP* gene, like the Swedish mutation (K670N and M671L), lead to changes close to the β- or γ-secretase cleavage site, thus affecting APP processing. Furthermore, mutations within the Aβ part of APP lead to alterations like the Arctic mutation (E693G), which enhances protofibril production [54, 55].

1.1.5 The physiological role of Aβ and Tau

The Aβ monomer has an amphipathic character with a hydrophilic N-terminus and a hydrophobic C-terminus. Its secondary structure depends on the chemical environment and can be random coiled, α-helical or show β-sheet character [56-58]. Therefore, physiological functions of the Aβ monomer could be attributed to secondary structure elements.

A broad range of physiological functions is suspected for Aβ. Soscia *et al.* [59] found out that Aβ could have a function in the innate immune system by resembling properties of an antimicrobial peptide (AMP) and inducing pro-inflammatory activities against a variety of microbes [59].

Other findings suggest that Aβ, although its sequence shows no nuclear localization signal (NLS), is active in the nucleus and impacts gene regulation. For instance, it represses gene transcription of LRP1 and KAI1 [60]. LRP1 (low density lipoprotein receptor-related protein 1) is a receptor which promotes intracellular signaling, lipid homeostasis and clearance of apoptotic cells. KAI1 is an invasion- and metastasis suppressor in a variety of solid tumors and has a significant role in development [61].

The neuroprotective functions of the Aβ peptide include enhancement of the survival of hippocampal neurons, the protection of mature neurons against

excitotoxic cell death and differentiation of neural progenitor cells into neurons ($A\beta_{1-40}$) or the astrocyte lineage ($A\beta_{1-42}$), respectively [51, 62, 63].

These results show that $A\beta$ is not neurotoxic *per se*, especially not in low concentrations, which prohibit the formation of oligomeric species. Additionally, the uptake of extracellular monomeric $A\beta$ does not take place through the cell-surface receptors which are involved in oligomer uptake [51].

Furthermore, Toneff *et al.* [64] were able to show that $A\beta_{1-40}$ and $A\beta_{1-42}$ undergo regulated secretion from dense core secretory vesicles in neurons together with neuropeptides like galanin, NPY (neuropeptide Y) or encephalin and catecholamines like dopamine, norepinephrine or epinephrine. Thus, both peptides are potentially involved in multiple neurotransmitter systems [64].

The intrinsically disordered protein family member Tau is a microtubule-associated protein. It is typically expressed in neurons but is also found in the nucleus and in oligodendroglial and astroglial cells. Its main physiological function is the promotion of microtubule assembly and stabilization of the microtubular network, thus making it important for axonal transport. Tau can also interact with mitochondria, the plasma membrane and nucleic acids, indicating a role in information exchange between organelles and the plasma membrane [8, 65].

1.1.6 Pathological aspects of Aβ and Tau

Despite the physiological effects of both proteins, they are claimed to have also pathological effects connected to several diseases including AD.

1.1.6.1   The role of Tau

Besides neurodegenerative diseases which are especially associated with tau (tauopathies), like frontotemporal dementia (FTD) or Pick´s disease, there is also a tremendous connection between tau and AD, even though the link between $A\beta$ and tau is poorly understood.

Tau is prone to be hyperphosphorylated, which leads to its detachment from the microtubules, misfolding and aggregation [66]. Aggregation of tau leads to the formation of oligomers and later to neurofibrillary tangles (NFTs). Thus, less free soluble tau can mediate axonal stability and transport [8-10]. The key mechanism which regulates the interaction of tau with tubulin is phosphorylation. Up to 20 % of the tau molecule can be phosphorylated. A modified protein kinase activity can lead to altered microtubule binding and toxicity [67]. In AD, up to 40 % of overall tau is hyperphosphorylated and therefore exhibits an altered conformation and self-assembly, mainly based on the hexapeptides ^{275}VQIINK^{280} and ^{306}VQIVYK^{311}, which mediate the formation of β-sheet structures [8, 68, 69].

1.1.6.2 The amyloid cascade hypothesis

For many years, plaques and fibrils consisting mainly of Aβ were thought to be the major toxic species in AD. Hardy and Higgins [70] postulated an amyloid cascade hypothesis that claims an imbalance between Aβ production and Aβ decomposition, leading to an increased deposition of Aβ in plaques as the main cause of AD. Those plaques were assumed to be the elicitor of AD [70].

In 1999, McLean *et al.* [71] showed that not only the amount of soluble Aβ is increased in AD but it also correlates with markers of disease severity in a higher degree than the level of insoluble Aβ. This led to the assumption that soluble Aβ oligomers are the major causative agent in AD, leading to neurotoxic effects [71]. Cizas *et al.* [72] showed in 2010 that small Aβ$_{1-42}$ oligomers are toxic to rat neurons but not to other cell types. Regarding these findings one must review the original amyloid cascade hypothesis and acknowledge soluble Aβ oligomers as toxic species, responsible for the development of AD pathology [72, 73].

As stated before, monomeric Aβ might have a physiological function and is assumed to play a role in neurological pathways. In 1992, Mori *et al.* [74] reported a N-terminally truncated species of Aβ which starts at position 3 with glutamate converted to pyroglutamate and features up to 20 % of the NH$_2$-terminal fragments in the brain [74]. This variation was shown to increase aggregation kinetics, toxicity and resistance to degradation in oligomers [75-77].

Moreover, small Aβ oligomers like dimers or trimers can convert to nucleation seeds or aggregate into large oligomers and later on to protofibrils, fibrils and plaques. The conversion between the stages is dynamic and reversible (Figure 5) [78]. The Aβ oligomers appear in manifold shapes and sizes like Aβ-derived diffusible ligands (ADDLs), annular oligomers or a 56-kDa dodecameric soluble Aβ assembly (Aβ*56). The oligomeric species and also protofibrils, fibrils and plaques were shown to be toxic in different modes of action [78, 79].
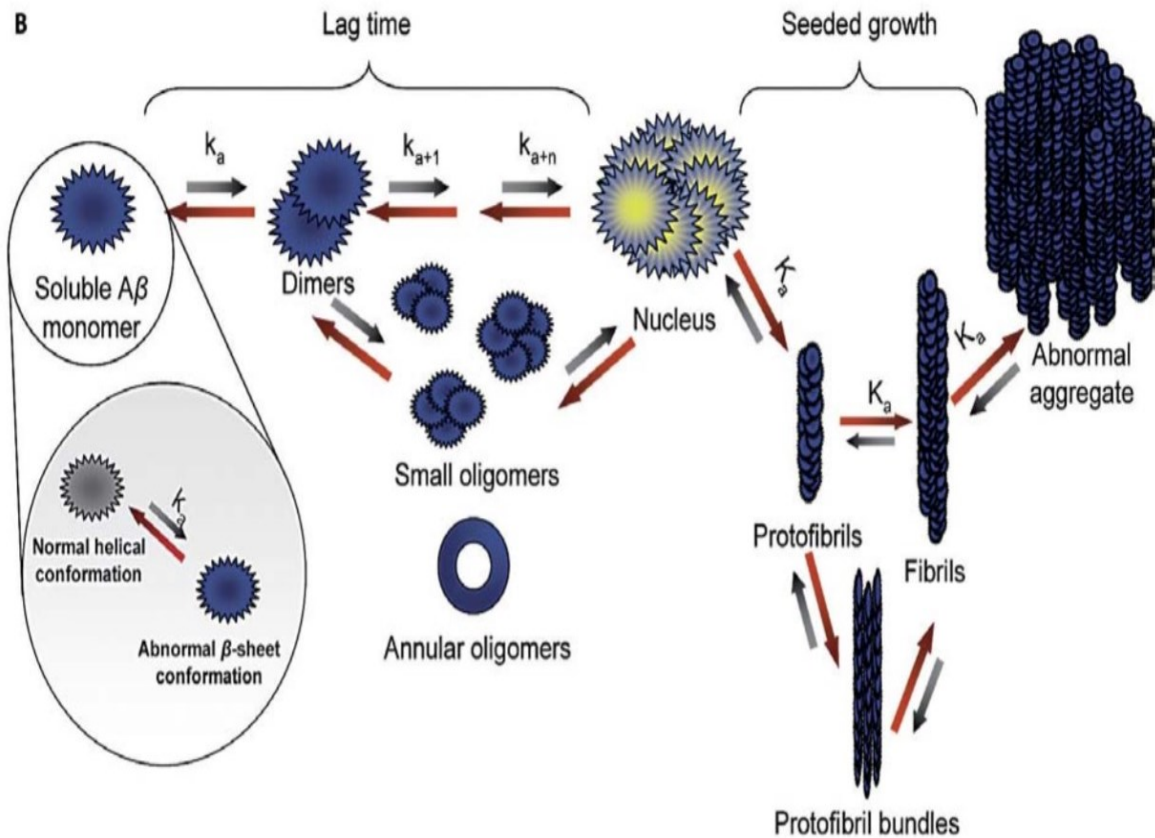
Figure 5: Schematic overview of Aβ aggregation.

The initial step towards aggregation of Aβ is the conversion of Aβ monomers from a helical conformation to an abnormal β-sheet conformation which is prone to aggregate with other Aβ molecules. The soluble abnormal monomer oligomerizes via distinct pathways and species to nucleation seeds, which are the foundation of seeded growth. They then form protofibrils, fibrils and aggregates. The oligomers can appear in many distinct forms like small oligomers or annular oligomers.

(taken from: Finder, VH & Glockshuber, R; Neurodegenerative Dis; 2007.).

Thus, Blennow *et al.* [80] revised the amyloid cascade hypothesis and incorporated the new outcomes regarding toxic species of Aβ. In Figure 6 the optimized amyloid cascade is shown [80].
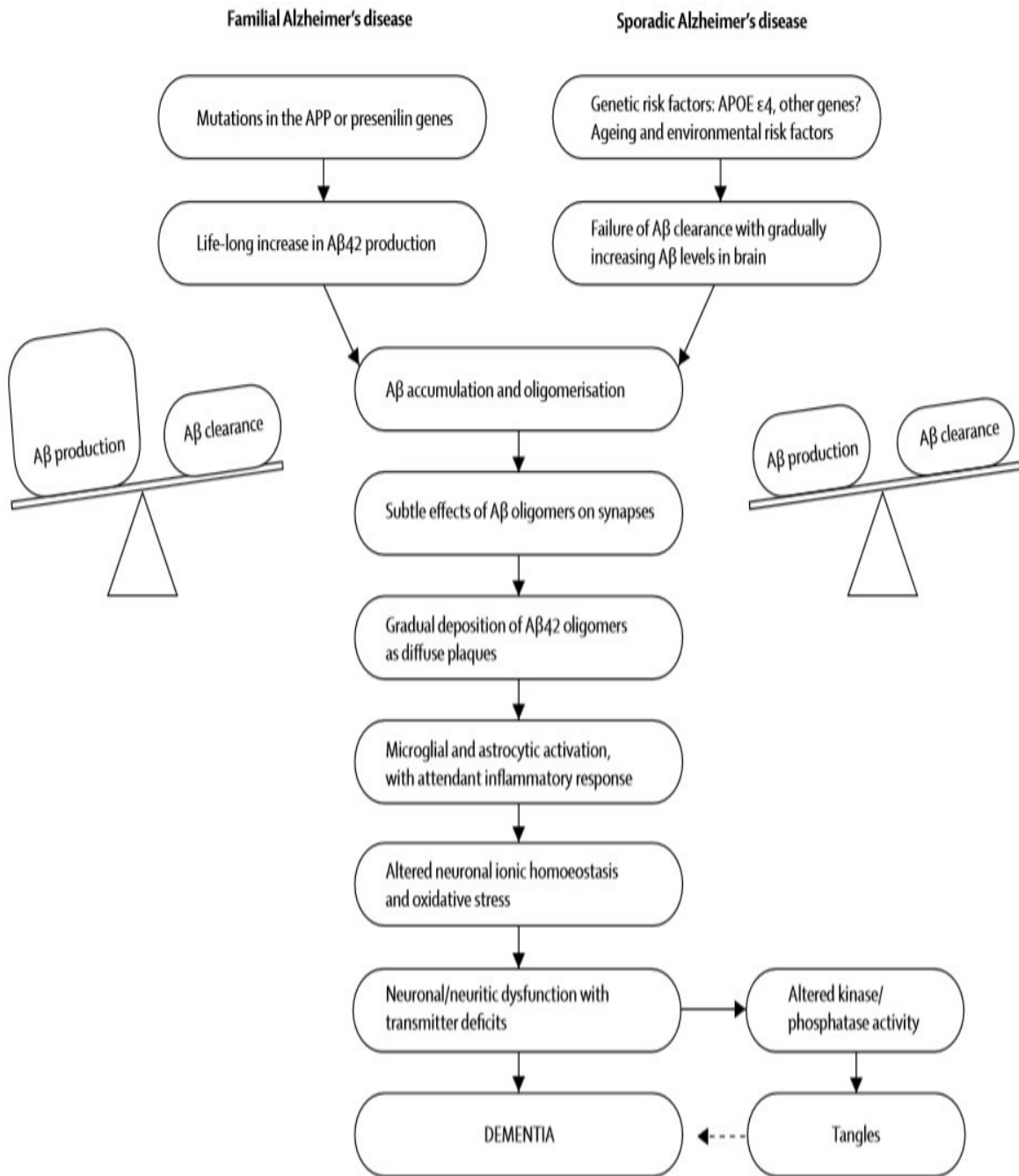
Figure 6: Revised amyloid cascade hypothesis.

While in familial AD the production of Aβ is increased over the whole lifetime, in sporadic AD the body fails to clear increased levels of Aβ from the brain. Both events can lead to accumulation and oligomerization of Aβ, harming synapses and neuronal pathways. The increasing deposition of oligomers as plaques leads to an inflammatory response as well as oxidative stress and an altered neuronal ion homeostasis. Finally, neuronal cells show severe dysfunctions and neurotransmitter deficits, leading to cognitive symptoms known as dementia.
(taken from: Blennow, K *et al*.; Lancet, 2006.)

1.1.6.3 Contribution of different Aβ species to AD

The pool of known toxic Aβ species as well as their modes of action is enormous. Already Aβ dimers were shown to be harmful by impairment of synaptic plasticity and memory as well as hyperphosphorylation of tau followed by neuritic degeneration [78, 81, 82]. Additionally, Aβ trimers and tetramers seem to have toxic properties due to an inhibition of long term potentiation [83].

Also larger soluble Aβ oligomers like ADDLs or Aβ*56 are known to be toxic. ADDLs were found to kill neurons at nanomolar concentrations and Aβ*56 assemblies induce synaptic dysfunction [84-86]. ADDLs might enable non-specific movement of ions across lipid bilayers by thinning the membrane just by their weight. Another potentially toxic species are annular pore forming oligomers as a subcategory of ADDLs. They enable another mechanism of ion homeostasis disturbance by forming channel-like structures (Figure 7) and thereby inducing cell toxicity [87, 88].
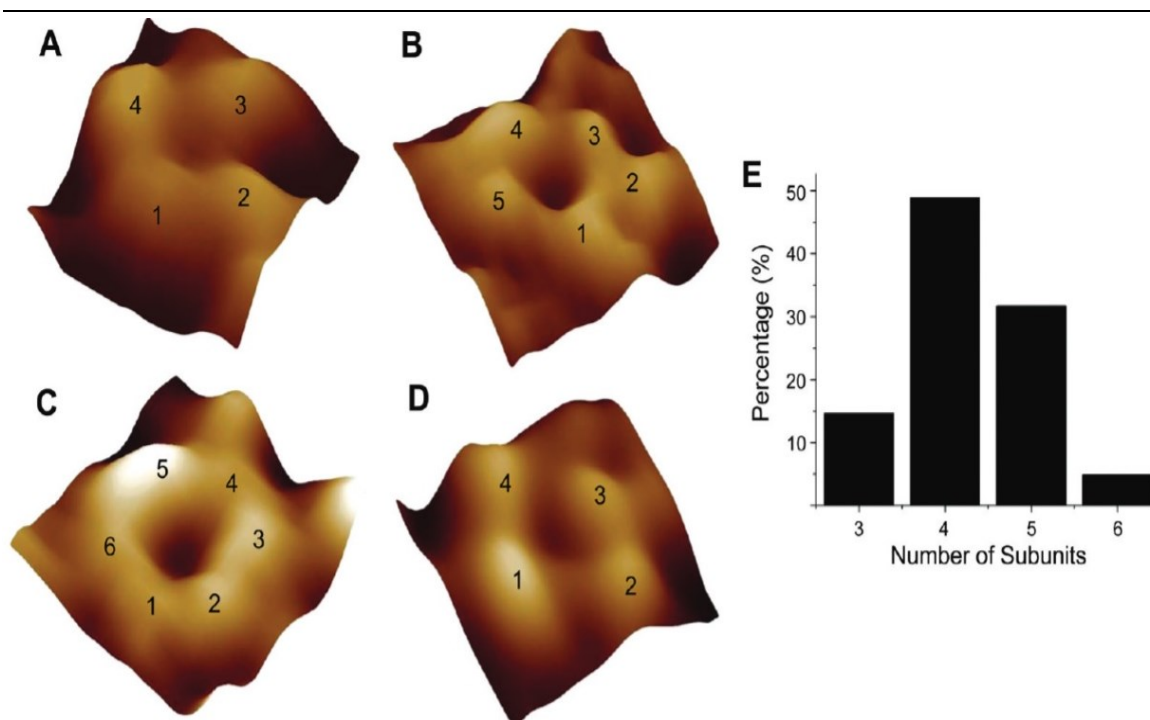
Figure 7: AFM images of D-Aβ$_{42}$ channels.

D-enantiomeric Aβ$_{42}$ is able to form channels in a lipid bilayer environment. Also the L-enantiomeric counterpart is able to form such channels. Tetrameric channels are the most common species, but also tri- to hexameric structures can be found. The channels might allow ions to cross the membrane non-specifically and therefore lead to impaired ion homeostasis.

(taken from: Connelly, L *et al.*, J Phys Chem, 2012.)

Aβ protofibrils are able to activate glial cells, which trigger an inflammatory response, subsequently leading to a chronic inflammatory state in the brain. Furthermore, Aβ protofibrils can change ion homeostasis by binding specific channels or membrane proteins [89, 90]. Moreover, also fibrils were shown to cause degeneration of neurons and activation of astrocytes and microglial cells, which are the driving force in plaque formation [91].

One can conclude that a wide variation of Aβ species contributes to symptoms of AD in a manifold manner. For example, Aβ seems to be directly or indirectly, by binding to RAGE (receptor for advanced glycation endproducts), involved in the production of reactive oxygen species resulting in lipid peroxidation [92-96], forms channel-like structures within the cell membrane which alter ion homeostasis [87], causes inflammation and immune response leading to lysosomal cell death [91] and induces neuronal cell death through the p75 neurotrophin receptor or caspase-mediated apoptosis in cerebral microvascular endothelial cells [97, 98]. Another pathway is the impairment of neuronal insulin receptors by Aβ, hence, connecting AD to a brain-specific form of diabetes [99-101]. Also discussed is a connection between AD and vascular dementia including blood-brain-barrier disruption, which leads to cerebral microangiopathy [102].

1.2 Diagnosis of AD

Other diseases like Morbus Parkinson or Creutzfeld-Jacob disease (CJD) show overlapping features and symptoms as AD, complicating the discrimination between different disease patterns. Until today AD can be diagnosed reliably only *post mortem* by the detection of Aβ deposits in the brain. However, several diagnostic methods can be used to narrow down the possible diseases, which come into question.

First of all, the affected person and family members can monitor the mental status. If there is evidence of an initiating dementia, a test on cognitive impairment (like the mini-mental state examination (MMSE)), mood, behavior and social life should be the next step [103]. By testing genetic alterations typical for AD (e.g. *ApoE4, PSEN1, PSEN2*) and biomarkers in body fluids like inflammatory markers or CSF

Aβ levels, diagnosis can be refined. However, *post mortem* immunohistological staining showed that the correlation between inflammation in the brain and AD declines with age and complicates interpretation of the data [104]. Moreover, MRI- or PET-imaging can show a decline of brain mass or elevated/decreased glucose uptake. Imaging compounds like Pittsburgh compound B (PiB) are currently tested as markers for Aβ deposits [105, 106].

In our working group, new sensitive assays for detection of Aβ and other amyloidogenic peptides in body fluids are developed. The surface-fluorescence intensity distribution analysis (sFIDA) enables detection of Aβ aggregates by two differently labeled Aβ-specific antibodies and determination of Aβ concentration [107-109].

1.3   Therapy of AD

To date, only palliative treatments for AD, which ease the symptoms, are approved. These drugs are mainly antidepressants and antipsychotics, which target accessory symptoms like sleep disorder or anxiety [110]. Only five drugs are approved by the US Food and Drug Administration (FDA), namely the N-Methyl-D-aspartate (NMDA) receptor antagonist memantine and four cholinesterase inhibitors [111].

Glutamatergic neurons are involved in the regulation of synaptic plasticity, neuronal growth, learning and memory. A glutamate cycle between pre- and post-synaptic neurons and astrocytes controls the glutamate which is available for receptors. Defects in this cycle lead to an extracellular glutamate accumulation and an increased activation of the NMDA receptor, resulting in neuronal toxicity. The Aβ peptide seems to be able to bind to NMDA receptors, leading to their persistant activation [112, 113]. Memantine, an uncompetitive NMDA-receptor antagonist, is able to block the channel and decrease the persistant activation without inhibiting physiological glutamate signal cascades [114, 115].

Acetylcholine (ACh) is an important neurotransmitter, binding to muscarinic and nicotinic ACh receptors, which modulate synaptic plasticity. Acetylcholinesterase is an enzyme which disintegrates ACh to acetate and choline. Thus, ACh is no more

available for the binding to ACh receptors. Inhibition of acetylcholinesterase can lead to an increased activity of ACh receptors and therefore improved long term potentiation. To date, tacrine, donepezil, rivastigmine and galantamine are the four drugs used for this purpose. Even though tacrine is rarely used nowadays because it shows hepatotoxicity, novel tacrine analogs, which show a higher acetylcholinesterase inhibition, are researched [111, 116].

Also other neurotransmission modifying drugs are tested, which modulate the serotonin or adenosine receptor signaling. Approaches targeting other pathways involved in AD are under research, such as inhibition of tau phosphorylation, oxidative stress reduction, anti-inflammatory therapies, metal chelation or the use of phytoextracts (e.g. anti-oxidative compounds like resveratrol from grapes and berries, *Ginkgo biloba* extracts or St. John´s wort) [111, 117, 118].

1.3.1 Therapies targeting the pathogenesis of AD

Drugs that can stop or reverse AD pathogenesis are not approved yet, but several approaches are being developed, such as immunotherapy and the modulation of APP processing and Aβ aggregation.

1.3.1.1 Immunotherapy

Immunization against Aβ can be afforded in two distinct pathways. Firstly, active immunization with full length Aβ or parts of it as antigen can lead to a humoral immune response and production of anti-Aβ antibodies. This approach led to promising results in PDAPP mice. The typical AD-like pathology was reduced when mice were treated with anti-Aβ antibodies [119, 120]. However, the active anti-Aβ vaccine AN1792 failed in clinical trials, since it caused meningoencephalitis in 6 % of the treated patients. Yet, second generation active vaccines are tested [121].

The second way of immunization is passive immunization. In this approach, already selected antibodies against Aβ are administered to the patient. The

antibodies bind to Aβ molecules and target them for clearance by the immune system [119]. In recent phase 3 studies on the humanized monoclonal antibodies targeting Aβ called Solanezumab and Bapineuzumab, the substances failed to improve cognition or functional ability in human patients [122-125]. However, there is hope that immunization could help if applied earlier in the disease progression [126].

More recently, passive immunization with antibodies which are specific for Aβ oligomers is investigated. Moreover, conformation sensitive single chain variable fragments (scFvs) are under consideration. The scFvs can be screened *in vitro* or *in vivo* by intracellular antibody capture technology [127-129]. Additionally, articifcial *S. aureus* protein A derived small antigen binding peptides, called affibodies, are researched. These peptides can be developed by combinatorial protein engineering principles or phage display for specific antigen binding. For example, the affibody protein $Z_{Aβ3}$ acts as a stoichiometric inhibitor of Aβ fibrillation [130-132].

Another promising approach in active immunization is the use of AFFITOPE vaccines as researched by AFFiRiS. AFFITOPES use short peptides, which mimick parts of the N-terminal native Aβ sequence as their antigenic component. AFFITOPES can be used with adjuvants and due to their length of six amino acids, they do not activate an Aβ-specific autoreactive T cell response. Also, the induced antibody response targets only Aβ and prevents crossreactivity with APP [133, 134].

1.3.1.2 Intervention of APP processing

Modulation of APP processing could reduce the activity of the amyloidogenic APP cleavage pathway, thus shifting the ratio of toxic cleavage products and amyloidogenic Aβ towards non-toxic species. This modulation can be achieved, for example, by enhancing α-secretase activity or by inhibiting or modulating β- and/or γ-secretase activity [135].

In the case of β-secretase modulation, the β-secretase inhibitor MK-8931 (Merck KGaA) will soon enter a safety and efficacy phase 2/3 trial (EPOCH) [136,

137]. However, several compounds from this class of drugs show only limited inhibitory activity or have side effects. Several β-secretase inhibitors failed in clinical trials. The study results of a phase 1 trial with the β-secretase inhibitor CTS-21166 (CoMentis and Astellas Pharma) is currently not available at the clinicaltrials.gov webpage provided by the US National Institutes of Health. Further investigation was terminated after completion of the phase 1 trial. Another example for the failure of a β-secretase inhibitor is LY2811376 (Eli Lilly). Trials were terminated due to long-term degenerative changes in the retinal epithelium of rats [136, 138].

In the case of γ-secretase modulators, most compounds failed in clinical trials because of their interference with the Notch signaling pathway, which gave rise to severe side effects in the liver, the spleen, or the gastrointestinal tract. The drug Avagacestat (Bristol-Myers Squibb) was tested in a global multicenter study with five groups of different dosage (placebo, 25, 50, 10 or 125 mg Avagacestat). Treatment led to mild gastrointestinal and dermatologic side effects including non-melanoma skin cancer at low doses (25 and 50 mg) and weight loss when higher doses were administered. Moreover, in all groups, cerebral microbleeds occurred with an incidence of at least 10 %. A decrease in $A\beta_{1-40}$ and $A\beta_{1-42}$ was observed only in high dose groups (100 and 125 mg), but accompanied by a decrease in cognitive function [136].

Semagacestat (Eli Lilly and Èlan) is another compound that was a potential γ-secretase inhibitor. Although Semagacestat can lower Aβ levels in plasma, cerebrospinal fluid (CSF) and brain in a dose-dependent manner in animals and also in human plasma and CSF, it showed adverse effects that are generally associated with Notch singaling activity. Moreover, in phase III clinical trials, Semagacestat was shown to be unable to slow disease progression accompanied by a decreased cognitive performance and an increased risk for skin cancer [136].

A novel approach for modulation of APP processing involves the direct binding of compounds to the APP molecule. As an example, tropisetron improves cognitive functions in transgenic mice and received approval for clinical trials with MCI (mild cognitive impairment) patients, in early 2014 [139].

1.3.1.3 Modulation of Aβ aggregation and degradation

The modulation of Aβ is defined as the conversion of low molecular weight species into non-toxic species before they can form toxic oligomers or the disassembly of aggregates.

This modulation can be achieved by upregulating or stimulating Aβ-cleaving proteases like insulin degrading enzyme (IDE) or neprilysin (NEP) which have been shown to retard or prevent Aβ plaque formation and pathology in mice. Leissring *et al*. [140] hypothesized one potential mode of action: Already formed Aβ deposits disaggregate into monomers under an equilibrium reaction due to the depletion of Aβ monomers by IDE or NEP. The liberated monomers could be cleared again by the proteases. Since IDE and NEP have several other substrates, modulating their activity may lead to side effects. Gene therapy trials with human patients raises also an ethical standpoint, but strategies to address protease stimulation without gene therapy are already under consideration [140, 141].

Additionally, the stimulation of autophagic clearance of Aβ has been studied. Autophagy seems to contribute considerably to Aβ clearance under physiological conditions and is reduced in AD patients [142, 143].

Moreover, aggregation of Aβ can be modulated by the conversion of toxic low molecular weight aggregates or oligomers into non-toxic species. For example, the interaction with heterocyclic aminopyrazoles can influence the amyloidogenic attributes of $A\beta_{1-42}$ [144-147].

In order to identify suitable compounds, phage display or rational drug design represent viable options [148]. In rational drug design, knowledge about the target peptide properties leads to the development of new or improved ligands. This work can be extended by computational drug design and modeling [149-153]. One example for rationally designed as well as chemically and computationally optimized compounds is the β-sheet breaking peptide iAβ5p [154]. Moreover, empirical drug design is possible, however its outcome can be improved when it is combined with complementary approaches such as molecular dynamics simulations [155].

1.4   Drug design by phage display

Selection of specific binding partners can be achieved by phage display. Phage display can be used to identify interactions between different molecules, determine epitope specificities of antibodies and characterize the binding specificities of nucleic acid binding proteins.

In principle, the phage display technique is based on the presentation of a library of peptides encoded by phages to the target molecule. The DNA sequence encoding the peptide is fused to a gene coding for a surface protein of the phage, resulting in physical linkage between DNA sequence and peptide sequence. This allows selection of binding partners for a target protein by iterative rounds of *in vitro* panning and amplification, followed by sequencing of the DNA that encodes the peptide insert [156, 157].

There are a variety of phage display methods and a number of different parameters can be changed, for example the phage vector, the target molecule, the fusion construct or the insert sequence length can be varied. Selection follows affinity of the presented ligand to the target molecule [158]. The most common constructs are randomized DNA libraries. Moreover, cDNA libraries or peptide/protein domain libraries can be used [158].

The most commonly used phage is the non-lytic filamentous bacteriophage M13. At one tip of each M13 phage particle five copies of the minor coat proteins pⅢ and pⅥ are attached. Both proteins are used mainly for presentation of the randomized peptide sequence, since they are involved in the attachment of phages to their host and therefore exposed to the environment. Additionally, the major coat protein pⅧ is used for insertion of a randomized sequence. For all three fusion variants, the rate of infectivity can decrease following creation of the fusion constructs. Different approaches described below are used to address this potential reduction in infectivity.

Using pⅢ as an example, the type 3 system is the most straightforward approach. All pⅢ molecules present the inserted randomized sequence fused to the N-terminus of the protein.

Another possibility is to include a fusion gene of pⅢ with the insertion sequence, additionally to the wild-type pⅢ genomic sequence. With this so called type 33 system the phage presents a mosaic of wild-type pⅢ and fusion pⅢ at its surface. The third option is the type 3+3 system. In this case, the phage encodes for the wild-type pⅢ and an inserted phagemid encodes for a recombinant pⅢ version. Within the host cell, phages are produced that present mixtures of wild-type and fusion pⅢ.

All three approaches share one disadvantage. The inserted sequence can interfere with phage infectivity and the replication rate of the phage presenting this sequence can be affected. [158].

Since the phage-displayed peptide has accessibility to solvent, it behaves basically as if it was not attached to the phage surface. Therefore, it retains its natural affinity and specificity for the target. Thus, affinity selections are easily achievable when applied in aqueous solution [158]. The affine phages bind to the target and non-binding phages are discarded. The bound phages are eluted by competition or pH shift and amplified in bacterial cells in order to obtain a pool of phages with increased affinity to the target for another round of panning. The efficiency of a selection can be increased by applying higher stringency conditions. However, this needs to be performed cautiously, as the background yield of the whole pool of phages can easily override the yield of the phages with the highest target affinities.

After enrichment of the phage pool, strongly binding single phage clones are amplified. The amino acid sequence of the phage-displayed peptide from a single phage clone is obtained by determining the corresponding coding sequence in the phage DNA [158-160].

Several articles where compounds have been selected via phage display are published. Peptides with diagnostic or therapeutic benefit against AD, acute myocardial infarction, human brain metastatic breast cancer, aggregation of human antibody light chains or TGF-β receptor binding were identified [161-165].

1.4.1 Mirror image phage display

Two of the major problems of selected peptides from biologically encoded libraries are that they are prone to degradation by enzymes and that they are likely to induce a humoral immune response [166, 167]. Therefore, Schumacher and colleagues [167] described a novel approach, called mirror image phage display, which enables identification of D-enantiomeric ligands [167].

A phage display library is selected for ligands which bind the chemical mirror image of the naturally occurring L-enantiomeric target molecule. The selection is performed as described in Chapter 1.4. After suitable ligands for the target molecule have been found, the corresponding DNA sequence of the phage genome is analyzed and translated into amino acid code. This resulting peptide sequence is then synthesized completely of D-enantiomeric amino acids. Since L- and D-enantiomeric versions of one molecule act as mirror images with identical properties (except for optical activity and accessibility for enzymes), the D-enantiomeric ligand should subsequently bind to the physiological L-enantiomeric form of the target molecule [167, 168].

As enzymes are stereo-specific, compounds consisting partially or completely of D-peptides are less prone to degradation than their L-enantiomeric counterparts. Therefore, they exhibit an extended biological half-life. Moreover, D-peptides are likely to show lower immunogenicity, although immunogenicity levels depend on the dose and frequency of administration [169-173].

Within the past years, several D-peptides, selected by mirror image phage display, have shown their suitability as diagnostic or therapeutic tools for cancer, HIV and AD. One example is the development of potent D-peptides which inhibit entry of HIV-1 into cells. The obtained peptides were used as templates for further mirror image phage displays and structure-assisted design. Subsequently, an inhibitor with a half maximal inhibitory concentration (IC$_{50}$) of 250 pM was found [168, 174].

In our group, compounds which can be used as diagnostic tools for AD, were found via mirror image phage display and improved by rational design [175, 176]. With a different mirror image phage display, van Groen *et al*. were able to select the specifically Aβ binding peptide D3, which has proven its suitability for AD

treatment *in vitro* and *in vivo*. Moreover, the peptide has a high blood brain barrier permeability [177-180]. In 2010, Müller-Schiffmann and colleagues [181] showed that the combination of different drug classes, for example the D-peptide D3 and a rationally designed β-sheet breaking aminopyrazole compound, leads to superior, synergistically acting hybrid molecules [181]. Members of our group were able to show that a competitive phage display is suitable for an increase in specificity to one ligand even though affinity decreases [182].

1.5   Objective of my thesis

AD is the most abundant type of dementia. This neurodegenerative disease involves the misfolding and subsequent aggregation of peptides in the brain.

The peptide Aβ is cleaved from its precursor protein APP. Besides Aβ peptides with 38 to 40 residues, $A\beta_{1-42}$ is highly abundant in patients suffering from AD. $A\beta_{1-42}$ readily aggregates and oligomers are considered to be the major toxic entity in AD, leading to cytotoxic effects, neuronal atrophy, cognitive decline and personality disorders.

Currently, neither an accurate *pre mortem* diagnosis nor curative therapy options are available. Thus, research on novel diagnosis and therapeutic tools are crucial.

The aim of this study was the selection of novel $A\beta_{1-42}$ monomer specific compounds and their subsequent characterization. For this purpose, a competitive mirror image phage display was designed, which allows the selection of $A\beta_{1-42}$ monomer specific peptide ligands and reduces undesirable binding to other $A\beta_{1-42}$ species. The selected D-enantiomeric peptides should preferentially bind and stabilize $A\beta_{1-42}$ in its monomeric state, which is likely to have a physiological value. Therefore, $A\beta_{1-42}$ monomers are removed from the dynamic equilibrium of different $A\beta_{1-42}$ species. Consequently, the dynamic equilibrium should be shifted towards disintegration of oligomeric Aβ species and larger aggregates, thereby eliminating the toxic species from the brain.

The selected peptides were characterized by several biological assays in order to obtain information on whether they can alter $A\beta_{1\text{-}42}$ aggregation and toxicity, and to analyze their therapeutic potential.

2. Materials

2.1 Peptides

The synthetic Aβ$_{1\text{-}42}$ peptides used are shown in Table 1. Peptides were purchased as RP-HPLC purified lyophilisates with a MALDI-TOF-MS stated purity of at least 95 %. Storage conditions were -20 °C.

Table 1: Synthetic Aβ peptides.

The name, amino acid sequence, chirality, modification and distributor are listed below.

name	amino acid sequence	chirality	modification	distributor
Amyloid beta$_{1\text{-}42}$	DAEFRHDSGYEVHHQKLVFFAED VGSNKGAIIGLMVGGVVIA-OH	L	none	Bachem Holding AG (Bubendorf, Switzerland)
Bio-Amyloid beta$_{1\text{-}42}$	Bio-DAEFRHDSGYEVHHQKLVFFAED VGSNKGAIIGLMVGGVVIA-OH	L	biotinyl group at the N-terminus	AnaSpec Inc. (Fremont, CA, USA)
Amyloid beta$_{1\text{-}42}$	daefrhdsgyevhhqklvffaedvgsnkgaiig lmvggvvia-OH	D	none	JPT Peptide Technologies GmbH (Berlin, Germany)
Bio-Amyloid beta$_{1\text{-}42}$	Bio-A-daefrhdsgyevhhqklvffaedvgsnkgaiig lmvggvvia-OH	D	biotinyl group at the N-terminus	JPT Peptide Technologies GmbH (Berlin, Germany)

Additionally, the peptides listed in Table 2 were selected by mirror image phage display and synthesized as all-D-enantiomeric peptides by peptides&elephants GmbH (Potsdam, Germany). The company provided RP-HPLC purified lyophilisates with a stated purity of > 95 %, specified via MALDI-TOF-MS. The peptides were stored at -20°C.

Table 2: Synthetic D-enantiomeric peptides selected via mirror image phage display.

The names, the amino acid sequences and modifications for all synthesized D-peptides selected during competitive mirror image phage display #5 are listed below.

clone number	name	alternative name	amino acid sequence	modification
5.80	MoRu1		htwttydyvwrl	amid group at C-terminus
5.57	MoRu2		gtmlkfsgmnlt	amid group at C-terminus
5.60	MoRu3	Mosd1	ysyltsyhmvwr	amid group at C-terminus
5.86	MoRu4		lipefywtywtn	amid group at C-terminus
5.52 & 5.81	MoRu5		hnwfywttepyd	amid group at C-terminus

2.2 Buffers, media, kits

All buffers and media used are listed in Table 3. All Kits used are listed in table 4.

Table 3: List of buffers and media.

Buffers and media compositions are listed below. Solutions and agar marked with an asterisk were autoclaved for 20 min at 121 °C.

description	composition
PBS *	140 mM NaCl; 2.7 mM KCl (pH 7.4)
TBS *	25 mM Tris-HCl; 0.9 % NaCl (pH 7.4)
Tris-HCl *	1 M Tris-HCl (pH 9.1)
Glycine-HCl *	200 mM Glycin-HCl (pH 2.2)
LB medium *	1 % (w/v) tryptone; 0.5 % (w/v) yeast extract; 0.5 % (w/v) NaCl
LB agar *	LB medium; 1.5 % (w/v) agar
TOP agar *	1 % (w/v) tryptone; 0.5 % (w/v) yeast; 0.5 % (w/v) NaCl; 0.7 % (w/v) agarose
PBS-T	PBS; 0.1 % (v/v) Tween-20
TBS-T	TBS; 0.1 % Tween-20
Elution buffer (SEC)	50 mM NaP$_i$; 150 mM NaCl (pH 7.4)
PEG/NaCl	20 % (w/v) Polyethylenglycol-8000; 2.5 M NaCl
IPTG/X-Gal	dimethylformamide; 5 % (w/v) IPTG; 4 % (w/v) X-Gal
Sodiumacetate buffer	3 M sodium acetate:Tris-EDTA (10:1)
Gel sample buffer	0.2 M Tris (pH 6.8); 40 % glycerin; 8 % SDS; 8 % β-mercaptoethanol;

(4x Laemmli)	Bromphenol blue
4x Tris-tricine gel sample buffer	4 % (w/v) SDS, 12 % (v/v) glycerin, 50 mM Tris, 2 % (v/v) β-mercaptoethanol, 0.01 % (w/v) SERVA BlueG (pH 6.8)
3x gel buffer	3 M Tris; 0.3 % (w/v) SDS; pH adjusted to 8.45
10x anode buffer	2 M Tris; pH adjusted to 8.9
10x cathode buffer	1 M Tris; 1M Tricine; 1 % (w/v) SDS; pH adjusted to 8.25
NP-40 lysis buffer	50 mM Tris-HCl (pH 7.8); 150 mM NaCl; 1 % Nonidet P-40; 1x protease inhibitor EDTA-free
LB-Tet medium	LB medium; 0.1 % (v/v) tetracycline
LB-Tet-IPTG/X-Gal agar	LB-medium; 1.5 % (w/v) agar; 0.1 % (v/v) tetracycline; 0.1 % (v/v) IPTG/X-Gal

Table 4: List of Kits.

The name, individual components and the manufacturer of the Kits are listed below.

description	components	manufacturer
MicroBCA-Kit	solution MA solution MB solution MC	Thermo Fisher Scientific Inc. (Waltham, MA, USA)
Ph.D.-12 Phage Display Peptide Library Kit	streptavidin 10 mM biotin *E. coli* K12 ER2738 -28 gⅢ sequencing primer (22-mer) (1 pmol/µl) -96 gⅢ sequencing primer (20-mer) (1 pmol/µl) Ph.D.-12 Phage Display Peptide Library (1x 10^{13} pfu/ml)	New England Biolabs Inc. (Ipswich, MA, USA)
SuperSignal West Dura Chemoluminescent Substrate	luminol/enhancer solution stable peroxide buffer solution	Thermo Fisher Scientific, Inc. (Rockford, IL, USA)
cell proliferation kit 1 (MTT)	MTT labeling agent solubilization solution	Roche Diagnostics GmbH (Mannheim, Germany)

2.3   Antibodies

The antibodies listed below were aliquoted upon arrival and frozen at -20 °C.

Table 5: List of antibodies.

The description, antigen, specificity, attached conjugate and manufacturer of the antibodies are listed below.

description	antigen	specificity	conjugate	manufacturer
Beta Amyloid, 1-16 (6E10) monoclonal antibody	human Aβ	mouse anti-Aβ	none	Covance Inc. (Princeton, NJ, USA)
Beta Amyloid, 1-16 (6E10) monoclonal antibody	human Aβ	mouse anti-Aβ	none	BioLegend (Dedham, MA, USA)
Anti-M13 monoclonal conjugate	bacteriophage M13 major coat protein (p8)	mouse anti-M13	HRP	GE Healthcare Europe GmbH (Freiburg, Germany)
Anti-Amyloid Precursor Protein, C-terminal (751-770) rabbit polyclonal	full-length APP & C-terminal soluble products CTFγ, CTFα and CTFβ	rabbit anti-APP	none	Merck KGaA (Darmstadt, Germany)
β-Actin (8H10D10) mouse monoclonal antibody	N-terminal human β-actin residues	mouse anti-β-actin	none	Cell Signaling Technology, Inc. (Danvers, MA, USA)
Goat anti mouse IgG-HRP	whole mouse IgG	mouse IgG	HRP	Santa Cruz Biotechnology, Inc. (Dallas, TX, USA)
Goat anti rabbit IgG-HRP	whole rabbit IgG	rabbot IgG	HRP	Santa Cruz Biotechnology, Inc. (Dallas, TX, USA)
Goat anti mouse IgG (H+L)-HRP	mouse IgG (H+L)	mouse IgG	HRP	Thermo Fisher Scientific Inc. (Rockford, IL, USA)

2.4   Bacterial strains

The bacterial strain *E. coli* K12 ER2738, included in the Ph.D.-12 Phage Display Peptide Library Kit, was used. The typical changes in the genotype for this strain are listed below.

F´*proA$^+$B$^+$ lacI^q Δ(lacZ)M15 zzf::Tn10(Tet^R)/fhuA2 glnV Δ(lac-proAB) thi-1 Δ(hsdS-mcrB)5*

2.5 Molecular weight markers

In order to determine the molecular weight of proteins in SDS-PAGE, Color marker ultra-low range (M.W. 1,060-26,600 Da) and Ultra-low range molecular weight marker (M.W. 1,060-26,600 Da) were used. Both markers were purchased from Sigma-Aldrich (St. Louis, MO, USA). Additionally, PageRuler prestained protein ladder 10-170 kDa from Thermo Fisher Scientific (Rockford, IL, USA) was used for γ-secretase inhibition assay.
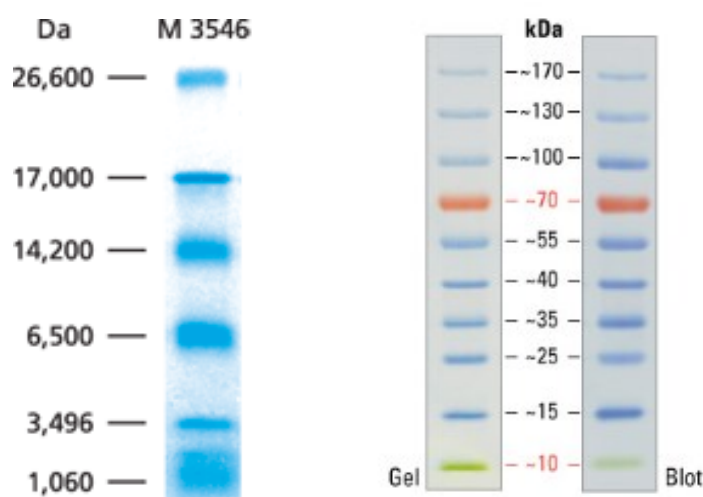
Figure 8: Scheme of protein molecular weight markers.

A gel run with 5 µl of a 1:20 dilution of the Sigma Ultra-low range molecular weight marker in a 10-20 % Tris-tricine SDS-PAGE gel and stained with EZBlue is shown exemplarily on the left. The bands are the same for the Color marker ultra-low range. An exemplary image of PageRuler prestained protein ladder 10-170 kDa on a 4-20 % Tris-glycine gel (SDS-PAGE) and subsequent transfer to membrane is shown on the right panel.

(taken from:

www.sigmaaldrich.com/life-science/proteomics/protein-electrophoresis/molecular-weight-markers.html & www.thermoscientificbio.com/protein-electrophoresis/pageruler-prestained-protein-ladder/).

2.6 Devices, laboratory equipment and software

In Table 6 devices, disposable laboratory equipment and machines used are listed.

Table 6: List of devices.

The devices and disposable laboratory equipment, machines as well as the corresponding manufacturers are listed below.

description	manufacturer
Protran BA83 nitrocellulose blotting membrane, 0.2 µm	GE Healthcare (Little Chalfont, UK)
Nunc 96-well Immobilizer Streptavidin microwell plate	Thermo Fisher Scientific Inc. (Waltham, MA, USA)
polypropylene microwell plates, 96-well	Bio TeZ Berlin Buch GmbH (Berlin, Germany)
polycarbonate microwell plates, 96-well	Bio TeZ Berlin Buch GmbH (Berlin, Germany)
Superdex 75 10/300 GL gel filtration column	GE Healthcare (Little Chalfont, UK)
ÄKTA purifier FPLC system	GE Healthcare (Little Chalfont, UK)
Rotilabo PS microwell plate, F96, clear	Carl Roth GmbH (Mannheim, Germany)
sterile filter unit 500 ml (0.22 µm)	Thermo Fisher Scientific Inc. (Waltham, MA, USA)
Nunc sealing tape for multiwell plates	Thermo Fisher Scientific Inc. (Waltham, MA, USA)
Protein LoBind Tubes, 1.5 ml	Eppendorf AG (Hamburg, Germany)
low retention pipette tips	Biotix Inc (San Diego, CA, USA)
15 ml & 50 ml centrifuge tubes	SARSTEDT AG & Co (Nümbrecht, Germany)
micro scale KB 800-2	Kern & Sohn GmbH (Bailingen, Germany)
micro scale CP225D	Sartorius AG (Göttingen, Germany)
gel documentation system GelDoc 2000	Bio-Rad Laboratories Inc. (Hercules, CA, USA)
gel documentation system ChemiDoc MP	Bio-Rad Laboratories Inc. (Hercules, CA, USA)
thermal printer P-95	Mitsubishi Electric Corp. (Chiyoda, Japan)
thermal paper K65HM for thermal printer P-95	Mitsubishi Electric Corp. (Chiyoda, Japan)
inverse laser microscope Olympus IX71	Olympus Europa Holding GmbH (Hamburg, Germany)
confocal laser scanning microscope Zeiss LSM 710	Carl Zeiss AG (Oberkochen, Germany)
objective EC Plan-Neofluar 40 x/1.30 Oil DIC M27	Carl Zeiss AG (Oberkochen, Germany)

objective Plan-Apochromat 63x/1.40 Oil DIC M27	Carl Zeiss AG (Oberkochen, Germany)
microplate reader POLARstar OPTIMA	BMG Labtech GmbH (Ortenberg, Germany)
UV/VIS spectrophotometer Lambda 25	PerkinElmer Inc. (Waltham, MA, USA)
NanoPhotometer P 300	Implen GmbH (München, Germany)
cuvette LG100-UV-G 7312 for NanoPhotometer	Implen GmbH (München, Germany)
cuvette lid factor 50 LP 0.2 mm	Implen GmbH (München, Germany)
Mini-PROTEAN Tetra Handcast Systems	Bio-Rad Laboratories Inc. (Hercules, CA, USA)
EPS 301 Power Supply	GE Healthcare (Little Chalfont, UK)
swinging bucket-rotor TLS-55	Beckman Coulter Inc. (Brea, Ca, USA)
centrifuge tube, Polyallomer, 2.2 ml, 11 x 35 mm	Beckman Coulter Inc. (Brea, Ca, USA)
Optima MAX-XP benchtop ultracentrifuge	Beckman Coulter Inc. (Brea, Ca, USA)
Infinity 1200 LC system for HPLC	Agilent Technologies Inc. (Santa Clara, CA, USA)
RP chromatography column Zorbax 300SB-C8	Agilent Technologies Inc. (Santa Clara, CA, USA)
LC injector valve syringe 50 µl FN 22/51/3	Agilent Technologies Inc. (Santa Clara, CA, USA)
Abbe refractometer AR4	A.Krüss Optotronic GmbH (Hamburg, Germany)
Formvar/carbon coated copper grid	Plano GmbH (Wetzlar, Germany)
Libra 120 transmission electron microscope	Carl Zeiss AG (Oberkochen, Germany)
sterile disposable cuvetes, PCR clean	Eppendorf AG (Hamburg, Germany)
incubuator Minitron	Infors AG (Bottmingen/Basel, Switzerland)

The software listed below was used for experiments and analysis. Additionally, Microsoft Office 2010 was used in order to analyze data and writing the thesis.

Table 7: List of software used for data analysis and presentation.

description	manufacturer
ZEN2008 for LSM 710	Carl Zeiss AG (Oberkochen, Germany)
ChemStation software for LC systems	Agilent Technologies Inc. (Santa Clara, CA, USA)
UV-WinLab V4.1.0.0230 Spectrometer software	PerkinElmer Inc. (Waltham, MA, USA)
SigmaPlot for Windows Version 11.0	Systat Software GmbH (Erkrath, Germany)
Adobe Photoshop CS5 Extended V12.0 x64	Adobe Systems Inc. (San José, CA, USA)
ImageLab Software	Bio-Rad Laboratories Inc. (Hercules, CA, USA)

2.7 Cell culture equipment

The equipment used in the cell culture including cells, culture flasks and chemicals is shown in Table 8. All equipment was manufactured under sterile conditions.

Table 8: List of cell culture equipment.

description	manufacturer / supplier
trypsin-EDTA solution	Sigma-Aldrich Corp. (St. Louis, MO, USA)
penicillin-streptomycin	Sigma-Aldrich Corp. (St. Louis, MO, USA)
Dulbecco´s Modified Eagle´s Medium (DMEM)	Sigma-Aldrich Corp. (St. Louis, MO, USA)
fetal bovine serum (FBS)	Sigma-Aldrich Corp. (St. Louis, MO, USA)
donor horse serum	PAA Laboratories GmbH (Pasching, Germany)
non-essential amino acid solution	Sigma-Aldrich Corp. (St. Louis, MO, USA)
cell culture flask (polystyrene, 75cm²)	SPL Life Sciences Co., Ltd. (Korea)
PC-12 rat adrenal pheochromocytoma cells	DSMZ - Deutsche Sammlung von Mikroorganismen und Zellkulturen GmbH (Braunschweig, Germany)
Neuro-2a (ATCC® CCL-131) mouse neuroblastoma cells	American Type Culture Collection (ATCC) (Manassas, VA, USA)
Neuro-2a cells, stably transfected with human APP695	Dr. Charlotte Teunissen (VMUC, Amsterdam, The Netherlands)
CO_2 incubator CB 150 l	Binder GmbH (Tuttlingen, Germany)
collagen A (1 mg/ml)	Biochrom GmbH (Berlin, Germany)
collagen 1 coated plate, 96-well (gibco)	Life Technologies Inc. (Carlsbad, CA, USA)
cell proliferation kit 1	Roche Diagnostics GmbH (Mannheim, Germany)
cell counting chamber (Neubauer, 0.1 mm, 0.0025 mm²)	Brand GmbH & Co. KG (Wertheim, Germany)
laminar flow clean bench	BDK Luft- und Reinraumtechnik GmbH (Sonnenbühl, Germany)
trypan blue solution (0.4 %)	Sigma-Aldrich Corp. (St. Louis, MO, USA)
DAPT (> 98 %)	Sigma-Aldrich Corp. (St. Louis, MO, USA)
centrifuge 5702R	Eppendorf AG (Hamburg, Germany)

2.8   Chemicals

The chemicals used are listed in Table 9.

Table 9: List of chemicals.

description	manufacturer
bovine serum albumin fraction V (BSA)	Roche Diagnostics GmbH (Mannheim, Germany)
nonfat dry milk powder	AppliChem GmbH (Darmstadt, Germany)
Tween-20	Carl Roth GmbH & Co. KG (Karlsruhe, Germany)
phosphate-citrate buffer with sodium perborate	Sigma-Aldrich Corp. (St. Louis, MO, USA)
sulfuric acid (95-97 %)	AppliChem GmbH (Darmstadt, Germany)
sodium bicarbonate	Carl Roth GmbH & Co. KG (Karlsruhe, Germany)
3,3´,5,5´-tetramethylbenzidine (TMB)	Sigma-Aldrich Corp. (St. Louis, MO, USA)
formic acid (98 % p.a.)	Carl Roth GmbH & Co. KG (Karlsruhe, Germany)
tryptone	AppliChem GmbH (Darmstadt, Germany)
yeast extract	AppliChem GmbH (Darmstadt, Germany)
sodium chloride	AppliChem GmbH (Darmstadt, Germany)
magnesium chloride hexahydrate	AppliChem GmbH (Darmstadt, Germany)
methanol (99.8 % p.a.)	AppliChem GmbH (Darmstadt, Germany)
agarose SERVA standard EEO	SERVA Electrophoresis GmbH (Heidelberg, Germany)
isopropyl β-D-1-thiogalactopyranoside (IPTG)	Carl Roth GmbH & Co. KG (Karlsruhe, Germany)
5-bromo-4-chloro-3-indolyl-β-D-galactopyranoside (X-gal)	Carl Roth GmbH & Co. KG (Karlsruhe, Germany)
N,N-Dimethylformamide (DMF)	Carl Roth GmbH & Co. KG (Karlsruhe, Germany)
agar for bacteriology	AppliChem GmbH (Darmstadt, Germany)
polyethylene glycol Avg. MW 8,000 (PEG-8000)	Sigma-Aldrich Corp. (St. Louis, MO, USA)
biotin (10 mM)	New England Biolabs Inc. (Ipswich, MA, USA)
ethanol absolute (99.9 % AnalaR NORMAPUR)	VWR international Ltd. (Lutterworth, Leicestershire, UK)
ethanol (96 % AnalaR NORMAPUR)	VWR international Ltd. (Lutterworth, Leicestershire, UK)
sodium acetate (anhydrous, > 99 %)	Sigma-Aldrich Corp. (St. Louis, MO, USA)
di-sodium hydrogen phosphate dihydrate (p.a.)	AppliChem GmbH (Darmstadt, Germany)
sodium dihydrogen phosphate dihydrate (p.a.)	AppliChem GmbH (Darmstadt, Germany)
guanidine hydrochloride (> 99.5 %)	Carl Roth GmbH & Co. KG (Karlsruhe, Germany)
sodium hydroxide (> 99 %)	Carl Roth GmbH & Co. KG (Karlsruhe, Germany)

acetic acid (p.a., 100 %, 17.5 M)	AppliChem GmbH (Darmstadt, Germany)
2-amino-2-hydroxymethyl-propane-1,3-diol (Tris)	AppliChem GmbH (Darmstadt, Germany)
N-(2-hydroxy-1,1-bis(hydroxymethyl)ethyl)-glycine (tricine)	AppliChem GmbH (Darmstadt, Germany)
OptiPrep density gradient medium (60 % iodixanol)	Axis-Shield PoC (Oslo, Norway)
acrylamide 4K-Solution (30 %) Mix 29:1	AppliChem GmbH (Darmstadt, Germany)
N,N,N′,N′-tetramethylethane-1,2-diamine (TEMED)	AppliChem GmbH (Darmstadt, Germany)
silver nitrate (> 99.9 %)	Carl Roth GmbH & Co. KG (Karlsruhe, Germany)
sodium carbonate (anhydrous, p.a.)	Merck KGaA (Darmstadt, Germany)
formaldehyde (36.5 %, p.a.)	Honeywell Specialty Chemicals Seelze GmbH (Seelze, Germany)
potassium hexacyanoferrate(III) (> 99 %, p.a.)	Fluka production GmbH (Buchs, Switzerland)
sodium thiosulfate (> 99 %)	Sigma-Aldrich Corp. (St. Louis, MO, USA)
sodium acetate (> 99 %, p.a., ACS, anhydrous)	Carl Roth GmbH & Co. KG (Karlsruhe, Germany)
acetonitrile (Rotisolv HPLC gradient grade)	Carl Roth GmbH & Co. KG (Karlsruhe, Germany)
2,2,2-trifluoroethanoic acid (TFA)	AppliChem GmbH (Darmstadt, Germany)

3. Methods

3.1 Competitive mirror image phage display

After several mirror image phage displays (mipd#1-4) that are described in the results part (Chapter 4), an improved protocol of competitive mirror image phage display (mipd#5) was established leading to the D-peptides MoRu1-5, which were characterized during my thesis. Since the elution procedure so far might have yielded only weak binding phages, the protocol of mipd#5 was revised again in order to enhance the elution of strongly binding phages to monomeric $A\beta_{1-42}$ (mipd#6). The improved competitive mirror image phage displays mipd#5 and mipd#6 are described in Chapter 3.1.1.

3.1.1 Selection rounds

The competitive mirror image phage display, later on refered to as mipd#5, was performed in order to obtain specifically $A\beta_{1-42}$ monomer binding peptides. Six panning rounds were performed. In order to reduce phages with an increased affinity to larger $A\beta_{1-42}$ species, oligomers and fibrils were added as counterselective agents starting at round two. Phages with an increased affinity to $A\beta_{1-42}$ oligomers and fibrils were subsequently depleted from the solution in order to enrich phages with an enhanced affinity towards monomeric $A\beta_{1-42}$ (Figure 9).

In order to avoid an enrichment of phages with an affinity to plastic surfaces or BSA, immobilization of the target peptide was performed by rotating between different streptavidin-coated surfaces (polystyrene/polypropylene/polycarbonate). Polystyrene plates were pretreated by washing each well three times with 300 µl of 1x TBS/0.05 % Tween-20 according to the manufacturer´s instructions.

Additionally, in every second round the surface was blocked with 150 µl of 1x TBS/0.1 % (v/v) Tween-20/1 % (w/v) BSA per well for one hour (h) at room temperature (RT) prior to the addition of the target peptide. This process was performed to reduce non-specific binding. Thus, no combination of plate surface

and blocking was used twice during the six panning rounds. Subsequently, SEC-derived, D-enantiomeric, N-terminally biotinylated $Aβ_{1-42}$ monomers were diluted in 1x TBS to a concentration of 63 nM and immobilized as target to the well. This concentration was chosen in accordance to the plates with the lowest streptavidin concentration per well and correlates with one third of the available binding sites per well. One-hundred microliters of the solution were loaded into the well followed by five minutes (min) incubation at RT. Afterwards, the well was washed three times with 150 µl of 1x TBS.
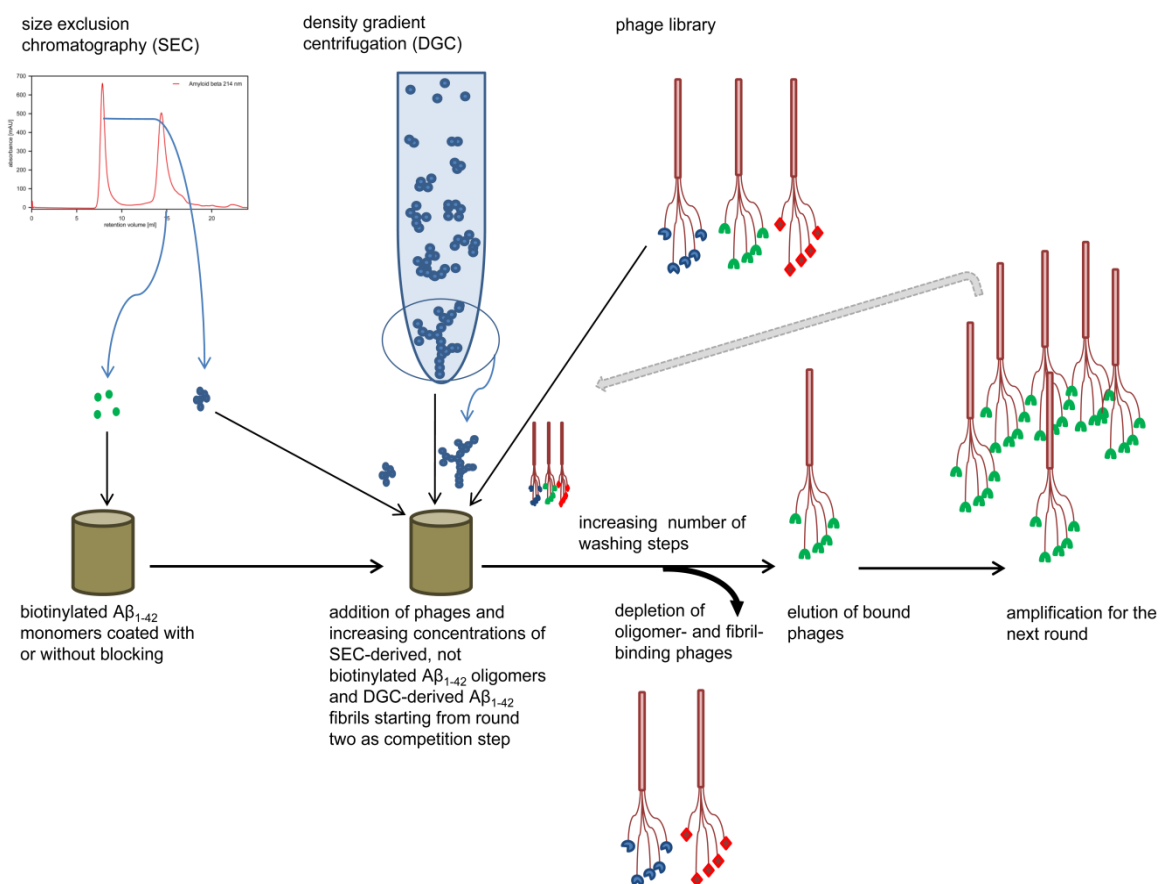
Figure 9: Scheme of a competitive mirror image phage display.

D-enantiomeric, biotinylated, SEC-derived monomeric $Aβ_{1-42}$ was immobilized at a concentration of 63 nM to different streptavidin-coated plastic surfaces (polystyrene/polypropylene/polycarbonate) and a commercially available phage library was incubated with the immobilized target peptide. 10 µM biotin were added in order to eliminate biotin competing phages. The supernatant including non-binding phages was removed. Target-bound phages were eluted, amplified and used in the following round. Starting from round two, increasing concentrations of SEC-derived, D-$Aβ_{1-42}$ oligomers and DGC-purified D-$Aβ_{1-42}$ fibrils were added together with amplified phages from the previous round in order to deplete phages with an increased affinity to $Aβ_{1-42}$ oligomers and fibrils. Moreover, the number of washing steps and the concentration of counterselective Aβ species was increased in each subsequent round.

In the first panning round 90 µl of 1x TBS and 10 µl (equates 1x 10^{11} phages) of the Ph.D.-12 Phage Display Peptide Library were added to the well and incubated for 5 min at RT. The supernatant was removed and 100 µl of 10 µM biotin in TBS-T was added to the well for 5 min at RT to reduce the number of streptavidin binding phages. Afterwards, the well was washed four times with TBS-T.

In order to elute the bound phages, 100 µl of 0.2 M glycine-HCl (pH 2.2) were added to the well and incubated for 10 min at RT. The solution containing the eluted phages was neutralized by the addition of 25 µl of 1 M Tris-HCl (pH 9.1). Twenty microliters were added to a new reaction tube in order to determine the phage titer following elution (output titer). The remaining 105 µl were used for amplification of the eluted phages.

Determination of the output titer as well as phage amplification was performed according to the manufacturer´s manual.
The output titer was determined by adding 10 µl of the eluate diluted to 100 µl with LB medium in a range of 10^{-2} to 10^{-7}, blended with 100 µl of *E. coli* ER2738 cells at an optical density of 0.6 and mixed afterwards. Eight-hundred microliters of TOP-agar and 200 µl of the phage dilutions with bacteria were plated onto 40 x 10 mm LB/Tet/IPTG/XGal Petri dishes and incubated overnight at 37 °C. The next day, plaques were counted and the titer was determined.

For phage amplification, a culture of 20 ml *E. coli* ER2738 with an optical density of 0.1 was incubated with the remaining phage elution (105 µl) for 4.5 h at 37 °C and 160 rpm. Additionally, 1x 10^{11} phages from the library were amplified in order to evaluate the affinity of non-selected phages to the target peptide in later on performed ELISA experiments. After 4.5 h the culture was centrifuged for 20 min at 2.990 x g and 4 °C. For ELISA experiments, one milliliter of the amplified phages was taken and stored at 4 °C. The remaining supernatant was precipitated overnight at 4 °C with 7 ml of a PEG-8000 / 2.5 M NaCl solution.

The next day the solution was centrifuged for 60 min at 2,990 x g and 4 °C and the supernatant was discarded. The pellet was dissolved in 1 ml of 1x TBS and centrifuged for 5 min at 9,300 x g at 4°C. The supernatant was mixed with 200 µl of PEG-8000 / 2.5 M NaCl followed by 1 h incubation on ice and a final centrifugation step for 20 min at 15,700 x g and 4 °C.

The pellet was resuspended in 100 µl of 1x TBS and the input titer after amplification was tested analogically to the output titration and according to the manufacturer´s protocol with dilutions ranging from 10^{-8} to 10^{-13}. The number of plaque forming units (pfu) was counted and phages were diluted to a concentration of $1x\ 10^{11}$ phages per well for the next panning round.

While the concentration of the target peptide remained stable at 63 nM over all panning rounds, D-enantiomeric $A\beta_{1-42}$ oligomers and high molecular weight (HMW) aggregates/fibrils without the N-terminal biotin tag were added at panning round two and subsequent panning rounds in increasing concentrations (round 2 (R2): 1/R3: 5/R4: 10/R5: 50/R6: 500 nM). $A\beta_{1-42}$ oligomers were isolated from SEC and fibrils were separated from monomers via DGC. For fibril preparation, 90 µg of $A\beta_{1-42}$ pretreated with 1,1,1,3,3,3-Hexafluor-2-propanol (HFIP) were dissolved in 250 µl 10 mM NaPi (pH 7.4) and incubated for > 24 h at RT and 600 rpm. Subsequently, 100 µl were loaded to the top of a discontinuous gradient of iodixanol, pre-formed by layering 260 µl of 30 % iodixanol at the bottom of an 11x34 mm polyallomer centrifuge tube, overlaid by 260 µl of 24 % iodixanol, 260 µl of 18 % iodixanol, 780 µl of 12 % iodixanol, 260 µl of 6 % iodixanol and 100 µl of 3 % iodixanol. The samples were spun at 259,000 x g for 3 h at 4 °C in an Optima MAX-XP ultracentrifuge with a TLS-55 rotor. After centrifugation, 14 fractions of 140 µl each were harvested with a pipette from top to bottom and fractions 12 to 14 were combined in order to obtain HMW aggregates and fibrils.

By including this additional competition step, the protocol was adjusted from the second panning round as follows: $1x\ 10^{11}$ phages from the prior panning round in 60 µl of 1x TBS were added to the target peptide. Shortly afterwards, 20 µl of SEC-derived $A\beta_{1-42}$ oligomers and 20 µl of DGC-derived $A\beta_{1-42}$ fibrils, each diluted to the desired concentration (e.g. 1 nM in R1; 5 nM in R2) in 1x TBS, were added to the sample. The solution was removed after 5 min of incubation at RT. Subsequently, a biotin competition step was performed and followed by washing four times with 1x TBS. The number of washing steps at each panning round was increased from 4 steps in round one to 6, 8, 10, 12 and 15 washing steps in rounds 2, 3, 4, 5 and 6, respectively. In the following chart (Table 10) the parameters of all six panning rounds are shown.

Table 10: Parameters in different panning rounds during the competitive mirror image phage display.

The polystyrene plates were washed prior to use as recommended by the manufacturer. Additionally, blocking with BSA was conducted in alternate rounds to reduce non-specific binding events. After allowing the naïve phage library to bind to $A\beta_{1-42}$ monomers in the first panning round, a competition step was added to the protocol, starting from round two, by elevating the concentration of $A\beta_{1-42}$ oligomers and fibrils as counterselective agents and competitive targets. PS = polystyrene, PP = polypropylene, PC = polycarbonate.

round	plate type	prewash	BSA blocking step	concentration of $A\beta_{1-42}$ monomers	concentration of $A\beta_{1-42}$ oligomers and fibrils	wash
1	PS	yes	yes	63 nM	0	4x
2	PP	no	no	63 nM	1 nM	6x
3	PC	no	yes	63 nM	5 nM	8x
4	PS	yes	no	63 nM	10 nM	10x
5	PP	no	yes	63 nM	50 nM	12x
6	PC	no	no	63 nM	500 nM	15x

For mipd#6, the protocol mentioned above was changed at two steps. Firstly, $A\beta_{1-42}$ fibril separation via DGC (Chapter 3.4) was performed with another iodixanol gradient with layers of 50/40/30/20/10/5 % iodixanol in 10 mM NaPi (pH 7.4) instead of 30/24/18/12/6/3 % iodixanol (mipd#5). Secondly, the elution procedure was significantly revised compared to all mirror image phage displays conducted before (mipd#1-mipd#5): One-hundred microliters of 0.2 M glycine-HCl (pH 2.2) were added to the well and incubated for 10 min at RT. The solution containing the eluted phages was then transferred to 25 µl of 1 M Tris-HCl (pH 9.1) in a clean reaction tube to neutralize the solution.

3.1.2 Enrichment ELISA

Enrichment ELISA was used to examine the affinity of the whole phage population to the target molecule and the counterselective agents in all panning rounds.

In mipd#5, 320 nM of each $A\beta_{1-42}$ species (biotinylated monomers, oligomers and HMW aggregates/fibrils) were immobilized in triplicates to streptavidin coated wells. Phages obtained after each panning round and the naïve phage library were

analyzed. Additionally, the different $A\beta_{1\text{-}42}$ species were immobilized in duplicates to assess the immobilization efficiency of $A\beta_{1\text{-}42}$ with the $A\beta$ specific antibody 6E10. Further controls included non-coated wells for each round, the naïve library, buffer and the antibody in duplicates. These controls were used to estimate non-specific binding events to the polystyrene plate or streptavidin.

The streptavidin coated 96-well polystyrene plates were prewashed as recommended by the manufacturer. After concentration determination of the aforementioned $A\beta_{1\text{-}42}$ species, the samples were diluted to 320 nM in 1x TBS and 100 µl per well were incubated on the plate for 15 min at RT. The plate was then washed twice with 150 µl of 1x TBS and blocked for 1 h at RT with 150 µl of 1 % (w/v) BSA in TBS-T. During this blocking step, the amplified phages from every panning round were mixed at a ratio of 1:1 with 1 % (w/v) BSA in 1x TBS and incubated on a shaker at RT for 20 min.

The wells were washed three times with 150 µl of TBS-T. The phage suspensions and the first antibody solution (6E10 1:10,000 in TBS-T), respectively, were added to the wells for 1 h at RT. After washing the wells five times with 150 µl of TBS-T, 200 µl of TBS-T were added to each well and the plates were incubated for 1 h at RT.

The supernatant was removed and 100 µl of mouse anti-M13:HRP antibody (1:5,000 in TBS-T) and secondary antibody goat anti-mouse:HRP (diluted 1:1,000 in TBS-T), respectively, were added to the wells. After 1 h of incubation at RT, the plate was washed ten times with 150 µl of TBS-T.

The detection was conducted by measuring the conversion of the substrate 3,3',5,5'-tetramethylbenzidine (TMB) by HRP accompanied with a color change. Therefore 50 µl of a TMB solution (one tablet of TMB was dissolved in 1 ml DMSO and diluted with 9 ml sterile filtered 0.05 M phosphate citrate buffer; pH 5.0) was added to each well and color development was stopped by adding 50 µl of 2 M H_2SO_4 when the solution in the wells turned turquoise. The absorption at 450 nm was measured in a microplate reader.

For mipd#6, the einrichment ELISA procedure was slightly revised. Firstly, the N-terminally biotinylated $A\beta_{1\text{-}42}$ species as well as the empty wells were all tested in duplicates. Secondly, since the coating efficiency for oligomeric species was

repeatedly higher compared with $A\beta_{1\text{-}42}$ monomers and fibrils in earlier performed ELISA experiments, the $A\beta_{1\text{-}42}$ oligomers were mixed in a ratio of 1:1 with $A\beta_{1\text{-}42}$ fibrils to an overall concentration of 320 nM. The immobilized $A\beta_{1\text{-}42}$ amounts for different species were now in a narrower range. Furthermore, mixing $A\beta_{1\text{-}42}$ oligomers and fibrils corresponds better with the counterselection step during the phage display itself in which oligomers and fibrils were added at the same time.

3.1.3 Single phage amplification

For the single phage ELISA and the preparation of phage DNA, single plaque forming units, each representing a group of phages grown from one single phage clone, were taken from the output titer plates of the panning rounds which had the highest affinity for $A\beta_{1\text{-}42}$ in the enrichment ELISA.

E. coli ER2738 cells were grown to an optical density of 0.1 in LB medium with tetracycline and each single phage clone was added to 5 ml of the culture in a test tube and amplified for 4.5 h at 37 °C and 160 rpm. Afterwards, the bacterial cultures where centrifuged for 20 min at 2,990 x g and 4 °C and the supernatant was dispensed. Two milliliters were later on used for DNA extraction and kept at 4 °C until usage. One milliliter was aliquoted for single phage ELISA experiments and stored at 4 °C and 0.5 ml were mixed with 0.5 ml 80 % sterile glycerol as backup and stored at -80 °C.

3.1.4 Single phage ELISA

The specificity and affinity of single phage clones towards the target (monomeric $A\beta_{1\text{-}42}$) and the counterselective agents ($A\beta_{1\text{-}42}$ oligomers and fibrils) was assayed by ELISA. The experimental setup was the same as for the enrichment ELISA (mipd#5) but instead of the whole phage eluate from each round, amplified single phage clones from the panning rounds, which had the highest affinity for $A\beta_{1\text{-}42}$, were used.

For mipd#6 each target was immobilized in duplicate for every clone or control. $A\beta_{1\text{-}42}$ oligomers and fibrils were mixed to an overall $A\beta_{1\text{-}42}$ concentration of

320 nM. This was done in order to achieve an $A\beta_{1-42}$ immobilization of these two species which is in closer range to $A\beta_{1-42}$ monomers and to reproduce the conditions of mipd#6 panning procedure. Additionally, a new batch of 6E10 antibody was used. For the single phage ELISA of mipd#6, the background signal of the anti M13 antibody values was subtracted. Additionally, the values received for binding of single phages to $A\beta_{1-42}$ oligomers/fibrils were normalized to the values received for binding to $A\beta_{1-42}$ monomers according to the outcome of coating efficiency controls with the $A\beta$ specific antibody 6E10.

3.1.5 Phage DNA preparation

The viral DNA was extracted in order to obtain the corresponding DNA of the target specific peptide dodecamer presented at the phage surface.

The solutions containing amplified single phage clones were centrifuged for 15 min at RT and 2,300 x g. The supernatant was transferred into a clean reaction tube and precipitated with 400 µl of PEG-8000/2.5 M NaCl. After inverting the solution, the sample was incubated for 40 min at RT. The mixture was then centrifuged for 10 min at 16,100 x g and 4 °C and the supernatant was removed. In order to discard the remaining supernatant, the reaction tubes were centrifuged again for 2 min at 16,100 x g and 4 °C and residual supernatant was carefully removed. The pellets were resuspended in 200 µl of 3 M sodium acetate buffer with TE buffer (10:1). Five-hundred microliters of 99.8 % ethanol were added to each sample followed by incubation for 15 min at RT. The samples were centrifuged for 10 min at 16,100 x g and 4 °C and the supernatant was removed. The pellets were washed with 70 % ethanol and centrifuged for 10 min at 16,100 x g and 4 °C. The supernatant was discarded and the pellet was dried in a vacuum centrifuge at 30 °C for 10 min. The pellet was resuspended in sterile ddH_2O and concentration was measured with a microvolume spectrophotometer.

Sequencing was performed by GATC Biotech AG. Therefore the DNA was prepared as recommended by the company. The sequencing primer -96 gpⅢ (sequence 5´-CCC TCA TAG TTA GCG TAA CG-3´) was provided at an amount of substance of 10 pmol.

3.2   Preparation of Aβ$_{1-42}$ monomers, - oligomers and -fibrils

3.2.1   General pretreatment of Aβ$_{1-42}$ samples

Generally, all Aβ$_{1-42}$ species were handled in siliconized reaction tubes with reduced sample to surface binding characteristics. All Aβ$_{1-42}$ preparations described later were pretreated as follows.

For dissolving any pre-existing aggregates of Aβ$_{1-42}$ and to assure the monomeric state, 1 mg Aβ$_{1-42}$ was dissolved in 700 µl of PTFE-filtered HFIP with a gastight Hamilton syringe at RT. The vial was sealed with parafilm and incubated at RT for at least 15 h. The dissolved Aβ$_{1-42}$ was transferred with a gastight syringe into a clean reaction tube. The original vial and the lid were rinsed with 300 µl of PTFE-filtered HFIP and also transferred into the new reaction tube. HFIP was evaporated in a vacuum centrifuge at RT without rotation. Afterwards the Aβ$_{1-42}$ film was dried overnight in the open reaction tube in a fume hood covered with a lintfree wipe to evaporate trace amounts of HFIP.

The Aβ$_{1-42}$ film was dissolved in 221 µl of PTFE-filtered HFIP transferred with a gastight pipette to give a 1 mM sample. The solution then was aliquoted as required, sealed with parafilm and frozen at -20 °C. HFIP was evaporated prior to use.

3.2.2   Separation of Aβ$_{1-42}$ species by size exclusion chromatography

In order to obtain monomeric and oligomeric Aβ$_{1-42}$ species, size exclusion gel filtration chromatography (SEC) was performed according to an optimized protocol of Johansson *et al.* [183].

HFIP was evaporated in a vacuum centrifuge and the resulting film of Aβ$_{1-42}$ was solved in filtered and degassed elution buffer at a concentration of 250 µM. After 1 min mixing, the sample was sonicated for 1 min and centrifuged for 1 min at 16,100 x g at RT to precipitate large aggregates and fibrils that otherwise would

clot the column. The supernatant was transferred to the chromatography system with a gastight syringe. The column used was a Superdex 75 10/300 GL connected to an ÄKTA purifier 900 system with a flow rate of 0.6 ml/min. Absorption was followed at 214 nm. The desired fractions (200 µl) were collected and pooled. $A\beta_{1-42}$ oligomers eluted at about 8 ml and the $A\beta_{1-42}$ monomers at approximately 14 ml.

3.2.3 Preparation of $A\beta_{1-42}$ samples with a broad range of differently sized species

In order to obtain a solution of $A\beta_{1-42}$ which resembles several toxic and nontoxic $A\beta_{1-42}$ species over a broad size range, HFIP pretreated $A\beta_{1-42}$ was incubated in 10 mM NaPi (pH 7.4) at a concentration of 80 µM for 4.5 h at RT and shaking at 600 rpm.

3.2.4 Preparation of $A\beta_{1-42}$ fibrils and high molecular weight aggregates

For preparation of $A\beta_{1-42}$ HMW aggregates and fibrils, 90 µg HFIP pretreated $A\beta_{1-42}$ were incubated in 250 µl 10 mM NaPi (pH 7.4) at RT for at least 24h while shaking at 600 rpm.

Separation of fibrils and HMW aggregates from remaining smaller $A\beta_{1-42}$ species, especially monomeric $A\beta_{1-42}$, was conducted by density gradient centrifugation (Chapter 3.4). Fractions containing $A\beta_{1-42}$ fibrils and HMW aggregates (F12-14) were used for further experiments.

3.3 Concentration determination of $A\beta_{1-42}$ samples

3.3.1 BCA assay

The concentration of $A\beta_{1-42}$ samples was determined via the bicinchoninic acid assay. This colorimetric quantitation method used to determine total protein content in a sample is based on the reduction of Cu^{2+} to Cu^{1+} by bicinchoninic acid (BCA). Two molecules of BCA chelate one Cu^{1+} ion and form a soluble purple product, which absorbs strongly at 562 nm. The linear absorbance rate can be used to calculate sample protein concentrations.

The protein samples of unknown concentration were mixed 1:1 with 6 M urea (final concentration 3 M) and incubated for 30 min at 60 °C to denature aggregates. Additionally, BSA at different concentrations (0/10/20/40 µg/ml) was used for calibration.

The BCA reagent kit was mixed (25 parts reagent A + 24 parts reagent B + 1 part reagent C) and added to the samples (protein of interest and BSA) at a ratio of 1:1. The mixture was incubated for 30 min at 60 °C. When the color change was clearly visible, 300 µl of each sample were transferred into a clear flat bottom 96-well microtiter plate and the absorbance was measured with a microplate reader. All samples were prepared in duplicates.

The protein concentration was measured proportionally to the BSA standard. The calibration with BSA was assigned and absorbance values of the $A\beta_{1-42}$ samples were converted to concentrations using the linear equation from the BSA standard calibration.

3.4 Density gradient centrifugation

The density gradient centrifugation method allows matrix-free separation and fractionation of different $A\beta_{1-42}$ species according to their sedimentation coefficients which depend on particle size and shape.

A discontinuous gradient of iodixanol was formed by pipetting different concentrations of iodixanol in 10 mM NaPi (pH 7.4) one upon the other as follows.

For the separation of Aβ$_{1-42}$ HMW aggregates and fibrils from smaller Aβ$_{1-42}$ species during mipd#5, 100 µl of HFIP pretreated Aβ$_{1-42}$ fibrils/HMW aggregates (Chapter 3.2.4) were mounted on top of an iodixanol gradient. The gradient consists of 260 µl of 30 % iodixanol at the bottom of an 11x34 mm polyallomer centrifuge tube, overlaid by 260 µl of 24 % iodixanol, 260 µl of 18 % iodixanol, 780 µl of 12 % iodixanol, 260 µl of 6 % iodixanol and 100 µl of 3 % iodixanol.

For experiments that require a broad range of Aβ$_{1-42}$ species, HFIP pretreated Aβ$_{1-42}$ (80 µM) was incubated in 10 mM NaPi (pH 7.4) for 4.5 h at RT and 600 rpm. In order to separate the different Aβ$_{1-42}$ species, 100 µl of the sample were mounted on top of an iodixanol gradient starting with 260 µl 50 % iodixanol at the bottom of an 11x34 mm polyallomer centrifuge tube overlayed by 260 µl of 40 % iodixanol, 260 µl of 30 % iodixanol, 780 µl of 20 % iodixanol, 260 µl of 10 % iodixanol and 100 µl of a 5 % iodixanol solution. This gradient was also used for the separation of Aβ$_{1-42}$ HMW aggregates/fibrils by DGC in mipd#6.

The samples were centrifuged at 259,000 x g for 3 h at 4 °C in a TLS-55 rotor using an OptimaXP centrifuge. After centrifugation, 14 fractions of 140 µl each were harvested with a pipette top to bottom. The residual pellet (60 µl) was mixed with 60 µl of 6 M guanidine hydrochloride and boiled for 10 min. This sample represents the fifteenth fraction. The density of the fractions increases from the top fraction one to the bottom fraction 15. Samples were later on analyzed by RP-HPLC and Tris-tricine-SDS-PAGE followed by silver staining.

3.5   Determination of iodixanol solution concentrations

Iodixanol concentrations in the fractions before and after ultracentrifugation were determined with an AR4 Abbé refractometer. After equilibration with ddH$_2$O and buffer, iodixanol solutions were analyzed. When the parting line, seen through the ocular, was adjusted to the crossing, the value for relative mass density [% Brix] was recorded, indicating the concentration of the solution.

3.6 Tris-tricine-SDS-PAGE

3.6.1 Casting gels

Proteins were separated by a polyacrylamide gel electrophoresis (PAGE). Protein samples adopt equivalent shapes and the intrinsic charge is covered by addition of sodium dodecylsulfate (SDS). This treatment leads to a separation due to the molecular mass and the size of the protein. Furthermore a Tris-tricine buffer system was used, since this is more suitable for small proteins with a mass smaller than 30 kDa [184-186]. In order to pour the gels, the Mini-PROTEAN Tetra Handcast System was used.

The resolving gel with an acrylamide ratio of 16.5 % was mixed as follows:

Acrylamide 4K solution 30 % (29:1 mix)	14.95 ml
3x gel buffer	9 ml
glycerine	2.82 ml
APS	0.2 ml
TEMED	15 µl

This amount is sufficient for four Mini-PROTEAN gels.

After the resolving gel was poured, it was overlayed with isopropanol to smoothen the surface and avoid contact with air, because air disturbes the radical polymerization reaction. After the gels were polymerized, the stacking gel with 4 % acrylamide was mixed as follows:

Acrylamide 4K solution 30 % (29:1 mix)	1.3 ml
3x gel buffer	2.5 ml
ddH$_2$O	6 ml
APS	0.2 ml
Bromphenol blue	a tip of a spatula

The Bromphenol blue allows an improved visibility of the gel pockets. The isopropanol was decanted and remaining relics were soaked with a piece of filter paper. After addition of 15 µl of TEMED, the stacking gel solution was filled into

the casting frames up to the top. Subsequently, 15 well combs were assembled into the frame.

3.6.2 Running SDS gels

Samples were mixed with sample buffer (4x Laemmli), boiled for 10 min and centrifuged shortly prior to the running of the gel.

The gels were adjusted into the Mini-PROTEAN Tetra Companion Running Module and put into the buffer tank. Into the running module 1x cathode buffer was poured and 1x anode buffer was inserted into the buffer tank. The combs were taken out of the gel and 18 µl of each sample were inserted into the gel pockets. Also 5 µl of a protein standard marker (Color Marker Ultra-low Range) were used in order to determine protein molecular weight in the lanes. Four gels were run at a fixed current of 190 mA.

3.7 Silver staining of SDS gels

In order to visualize even small amounts of protein the gels were silver stained. Gels were fixed in 50 % ethanol with 10 % acetic acid at RT for at least 1 h. Afterwards, the SDS was withdrawn by incubating the gels twice for 5 min at RT in a solution containing 10 % ethanol and 5 % acetic acid. The following incubation in Farmer´s reagent for at most 1 min led to the removal of excess dye. Incubating the gels afterwards for 20 min in staining solution (12 mM $AgNO_3$ in ddH_2O) led to an accretion of silver ions to the negatively charged side chains of the proteins. Excess silver ions were washed from the gel with ddH_2O for 20 seconds three times. The incubation with developer solution (280 mM Na_2CO_3 and 0.05 % (v/v) formaldehyde in ddH_2O) visualized the protein bands. After the desired intensity was reached, gels were incubated in an aqueous 1 % acetic acid solution for 10 min to stop the reaction and stored in tap water until detection. Detection of the bands was carried out with the gel documentation system ChemiDoc MP.

3.8   Thioflavin T assay

In order to determine the relative amount of fibrillar $A\beta_{1-42}$ over time in presence of $A\beta_{1-42}$ binding peptides, Thioflavin T (ThT) assays were performed.

The fluorescent dye ThT interacts with β-sheet structures and thereby its fluorescence emission is shifted to 490 nm. The change in fluorescence intensity is directly proportional to the amount of β-sheets in the given sample, which allows identification and quantification of Aβ fibrils and fibrilization kinetics (Figure 10) [187].

To see whether and how a peptide influences $A\beta_{1-42}$ fibrilization, the peptide was added together with ThT to HFIP pretreated $A\beta_{1-42}$ and fluorescence intensity was measured over time.
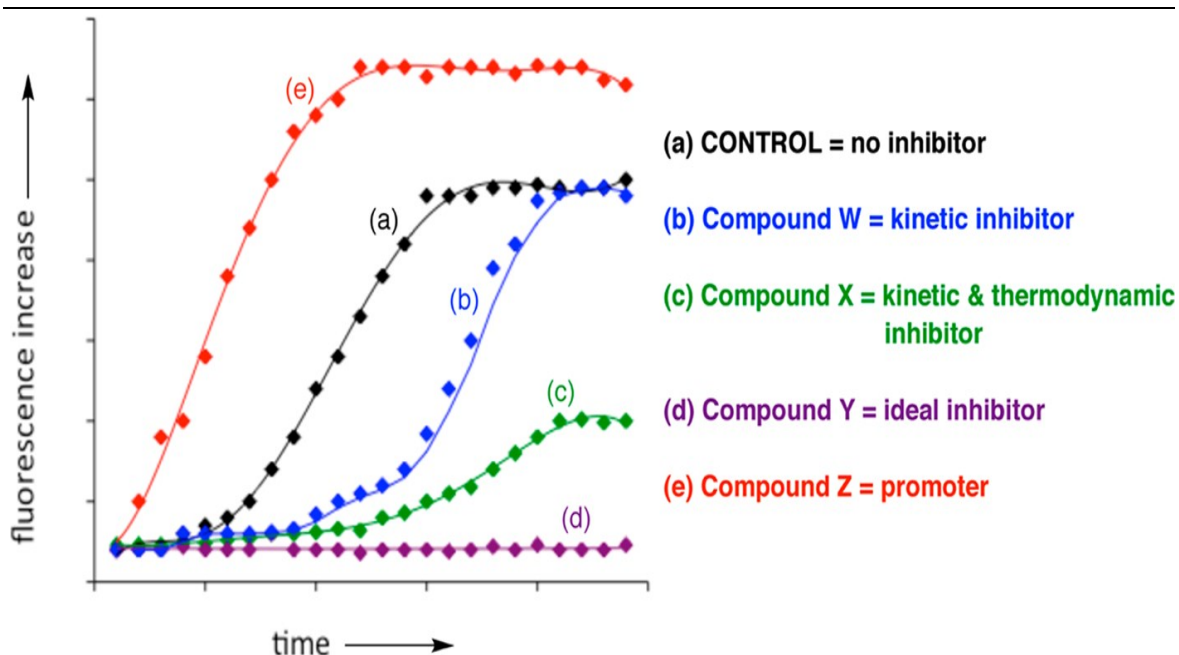
Figure 10: Influence of compounds on β-sheet developing proteins.

The graph shows several potential ways how compounds may affect the formation of β-sheets. Shown in black is a standard curve of an amyloidogenic peptide with a lag-, a log- and a stationary phase and a consistent increase of fluorescence. The red graph shows a substance that promotes β-sheet formation whereas the blue, green and purple curves show inhibiting substances. Blue displays a kinetic inhibitor prolonging the lag-phase of β-sheet formation while the green graph shows an inhibitor that is able to prolong the lag-phase and the overall increase of fluorescence. The purple line displays an ideal inhibitor that shows no formation of β-sheet content at all. (taken from: Jameson, LP *et al.*; ACS Chem Neurosci; 2012.)

The ThT assays were performed as follows. HFIP pretreated $A\beta_{1-42}$ was aliquoted and HFIP was evaporated in a vacuum centrifuge for 30 min. In order to remove residual HFIP, the $A\beta_{1-42}$ film was dried with an open lid under the fume hood. The peptides were aliquoted from their stock solutions and dried as described for the $A\beta_{1-42}$ samples.

The peptides were dissolved in filtered 1x PBS (pH 7.4) and 1 mM ThT in 1x PBS (pH 7.4) was given to the solution in order to obtain a final peptide and ThT concentration of 10 µM each. Afterwards, the solution was given to the $A\beta_{1-42}$ film which led to a final $A\beta_{1-42}$ concentration of 10 µM. After a short incubation time and flipping of the reaction tubes, 100 µl of each experimental approach (1x PBS; 10 µM $A\beta_{1-42}$; 10 µM peptide; 10 µM $A\beta_{1-42}$ + 10 µM peptide) were given into a black polystyrene 96-well flatbottom microtiter plate in sextuplicates. The plate was sealed with a polyolefine tape.

The microplate reader was adjusted to an excitation filter of 440 nm and an emission filter of 490 nm and heated to 37 °C. The samples were measured for 20 h with 20 min intervals and 1 mm double orbital shaking for 60 seconds before each cycle.

The buffer data was subtracted at every time point from all other experimental approaches and relative fluorescence units were plotted over time. At the point in time when the 10 µM $A\beta_{1-42}$ curve reached its saturation point, the relative fluorescence value of $A\beta_{1-42}$ was set 100 %. Values of the other approaches at this point in time were set into relation in order to gain information of the relative fluorescence representing the β-sheet content in the sample.

3.9 Transmission electron microscopy

In order to analyze which $A\beta_{1-42}$ species have formed after incubation with the selected peptides, transmission electron microscopy (TEM) images were taken. 10 µM HFIP pretreated $A\beta_{1-42}$ was incubated with or without 10 µM of peptide for 24 h at 25 °C. Twenty microliters of each sample were spotted on a formvar/carbon coated copper grid for 3 min. Afterwards, the solution was

detached with filter paper and the grid was washed three times with 20 µl of ddH$_2$O and once with 5 µl of 1 % aqueous uranylacetate solution. Then, 5 µl of 1 % uranylacetate were applied for 1 min and afterwards removed with a filter paper. The grids were airdried overnight. The samples were analyzed with a Libra 120 transmission electron microscope operating at 120 kV.

3.10 Reversed phase high performance liquid chromatography

Aβ$_{1-42}$ concentrations were quantified by isocratic reversed phase high performance liquid chromatography (RP-HPLC). The column used was a Zorbax SB-300-C8 on a 1260 Infinity HPLC system. Twenty microliters of the sample were injected and run with 1 ml/min in aqueous 30 % (v/v) acetonitrile/0.1 % (v/v) trifluoric acid buffer as mobile phase and 80 °C column temperature to denature Aβ$_{1-42}$ in the sample and separate it from other components, especially iodixanol. The signals were detected at an absorbance of 214 nm. The data was recorded and the peaks were integrated with the ChemStation software. To calibrate the column, Aβ$_{1-42}$ solutions of known concentrations were used to plot peak area versus Aβ$_{1-42}$ concentration. The plot equation then allowed calculation of Aβ$_{1-42}$ concentration within the samples.

3.11 Turbidity assay

In order to verify the generation of large particles in coincubations of Aβ$_{1-42}$ with peptide, a turbidity assay was performed. Measuring samples at a wavelength of 355 nm allows to detect only the scattering of light due to particle size and avoids detection of protein absorbance, since a smaller wavelength is required to detect the absorbance of peptides. Using 355 nm, and not for instance 500 nm, thereby enables one to see small particles scattering already.

HFIP pretreated Aβ$_{1-42}$ films were dissolved in 10 mM NaPi (pH 7.4) to a concentration of 25 µM either without or with peptide in different concentrations (10/25/50 µM). Samples were mixed two times for ten seconds and measured in

sextuplicates in an UV-/VIS spectrophotometer Lambda 25 right after mixing. Additionally, the samples were measured again after 24 h incubation at 21 °C.

3.12 Cell culture

3.12.1 Cultivation of PC-12 cells

The PC-12 cell line is derived from a pheochromocytoma of rat adrenal medulla. Even though these cells have an embryological origin, they can differentiate to neuronlike cells and share properties similar to neurons.

The cells were cultured in tissue culture flasks at 37 °C and 5 % CO_2 in a humidified incubator in DMEM with 10 % fetal bovine serum, 5 % horse serum and 1 % antibiotics (Penicillin/Streptomycin). Medium was changed every two to three days and the cells were passaged according to their confluence every three to five days.

Working conditions were sterile, using a clean bench and sterile media, buffer, disposable pipettes, plugged pipette tips and reaction tubes. Everything that was used under the clean bench was wiped with disinfectant.

3.12.2 Microscopy of PC-12 cells

In order to check the confluence, vitality, morphology and equal distribution of cells used for the MTT assay, the cells were observed with an inverse laser microscope (Olympus IX71) with transmission light.

3.12.3 Coating of tissue culture flasks

In order to grow PC-12 cells adherently, the tissue culture flasks needed to be covered freshly with the adhesion factor collagen. For a tissue culture flask with an

area of 75 cm², 5 ml of Collagen A were mixed with 5 ml of 1x PBS (pH 7.4) and pipetted onto the bottom of the flask. After distribution of the solution over the whole bottom, the flask was incubated at 37 °C for 40 min. Afterwards the solution was removed and the flask was washed two times with 5 ml of 1x PBS.

3.12.4 Medium change and passaging of cells

In order to supply the cells with nutrients and discard waste products and debris, which can affect the pH of the medium and therefore the wellbeing of the cells, the medium was changed every two to three days.

The medium was removed and adherent cells were washed two times with 5 ml of 1x PBS (pH 7.4). Fresh medium was added in a volume of 24 ml and the flasks were incubated again at 37 °C and 5 % CO_2.

When the cells reached a confluence of approximately 80 %, they needed to be passaged into a new collagen covered tissue culture flask, since with a lack of space the cells stop dividing or die because of nutrient limitation. Therefore, the medium was taken off the flask and the cells were washed with 5 ml of 1x PBS (pH 7.4). Afterwards, the cells were incubated for 5 min in the incubator with 1 ml of a trypsin/EDTA mixture which led to the detachment of cells. The reaction was stopped by adding 5 ml of 1x PBS (pH 7.4). The suspension was then pipetted a few times over the bottom of the flask to detach remaining cells and the total volume was transferred into a 15 ml reaction tube and spun down for 2 min at 2,000 x g to precipitate the cells.

The supernatant was discarded and cells were resuspended in 2 ml of medium. As PC-12 cells tend to accumulate and aggregate, they were singularized by drawing them up into a 5 ml syringe with a 22G canula for 15 times. Depending on the desired initial cell density the suspension was mixed with 25 ml of medium and added to a tissue culture flask freshly coated with collagen A and incubated at 37 °C and 5 % CO_2.

3.12.5 Cell count determination with a Neubauer counting chamber

In order to determine the number of cells given in a tissue culture flask after detachment, the cells were counted in a Neubauer counting chamber. For this purpose, 10 µl of singularized cells were mixed in a 1.5 ml reaction tube with 80 µl of medium and 10 µl of trypan blue to stain dead cells. The counting chamber was covered with a cover slip and 10 µl of the sample were given in between the chamber and the cover slip. Using a microscope, living cells within the four big squares of the Neubauer counting chamber were counted. The number of cells present in 1 ml was calculated in consideration of the dilution factor and the factor of the counting chamber.

3.12.6 Cell viability assay (MTT reduction assay)

In order to quantify the toxicity of peptides on eukaryotic cells, the MTT reduction assay was performed.

The tetrazolium dye 3-(4,5-dimethythiazol-2-yl)-2,5-diphenyltetrazolium bromide (MTT) can be reduced to insoluble, purple formazan in living cells by NAD(P)H-dependent cellular oxidoreductase enzymes and therefore can be used to determine the amount of cells which are metabolically active.

In a collagen coated 96-well flat bottom microtiter plate, $1x\ 10^4$ cells (PC-12) were seeded in a volume of 100 µl into the inner wells to avoid evaporation effects in the edge wells. The outer wells were filled with 100 µl of medium and the plate was incubated for 24 h in the incubator (37 °C / 5 % CO_2).

HFIP pretreated $A\beta_{1-42}$ was dissolved in sterile 10 mM NaPi (pH 7.4) and incubated for 4.5 h at 21 °C and 600 rpm. After incubation, peptides were added in different concentrations to gain total concentrations of 80 µM $A\beta_{1-42}$ and 0/40/80 µM peptide. Incubation continued for 40 min at 21 °C without shaking.

A volume of 1.25 µl was removed from every well containing cells and replaced with 1.25 µl of the aforementioned preparations in order to gain a total concentration of 1 µM $A\beta_{1-42}$ and 0/1/0.5 µM peptide, respectively. Every

preparation was tested at least in quintuplicates. The plate was incubated for 24 h at 37 °C and 5 % CO_2. Ten microliters were taken out of every well (also the ones containing only buffer) and 10 µl of MTT reagent were added. After incubation at 37 °C and 5 % CO_2 for 4 h, 100 µl of solubilization reagent were added to all wells and the plate was incubated at 37 °C/5 % CO_2 overnight.

The plate was shaken on a table shaker for 5 min in order to equally distribute the purple colored solution. Absorbance was measured at 660 nm as reference and 570 nm for the formazan. The reference values were subtracted from the 570 nm values. Afterwards, the mean value of cell-free wells was subtracted as background. The arithmetic mean of all measurements per approach was calculated. Results are represented as percentage of MTT reduction normalized to the values of the control wells (medium only) which were set 100 %. Cells treated with 0.1 % TritonX-100 in 10 mM NaPi (pH 7.4) served as control for dead cells.

3.12.7 Western blot for γ-secretase inhibition

Neuro-2a cells and Neuro-2a cells which are stably transfected with human APP695 were cultured in DMEM with 10 % fetal calf serum and 1x non-essential amino acids in tissue culture flasks. 5x 10^4 cells per well were seeded in a volume of 500 µl in a 24-well microtiter plate and incubated for 24 h at 37 °C and 5 % CO_2 to facilitate attachment to the surface.

A 1 mM stock solution of MoRu3 was prepared in sterile water and the γ-secretase inhibitor DAPT was diluted to 5 mM in DMSO. The dilutions were spun at 1,000 x g for 1 min prior to use. Then 0/10/100 µM MoRu3 and 1 µM DAPT were added to the cells and DMSO and water were additionally analyzed and served as controls. The cells were incubated at 37 °C and 5 % CO_2 for 24 h. Cell viability and morphology were analyzed with the laser scanning microscope LSM 710. The cells were washed three times with 1x PBS (pH 7.4) and lysed with 60 µl of NP-40 lysis buffer for 15 min. Lysates were resuspended, transferred to reaction tubes and centrifuged for 5 min at 12,000 x g. The supernatants were transferred to reaction tubes and protein concentration was determined by the microBCA assay. For gel electrophoresis the lysates were adjusted to the lowest measured protein

concentration. All samples were mixed with 4x Tris-tricine gel loading buffer at a ratio of 1:3 and boiled for 10 min. Gel electrophoresis was conducted with 10 % Tris-tricine gels at a constant voltage of 120 V. The PageRuler prestained protein ladder 10-170 kDa served as size marker. After gel electrophoresis, proteins were transferred via semi-dry blotting to a PVDF membrane. Protein transfer took place at 1 A and 25 V for 30 min. Subsequently, the membrane was blocked with 5 % non-fat dry milk powder in TBS-T at 4 °C overnight. The membrane was washed three times with TBS-T. The primary antibody for the detection of C-terminal fragment (anti-Amyloid Precursor Protein, C-Terminal (751-770) Rabbit pAb) was diluted 1:5,000 in TBS-T. Simultaneously, the anti-β-actin antibody (β-Actin (8H10D10) Mouse mAb) was diluted 1:1,000 in TBS-T and both antibodies were added to the membrane and incubated overnight at 4 °C on a roller mixer. The membrane was washed three times with TBS-T and incubated with the secondary antibodies goat anti-rabbit IgG:HRP diluted 1:5,000 in TBS-T and goat anti-mouse IgG:HRP diluted 1:10,000 in TBS-T for 3 h at RT on a roller mixer. After three washing steps with TBS-T, the membrane was incubated with the substrate for enhanced chemoluminescence for 5 min at RT in the dark. The signal was detected with the ChemiDoc MP gel documentation system.

4. Results

4.1 Development of an Aβ$_{1-42}$ monomer specific mirror image phage display

The main aim of this Ph.D. thesis was to select small D-enantiomeric peptides that bind specifically to monomeric Aβ$_{1-42}$.

In order to obtain Aβ$_{1-42}$ monomer specific binding partners, a mirror image phage display based on a protocol from earlier work was applied (mipd#1). With this protocol the peptide D3 was selected by Katja Wiesehan in our group [180].

The procedure of mipd#1 was as follows: HFIP pretreated, N-terminally biotinylated, D-enantiomeric Aβ$_{1-42}$ was diluted to 2 nM in 1x TBS in order to assure a solely monomeric target peptide population. One-hundred microliters of the sample were immobilized for 15 min at RT and 600 rpm in streptavidin coated wells for six rounds. The wells were washed twice with 100 µl of 1x TBS. Subsequently, 100 µl of 1x TBS were added to each well and the wells were frozen at -20 °C until required. In each round, three different libraries were used: phages presenting (i) dodecameric (12), (ii) heptameric (7) or (iii) heptameric residues with cysteines at both ends (C7C). For each phage library, one well per round was used and 1x 10^{11} phages were added in 100 µl of 0.1 % BSA in TBS-T. The binding reaction ran for 10 min at RT. The supernatant was removed and each well was washed ten times with 150 µl of TBS-T. The phages were eluted and neutralized in the same well and amplified as described in Chapter 3.1.1.

In order to determine in which panning round the pool of phages had the highest affinity for the Aβ$_{1-42}$ target, an enrichment ELISA was performed with the amplified phage pools of all panning rounds from all three approaches (12, 7, C7C) of mipd#1. In each approach, an enrichment of the binding affinity to Aβ$_{1-42}$, as shown by an increase in the absorbance values, was achieved. However, the affinity increased also for the streptavidin coated surface without immobilized Aβ$_{1-42}$. Ten phages from each round were amplified and tested in a single phage ELISA. The clones were given a continuing number (e.g. 1.1, 1.2,…). No single

phage clone was found that bound with a considerably higher affinity to the $A\beta_{1-42}$ target than to the streptavidin coated surface. As an example, all tested single phage clones from the approach with the C7C phage library (iii) had lower signals for the target peptide $A\beta_{1-42}$ than for the streptavidin-coated surface (Figure 11). Some of the clones, e.g. 1.8, showed no affinity for both targets.
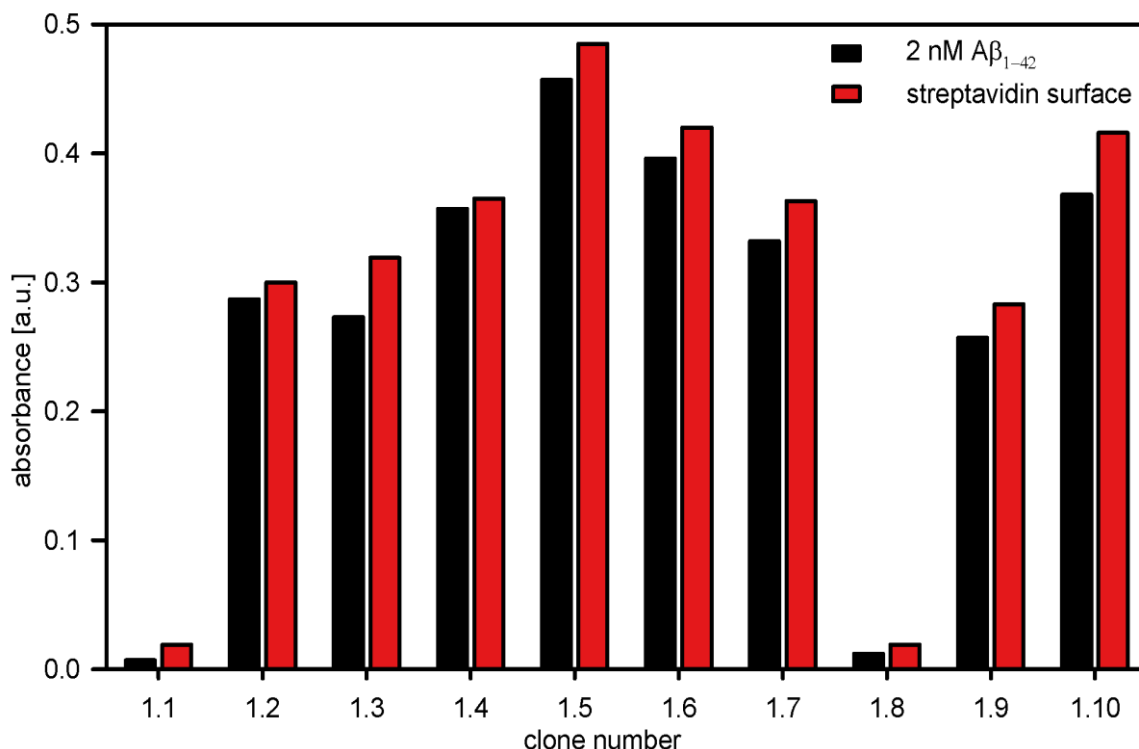
Figure 11: ELISA for relative quantification of binding affinity of single phage clones from the C7C library of mipd#1.

The relative binding affinity of single phage clones of the C7C library from mipd#1 to $A\beta_{1-42}$ and the streptavidin-coated surface was analyzed. The M13 phage-specific antibody was used for quantification of bound phages. The enzymatic transformation of the substrate by the antibody-conjugated HRP was measured at 450 nm. The relative absorbance values are plotted. Ten amplified single phage clones (1.1 – 1.10) from panning round six were added to streptavidin-coated wells which were coated with 2 nM biotinylated $A\beta_{1-42}$ (black) or not coated (red).

Since no single phage clone was identified that yielded specificity for $A\beta_{1-42}$, the protocol was revised leading to mipd#2. In this approach two steps of the mipd#1 protocol were revised. Firstly, after immobilization of $A\beta_{1-42}$ and prior to the washing steps with 1x TBS, the wells were blocked with 120 µl of 0.1 % BSA in TBS-T for 15 min at RT. The second revision was included prior to the washing steps and after phage panning procedure. The $A\beta_{1-42}$ coated wells were incubated

for 5 min at RT with 100 µl of 100 µM biotin in TBS-T. This step was used in order to displace streptavidin binding phages which compete with biotin. All other parts of the protocol were not modified.

After performing an enrichment ELISA with the pooled phages of each panning round, 22 single phage clones from each library used in mipd#2 were amplified and tested in a single phage ELISA. In order to assure a saturated surface and a sufficient amount of binding sites for the phage clones, 2 µM $A\beta_{1-42}$ was used for immobilization. The phage clones were tested against streptavidin coated wells with and without immobilized $A\beta_{1-42}$ (2 µM).

Phages were identified, which bound strongly to $A\beta_{1-42}$, even though they were never exposed previously to $A\beta_{1-42}$ (i.e. control panning with the dodecamer library against streptavidin coated wells without immobilized $A\beta_{1-42}$; data not shown). Additionally, many phages contained no insert or the inserted sequence corresponded to the amino acid sequence of the typical streptavidin binding motif HPQ.

In the next approach (mipd#3), D-enantiomeric $A\beta_{1-42}$ was immobilized by amine coupling to the well surface in order to avoid streptavidin binding of phages. $A\beta_{1-42}$ was immobilized at a concentration of 6.65 nM. In order to obtain predominantly monomeric $A\beta_{1-42}$ purification via SEC was performed. The monomeric fraction was diluted in SEC elution buffer to the desired concentration of 6.65 nM and immobilized for 2 h at RT. The wells were washed with 300 µl of 0.1 % Tween-20 in 1x PBS (PBS-T) and incubated for 1 h at RT with 100 µl of 10 nM ethanolamine in 100 µM $NaHCO_3$ buffer (pH 9.6). Afterwards, the wells were filled with 150 µl of PBS-T and frozen at -20 °C until required.

Prior to each round, possible aggregates in the wells were denatured by applying two times 300 µl of 6 M guanidine hydrochloride to each well for 10 min. Subsequently, the wells were washed two times with 300 µl of TBS-T. 1x 10^{11} phages in 100 µl of TBS-T were added to the wells for 10 min at RT. The wells were washed ten times with 150 µl of TBS-T. Elution and amplification were performed as described in the methods part (Chapter 3.1.1). After four rounds of panning, an enrichment ELISA with $A\beta_{1-42}$ concentrations of 6.65, 222 and 500 nM and uncoated wells was performed. Phages from the heptameric and the

dodecameric libraries showed an increasing affinity for $A\beta_{1-42}$ and the non-coated wells over all panning rounds. However, no difference in the absorbance signal was detected for the three concentrations and the uncoated wells (Figure 12).
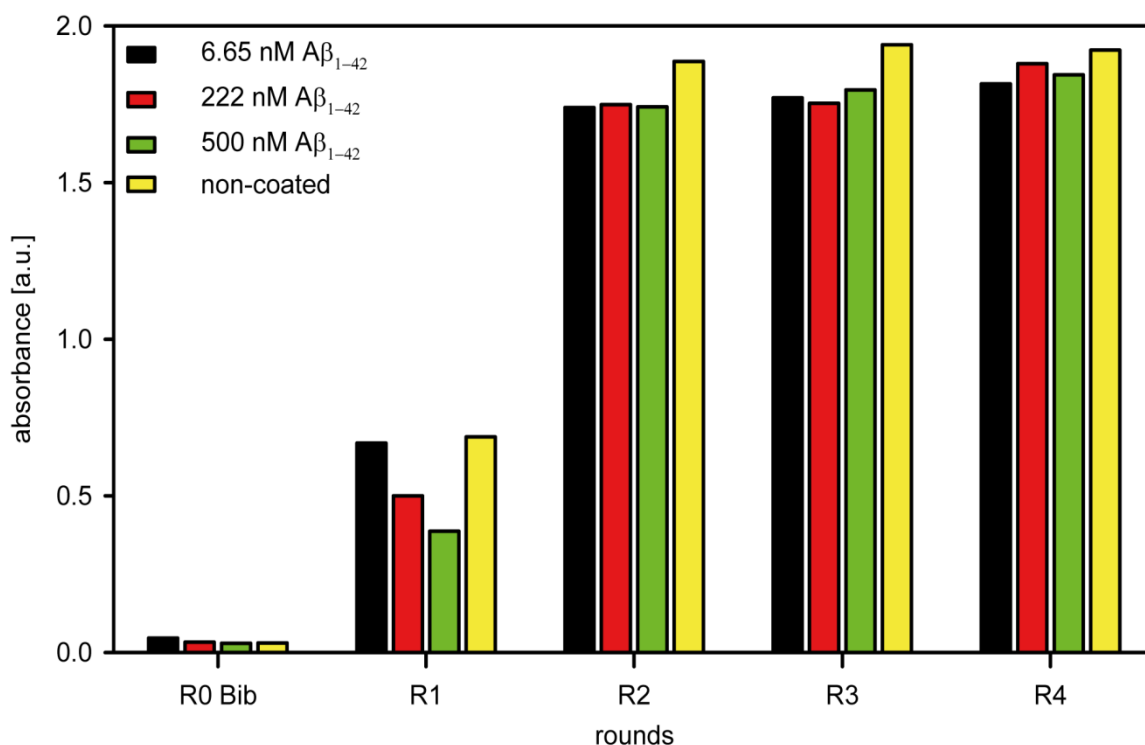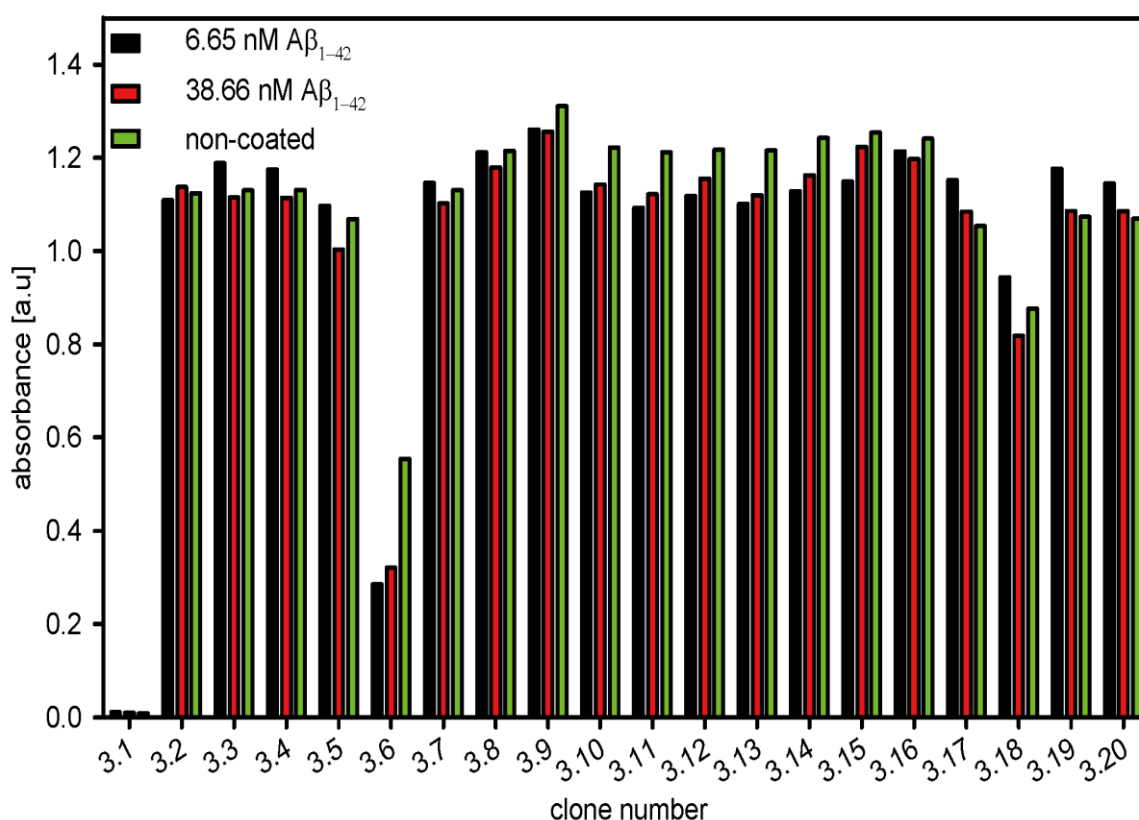

Figure 12: ELISA for relative quantification of binding affinity of phages from the dodecameric phage library from mipd#3 towards different $A\beta_{1-42}$ concentrations.

The relative binding affinity of amplified phage pools from the dodecameric library during mipd#3 to $A\beta_{1-42}$ was analyzed. The M13 phage-specific antibody was used for quantification of bound phages. The enzymatic transformation of the substrate by the antibody-conjugated HRP was measured at 450 nm. Relative absorbance values are plotted. Amplified phages from round one to four (R1–R4) and phages from the naïve library (R0) were added to different concentrations of HFIP treated $A\beta_{1-42}$ immobilized to the wells. The absorbance values for 6.65 nM $A\beta_{1-42}$ (black), 222 nM $A\beta_{1-42}$ (red), 500 nM $A\beta_{1-42}$ (green) and 0 nM $A\beta_{1-42}$ (yellow) are plotted.

Single phage clones from round three of the heptameric and dodecameric libraries were amplified. A single phage ELISA was performed using SEC-derived D-enantiomeric $A\beta_{1-42}$ monomers, immobilized at two different concentrations (6.65 and 38.66 nM). Additionally, all clones were tested for their affinity to uncoated wells. For most single phage clones from both libraries, a concentration dependency was not observed. Additionally, the background signals from uncoated wells were as high as for $A\beta_{1-42}$ coated wells. Figure 13 shows the results from a single phage ELISA with clones from the dodecameric library after

the third panning round of mipd#3.

Figure 13: ELISA for relative quantification of binding affinity of single phage clones from the dodecameric phage library during mipd#3 to Aβ$_{1-42}$.
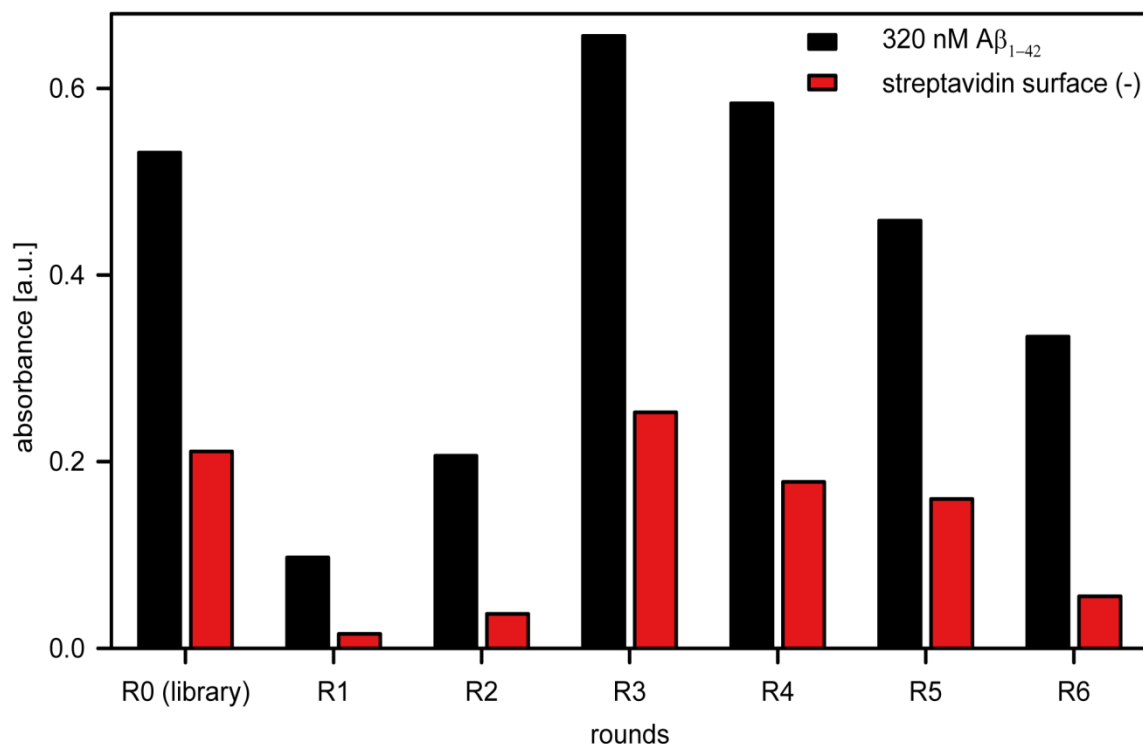
The relative binding affinity of single phage clones to SEC-derived Aβ$_{1-42}$ monomers was analyzed. The M13 phage-specific antibody was used for quantification of bound phages. The enzymatic transformation of the substrate by the antibody-conjugated HRP was measured at 450 nm. Relative absorbance values are plotted. Twenty amplified single phage clones (3.1 - 3.20) from the dodecameric library after panning round three used in mipd#3, were added to wells. Results from samples with 6.65 nM Aβ$_{1-42}$ (black), 38.66 nM Aβ$_{1-42}$ (red) or 0 nM Aβ$_{1-42}$ (green) immobilized to wells are plotted.

Sequencing of the DNA from clones originating from the heptameric library resulted in the sequence LPPNPTK. This sequence was found in 23 out of 24 sequenced clones and resembles a BSA binding motif. Since identification of suitable, specifically Aβ$_{1-42}$ binding phages was not achieved, the protocol was refined, leading to mipd#4.

In this new approach (mipd#4) streptavidin-biotin coupling for immobilization was used again and a competition step in order to reduce selection of phages with increased affinity to Aβ$_{1-42}$ oligomers and fibrils was included. Therefore,

non-biotinylated D-enantiomeric $A\beta_{1-42}$ oligomers and fibrils were added to the approach, which contained monomeric N-terminally biotinylated D-enantiomeric $A\beta_{1-42}$. With this step, phages that preferentially bind to $A\beta_{1-42}$ oligomers and fibrils should be depleted and phages with a considerably higher affinity for monomeric $A\beta_{1-42}$ should be enriched. Additionally, the binding of phages to the target and the competition step were carried out in solution. Only after the panning procedure the solution was added to a streptavidin well in order to enable the immobilization of biotinylated $A\beta_{1-42}$ monomers. Subsequently, non-biotinylated $A\beta_{1-42}$ oligomers and fibrils and phages which had bound to these species, were washed away. Additionally, a biotin competition step was included in order to reduce the number of phages that bind to the biotin binding site of streptavidin. Furthermore, the number of washing steps was increased from one round to the next. Only the dodecameric library was used and three different approaches were conducted in parallel. One approach (mipd#4-A) did not include competition with $A\beta_{1-42}$ oligomers and fibrils. The second approach (mipd#4-B) included a competition step with $A\beta_{1-42}$ oligomers and fibrils in every second panning round. The third approach (mipd#4-C) included competition steps with $A\beta_{1-42}$ oligomers and fibrils in every panning round. $A\beta_{1-42}$ monomers and oligomers were SEC-purified and fibrils were grown for 24 h and isolated from smaller $A\beta_{1-42}$ species by centrifugation. Inorder to avoid rapid monomer aggregation during concentration determination, the eluted fractions from SEC runs were stored at -20 °C.

An enrichment ELISA, using 320 nM HFIP pretreated biotinylated $A\beta_{1-42}$ as target was performed with the amplified phage pools from every panning round. The approach mipd#4-C, in which continuous competition with $A\beta_{1-42}$ oligomers and fibrils was applied, showed that affinity of phages for $A\beta_{1-42}$ exceeded affinity for streptavidin coated wells. Additionally, affinity for $A\beta_{1-42}$ increased until round three and afterwards decreased again. At the same time, affinity of phages for the streptavidin coated surface also increased from round one to three and decreased from panning round 3 to 6 (Figure 14). Thus, taking the signal-to-noise ratio as a basis, single phage clones from round 3 to 5 of the approach mipd#4-C were amplified.

Figure 14: ELISA for relative quantification of binding affinity of phages from mipd#4-C towards different Aβ$_{1-42}$ concentrations after six panning rounds.

The relative binding affinity of phages from the dodecameric library to HFIP pretreated Aβ$_{1-42}$ was analyzed. The M13 phage-specific antibody was used for quantification of bound phages. The enzymatic transformation of the substrate by the antibody-conjugated HRP was measured at 450 nm. The relative absorbance values are plotted. Amplified phages of round 1 to 6 (R1–R6) from mipd#4-C and phages from the naïve library (R0) were added to streptavidin coated wells (red) or to HFIP pretreated biotinylated Aβ$_{1-42}$, immobilized at a concentration of 320 nM to streptavidin coated wells (black).

For the single phage ELISA, D-enantiomeric, N-terminally biotinylated Aβ$_{1-42}$ monomers, oligomers (both SEC-derived) and fibrils (> 24 h incubation at RT) were immobilized each to a streptavidin microtiter plate at a concentration of 320 nM. Four single phage clones (4C.20, 4C.46, 4C.62 and 4C.72) from the mipd#4-C approach showed a high affinity to Aβ$_{1-42}$ monomers when compared with their affinity towards oligomers, fibrils and uncoated wells (Figures 15 and 16).
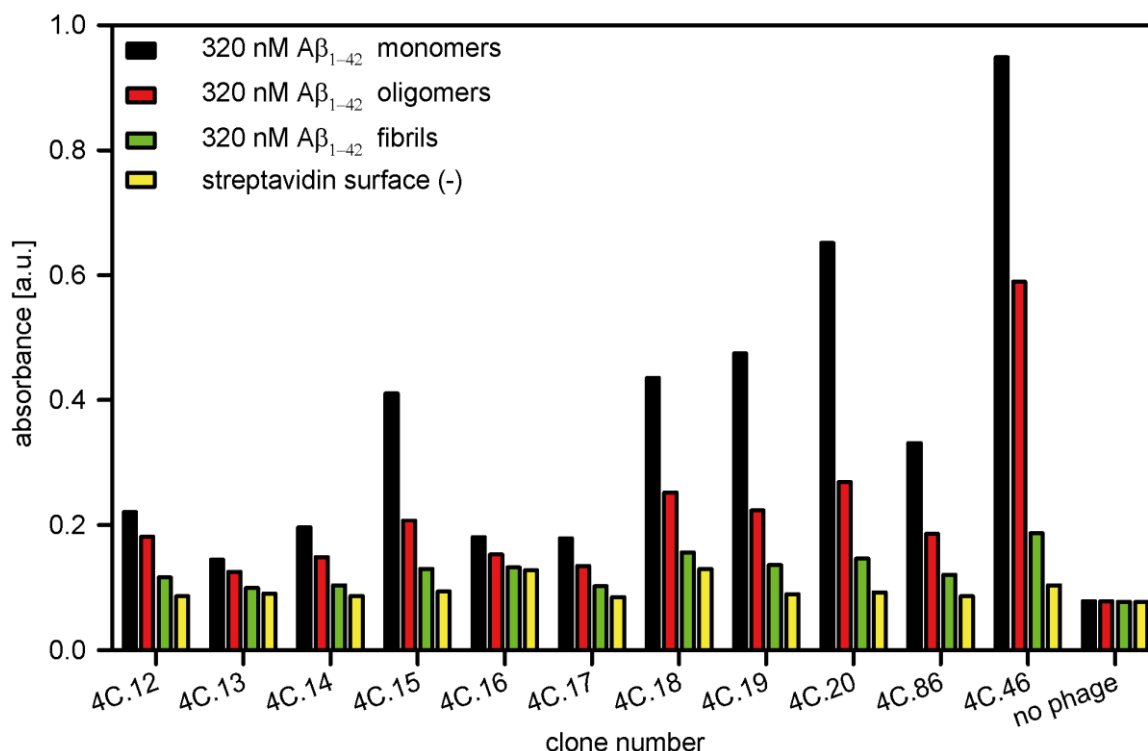
Figure 15: ELISA for relative quantification of single phage clones from the dodecameric phage library used in mipd#4-C towards different species of Aβ$_{1-42}$.

The relative binding affinity of single phage clones to different Aβ$_{1-42}$ species was analyzed. The M13 phage-specific antibody was used for quantification of bound phages. The enzymatic transformation of the substrate by the antibody-conjugated HRP was measured at 450 nm. The relative absorbance values are plotted. Amplified single phage clones from the dodecameric library (4C.xx) as well as a sample without phages were analyzed. Results from wells containing immobilized SEC-derived biotinylated Aβ$_{1-42}$ monomers (black), SEC-derived biotinylated oligomers (red) or biotinylated fibrils (green), all immobilized at a concentration of 320 nM, are shown. Results from streptavidin coated wells without immobilized Aβ$_{1-42}$ are plotted in yellow.

Clone 4C.20 was chosen because of its high absorbance values in wells with Aβ$_{1-42}$ monomers. The value represents the relative affinity of this clone for monomeric Aβ$_{1-42}$. Moreover, clone 4C.20 exhibits low affinities for other Aβ$_{1-42}$ species and uncoated wells. In addition, clone 4C.46 was chosen, as it had the highest affinity for monomeric Aβ$_{1-42}$ (Figure 15). In all cases, binding affinity of phages to Aβ$_{1-42}$ fibrils and uncoated wells was lower when compared with earlier mirror image phage display approaches (mipd#1-3). A sample without phages served as a control for cross reactivity of the M13 phage-specific antibody. The corresponding absorbance values were low, thus, the antibody neither reacted with the streptavidin coated surface nor with Aβ$_{1-42}$ species.
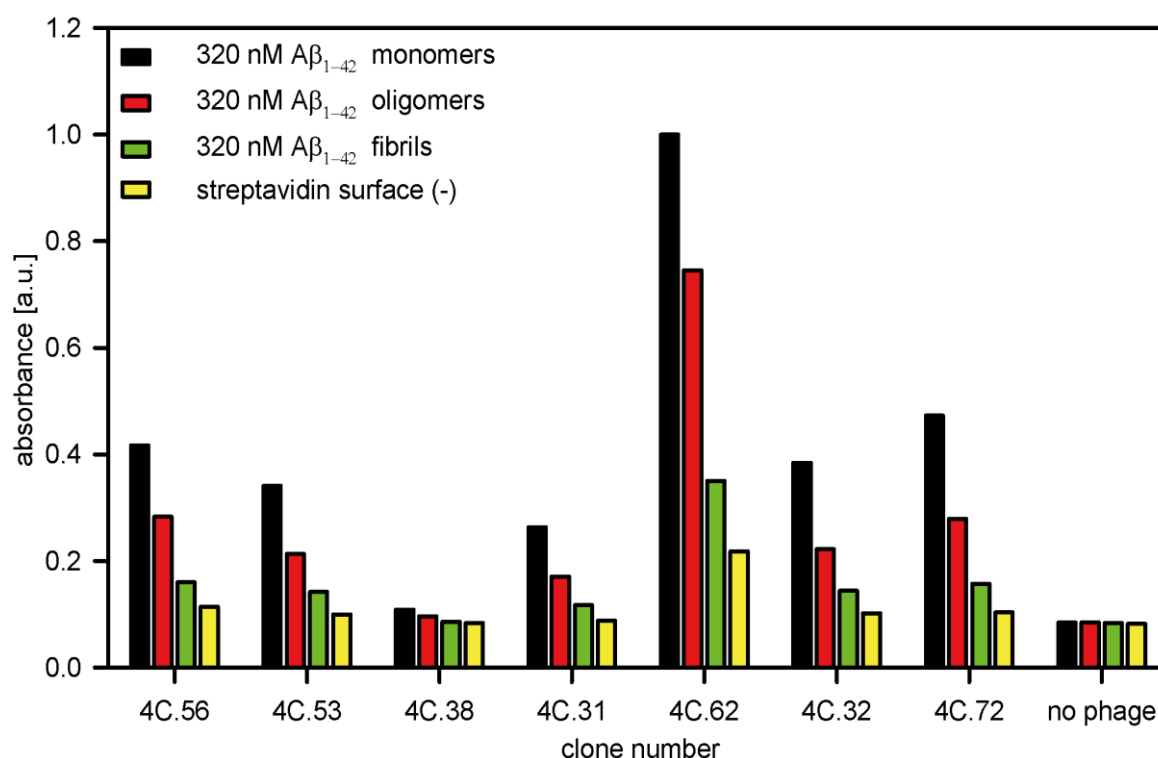
Figure 16: ELISA for relative quantification of single phage clones from the dodecameric phage library used in mipd#4-C towards different species of Aβ$_{1-42}$.

The relative binding affinity of single phage clones to different Aβ$_{1-42}$ species was analyzed. The M13 phage-specific antibody was used for quantification of bound phages. The enzymatic transformation of the substrate by the antibody-conjugated HRP was measured at 450 nm. The relative absorbance values are plotted. Amplified single phage clones from the dodecameric library (4C.xx) and a sample without phages were analyzed. Results from wells containing immobilized SEC-derived biotinylated Aβ$_{1-42}$ monomers (black), SEC-derived biotinylated oligomers (red) or biotinylated fibrils (green), all immobilized at a concentration of 320 nM, are shown. Data from streptavidin coated wells without immobilized Aβ$_{1-42}$ are presented in yellow.

Clone 4C.62 was chosen because of its selectivity for monomeric Aβ$_{1-42}$ (Figure 16), as observed from the absorbance measurements. However, oligomer-, fibril- and non-coated wells also exhibited high values. Nonetheless, the clone was chosen because of its overall binding characteristics. Clone 4C.72 has a proportionally low overall affinity, as shown by the low absorbance values. However, the signal-to-noise ratio (Aβ$_{1-42}$ monomer signal versus streptavidin coated wells) was high and therefore crucial (Figure 16). The DNA sequence inserted to each clone was sequenced, translated into the corresponding amino acid sequence and produced as D-enantiomeric peptides (Table 11).

Table 11: The amino acid sequences of selected clones.

The DNA from the selected single phage clones was sequenced and converted into the corresponding amino acid sequence presented in one letter code.

clone	name	sequence
4C.20	SRM1	SLLTFHEWHVNL
4C.46	SRM2	SVSYFVSMDWPW
4C.72	SRM3	TTYVQHNYVVRH
4C.62	SRM4	DSWHWWYDHFHS

Dissolution of these peptides in various buffers failed. Thus, a new selection process was conducted.

4.2 Competitive mirror image phage display for monomeric Aβ$_{1-42}$ with alternating plastic surfaces

The next mirror image phage display (mipd#5) was based on the knowledge and awareness of previous problems in the earlier attempts. In this approach, all potential unwanted binding events should have been avoided.

SEC-derived, D-enantiomeric, N-terminal biotinylated monomeric Aβ$_{1-42}$ was used as target protein in a concentration of 63 nM. This concentration correlates with an amount of substance, which saturates one third of all possible binding sites in a streptavidin coated well. In order to reduce instant aggregation of monomeric Aβ$_{1-42}$, the target protein was coated for only 5 min right after elution, estimation of concentration from the SEC peak hight and subsequent dilution. Estimating the concentration did not always correlate with the later on performed BCA assay, but was close to the defined 63 nM. This low variability of immobilized monomeric Aβ$_{1-42}$ concentration should not alter the monomeric state of the target.

In order to reduce phages with an increased affinity for polystyrene, the surface was altered every round from polystyrene to polypropylene to polycarbonate and anew. Furthermore, in every second round a BSA blocking step was included in order to deplete plastic binders and additionally to deplete BSA binders in the rounds without a blocking step. This approach assured that no surface condition was used twice during the panning procedure. Additionally, phages that compete

with biotin (i.e. bind to the biotin binding site of streptavidin) were depleted by adding a biotin competition step in every round.

As the overall goal was to select $A\beta_{1-42}$ monomer specific binding partners, a competition step with increasing concentrations of non-biotinylated SEC-derived $A\beta_{1-42}$ oligomers and non-biotinylated DGC-derived $A\beta_{1-42}$ fibrils and aggregates was included. Thus, the selective pressure was increased from one round to another. Both species were produced and the concentrations were determined before the SEC run for monomeric $A\beta_{1-42}$. Thus, all $A\beta_{1-42}$ species were at hand at once, which reduced the time for the $A\beta_{1-42}$ monomers to aggregate before immobilization. With an increased number of washing steps after each panning round, the amount of weak binding phages should be reduced.

4.2.1 Preparation of SEC-derived $A\beta_{1-42}$ monomers and oligomers and DGC-derived aggregates and fibrils

In order to obtain monomeric $A\beta_{1-42}$ species, size exclusion chromatography was performed with a SD75 10/300 GL column using an ÄKTA purifier FPLC system. The protocol is based on the publication from Johansson *et al.* [183].

In order to ensure that the lyophilized $A\beta_{1-42}$ was free of huge aggregates, every sample was pretreated with HFIP to provide predominantly monomeric Aβ species. HFIP pretreated $A\beta_{1-42}$ was dissolved in elution buffer at a concentration of 250 µM. The sample was mixed, sonicated and centrifuged for 1 min each in order to dissolve the $A\beta_{1-42}$ film and separate remaining large particles. The $A\beta_{1-42}$ species in the supernatant were separated by SEC. A chromatogram of N-terminally biotinylated $A\beta_{1-42}$ is plotted in Figure 17.
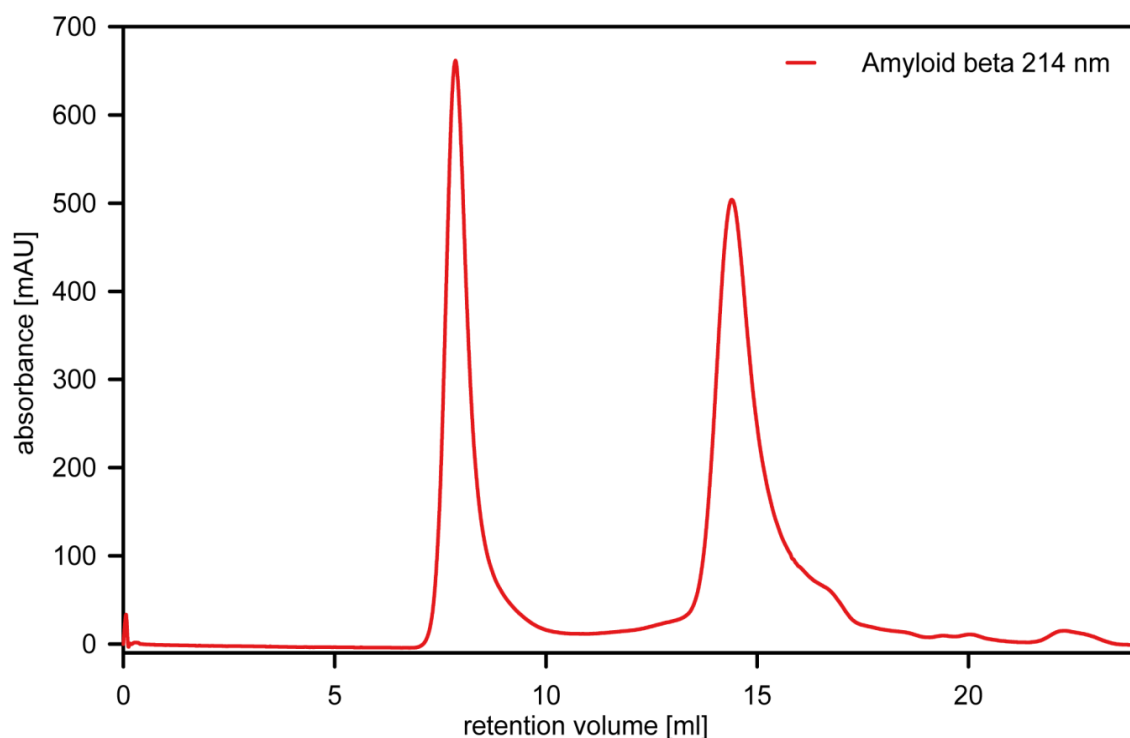
Figure 17: Size exclusion chromatogram of biotinylated Aβ$_{1-42}$.

HFIP pretreated biotinylated Aβ$_{1-42}$ was dissolved in SEC elution buffer at a concentration of 250 µM and applied to a Superdex 75 10/300 GL column connected to an ÄKTA purifier FPLC system. The absorbance (mAU = milli absorption units) at 214 nm is plotted against the retention volume. Oligomers of biotinylated Aβ$_{1-42}$ eluted essentially with the void volume of the column (7.8 ml), whereas the biotinylated Aβ$_{1-42}$ monomers eluted at 14.4 ml.

According to previous calibration runs, these elution volumes correspond to an estimated molecular weight of ≥ 100 kDa for the oligomers and ~ 10 kDa for the Aβ$_{1-42}$ monomer fraction (4.7 kDa). As the calibration refers to globular shaped proteins, these estimated molecular masses do not represent the actual molecular masses of the non-globular Aβ$_{1-42}$ peptide species.

In order to verify the monomeric and oligomeric status, the pooled peak fractions of $A\beta_{1-42}$ oligomers and monomers from SEC runs with N-terminally biotinylated D-enantiomeric $A\beta_{1-42}$ were analyzed by DGC, Tris-tricine SDS-PAGE and silver staining as explained in the methods part. The $A\beta_{1-42}$ oligomer fractions comprise a broad range of species. The strongest signals were found in fractions five to six, representing oligomers (Figure 18 A). In contrast the fractions of the $A\beta_{1-42}$ monomer peak include monomers as shown by protein bands at a molecular weight of 4.5 kDa within DGC fractions 1 and 2 only (Figure 18 B).
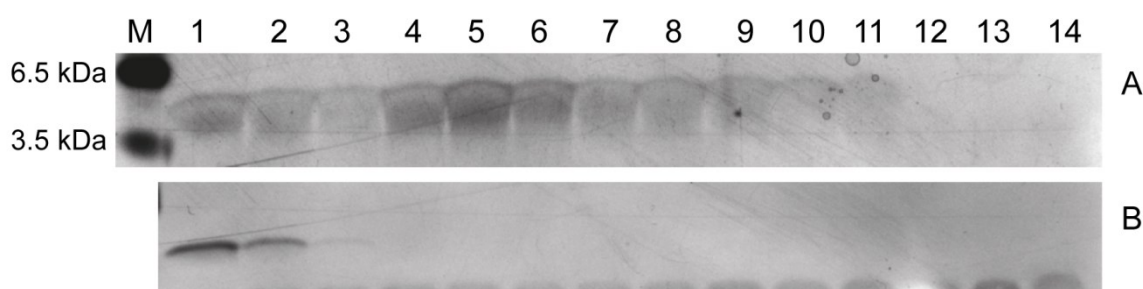
Figure 18: Silver stained Tris-tricine SDS-PAGE after DGC of $A\beta_{1-42}$ SEC peaks.

Pooled peak fractions from a SEC run with N-terminally biotinylated $A\beta_{1-42}$ were analyzed by DGC, Tris-tricine SDS-PAGE and silver staining. The silver stained gel shown in panel A represents the distribution of $A\beta_{1-42}$ from the 7.8 ml peak with a maximum of $A\beta_{1-42}$ signal in DGC fractions five and six. The gel in panel B represents the distribution of $A\beta_{1-42}$ from the 14.4 ml peak with a maximum of detectable $A\beta_{1-42}$ in fraction one and two.

In order to obtain $A\beta_{1-42}$ fibrils and HMW aggregates, 80 µM HFIP pretreated D-enantiomeric $A\beta_{1-42}$ wase incubated for at least 24 h at RT in 10 mM sodium phosphate buffer (pH 7.4). The formed species were separated according to their mass and shape by DGC. Figure 19 shows a scheme of the density gradient approach.
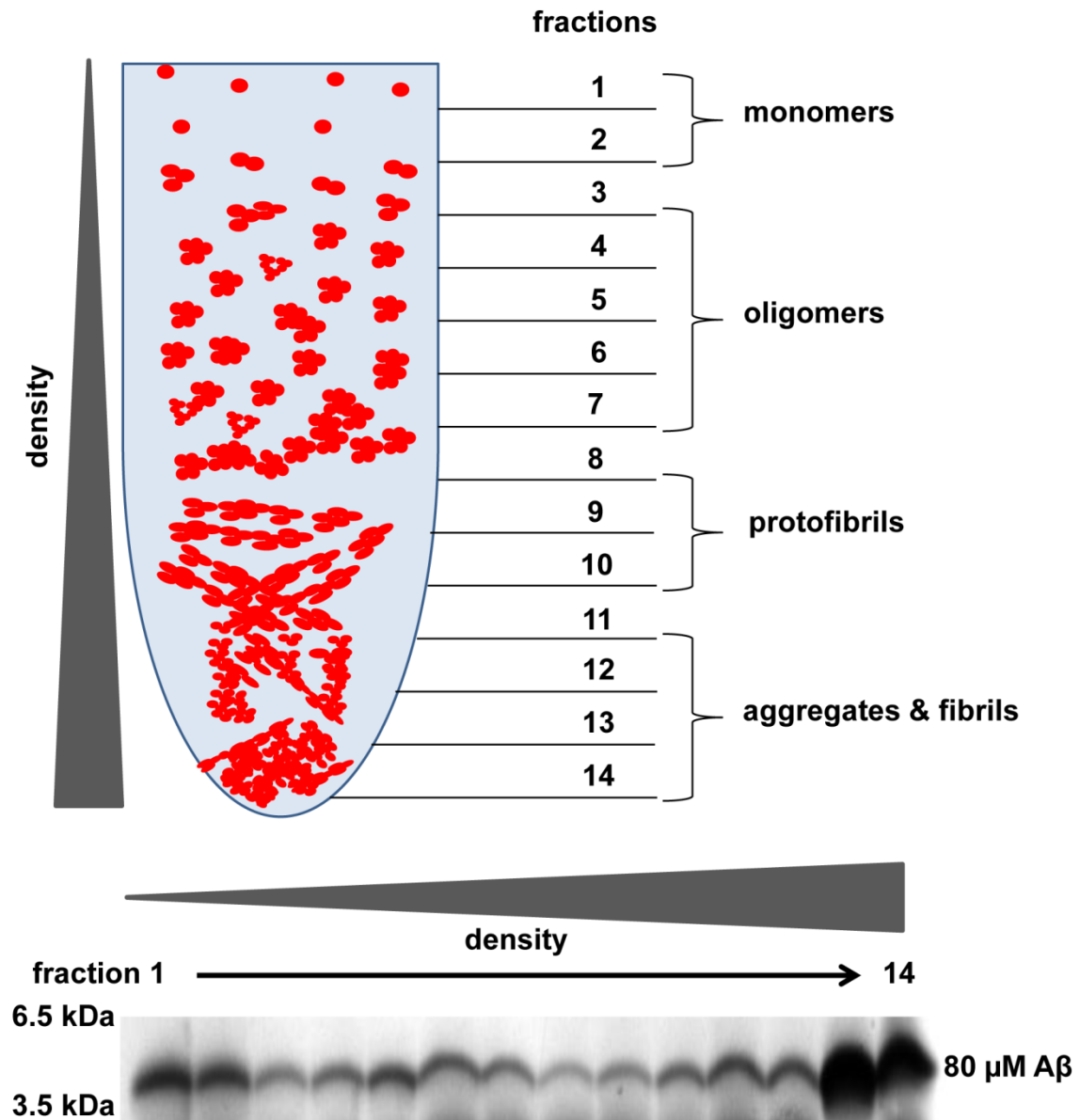
Figure 19: Schematic overview of the Aβ$_{1-42}$ fibril preparation via DGC.

In order to separate Aβ$_{1-42}$ species, density gradient centrifugation can be performed. The sample is loaded onto a discontinuous iodixanol gradient. The different species penetrate into the gradient during centrifugation, according to their mass and shape. Small species, such as Aβ$_{1-42}$ monomers, are found in the first fractions of the gradient with a low density. The larger and heavier species penetrate further into the gradient. After centrifugation, the solution was separated into 14 fractions and analyzed with a Tris-tricine SDS-PAGE in order to determine the distribution of Aβ$_{1-42}$. The upper part of the figure shows a schematic distribution of Aβ species in the iodixanol gradient after centrifugation. The lower part of the figure shows a silver stained Tris-tricine SDS-PAGE gel with samples from a DGC-separated fibril preparation of 80 μM Aβ$_{1-42}$. Aβ can be detected in all fractions at ~ 4.5 kDa.

The generation of Aβ$_{1-42}$ fibrils and HMW aggregates, and their separation from smaller species was confirmed by silver staining of a Tris-tricine SDS-PAGE gel. The distribution of an Aβ$_{1-42}$ fibril preparation from panning round six following DGC is shown in Figure 20. The strongest signal intensity was detected in fractions F13 and F14. These fractions include the most dense and largest Aβ$_{1-42}$ species, including HMW aggregates and fibrils. Smaller amounts of Aβ$_{1-42}$ were detected in fractions F1 to F12.
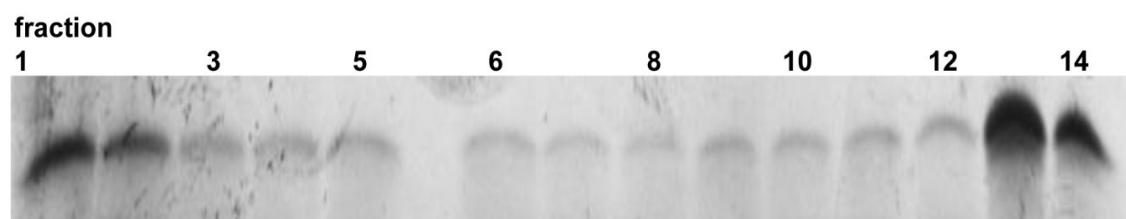
Figure 20: Silver stained Tris-tricine SDS-PAGE of a DGC-derived Aβ$_{1-42}$ fibril preparation.

80 μM Aβ$_{1-42}$ was incubated for at least 24 h in order to obtain fibrillar species. To separate fibrils from other Aβ species, the sample was loaded onto a discontinuous iodixanol gradient and centrifuged. After centrifugation, 14 fractions were obtained by upward displacement and loaded onto a Tris-tricine SDS gel. Following electrophoresis, the gel was silver stained.

In order to verify the results from DGC, the fractions F12 and F13 were spotted onto a formvar/carbon copper grid, stained with uranyl acetate and analyzed by transmission electron microscopy (TEM). Figure 21 shows manifold shapes of Aβ$_{1-42}$, including short fibrils and large aggregates, thus supporting the concept that DGC can effectively separate various Aβ species. Aβ$_{1-42}$ oligomers can be seen as black spherical particles in panels A (fraction 12) and B (fraction 13). Moreover, in panel B, branched, thick protofibrils and fibrils can be seen. Panels C and D show Aβ$_{1-42}$ protofibrils, fibrils and oligomers obtained from fraction 13.
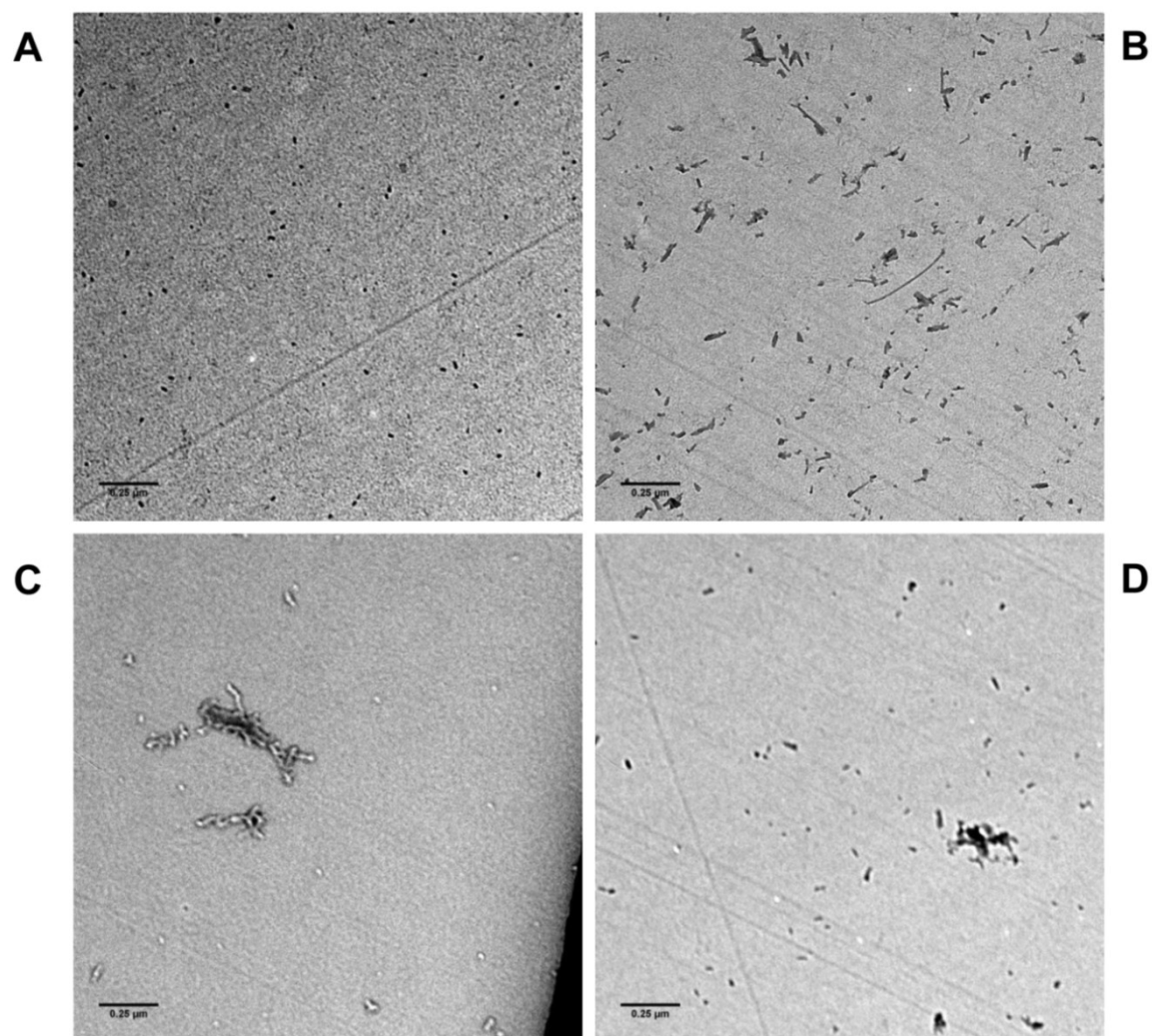
Figure 21: TEM pictures of high molecular weight Aβ$_{1-42}$ species from DGC fractions F12 and F13.

After separation of an Aβ$_{1-42}$ fibril preparation via DGC, samples from fractions 12 (A) and 13 (B to D) were spotted onto a formvar/carbon copper grid and stained with uranyl acetate. The grids were analyzed by TEM operating at 120 kV. The scale bars represent 0.25 µm.

## 4.2.2 Enrichment ELISA

In order to analyze whether the phage-displayed peptides show an increased affinity to monomeric $A\beta_{1-42}$ from one round to the next and which round is suitable for picking single phages, an enrichment ELISA was performed (Chapter 3.1.2).

Biotinylated $A\beta_{1-42}$ monomers, oligomers and fibrils were produced as in the panning rounds of mipd#6 and immobilized at a concentration of 320 nM to streptavidin coated wells in triplicates. Wells without immobilized $A\beta_{1-42}$ served as control for unspecific binding of phages to the plastic surface or streptavidin.The eluted phage pools of each panning round as well as the naïve phage library were subsequently analyzed for their binding affinity to all immobilized $A\beta_{1-42}$ species and the uncoated wells.

In order to analyze a potential cross-reactivity of the M13 phage-specific antibody with $A\beta_{1-42}$ or the streptavidin coated surface, control wells with and without immobilized $A\beta_{1-42}$ species were incubated with buffer instead of phages. Afterwards, the M13 phage-specific antibody was added and substrate transformation by HRP conjugated to the M13 phage-specific antibody, was measured.
Furthermore, immobilization efficiency was tested. $A\beta_{1-42}$ monomers, oligomers and fibrils were immobilized and detected with the $A\beta$-specific antibody 6E10. Subsequently, 6E10 was detected with a HRP conjugated goat anti mouse antibody and the values of substrate transformation by HRP were measured at 450 nm (Figure 22).
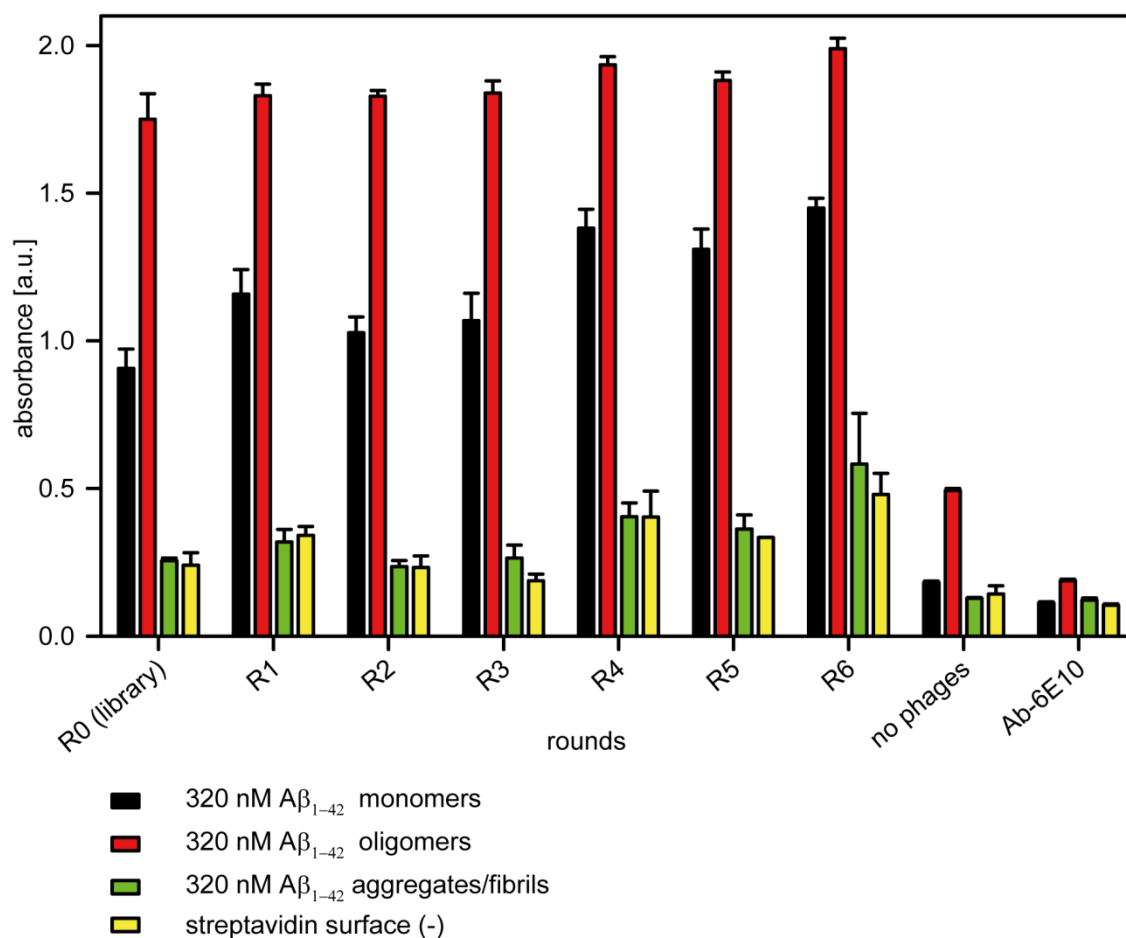
Figure 22: ELISA for relative quantification of binding affinity of phages from mipd#5 towards different Aβ₁₋₄₂ species after six panning rounds.

The relative binding affinity of phages from the dodecameric phage library to SEC-derived biotinylated Aβ$_{1-42}$ monomers and oligomers as well as DGC-derived biotinylated Aβ$_{1-42}$ fibrils was analyzed. The M13 phage-specific antibody was used for quantification of bound phages. The enzymatic transformation of substrate by the antibody-conjugated HRP was measured at 450 nm. The relative absorbance values are plotted. Amplified phages from round one to six (R1–R6) as well as phages from the naïve library (R0) were added to monomeric (black), oligomeric (red) or fibrillar Aβ$_{1-42}$ (green), all immobilized at a concentration of 320 nM. The phages were also added to uncoated wells (yellow). Cross reactivity of the M13 phage-specific antibody was tested in an approach without addition of phages (no phages). In order to verify the immobilization efficiency of the different Aβ$_{1-42}$ species, the Aβ-specific antibody 6E10 was added to wells instead of the anti-M13 antibody. 6E10 binding was detected with a HRP conjugated secondary antibody.

The affinity of phages towards Aβ$_{1-42}$ increased from the naïve library to phages from panning round one and again from round three to four. The increase of the absorbance signal of phages binding to monomeric Aβ$_{1-42}$ was from 0.9 to 1.45 absorbance units in the sixth round. Yet, the absorbance signal of phages binding

to Aβ$_{1-42}$ oligomers increased from initially 1.7 to 2.0 absorbance units and is therefore constantly higher over all rounds. Even though the absolute absorbance signals were higher for Aβ$_{1-42}$ oligomers, the increase of absorbance was higher for monomer binding phages. Also the relative affinity to Aβ$_{1-42}$ fibrils and the well surface increased over time, however these values were considerably lower than for Aβ$_{1-42}$ monomers and oligomers. The controls showed, that the M13 phage-specific antibody cross reacted with oligomeric Aβ$_{1-42}$. Furthermore, the efficiency of immobilization was higher in case of oligomeric Aβ$_{1-42}$ compared to Aβ$_{1-42}$ monomers and fibrils, which barely exceeded the value for uncoated wells.

Regarding the overall values and the signal-to-noise ratio, single phage clones from round five and six were amplified. Their DNA was sequenced and the single phage clones were tested in an ELISA.

4.2.3 Single phage ELISA

In parallel to single phage DNA sequencing, the amplified single phage clones were tested for their relative affinity towards different Aβ$_{1-42}$ species. The assay was performed as explained in Chapter 3.1.4. It differs from the enrichment ELISA only by the analytes, which are not pooled phages from each panning round but single phage clones. The single phage ELISA was performed on three plates due to the amount of phage clones tested. Due to this issue, the cross reactivity of the anit M13 antibody with different Aβ$_{1-42}$ species as well as coating efficiency of Aβ$_{1-42}$ with the 6E10 antibody was tested independently on every plate. On each plate, the M13 phage-specific antibody showed cross reactivity with Aβ$_{1-42}$ monomers and oligomers. Additionally, more Aβ$_{1-42}$ oligomers were immobilized to the wells compared to Aβ$_{1-42}$ monomers or fibrils, which barely exceeded the signal intensity of wells without immobilized Aβ$_{1-42}$. Thus, the high affinities of single phage clones to oligomeric Aβ$_{1-42}$ have to be considered with caution in the interpretation of the outcome (Figures 23 to 25.)
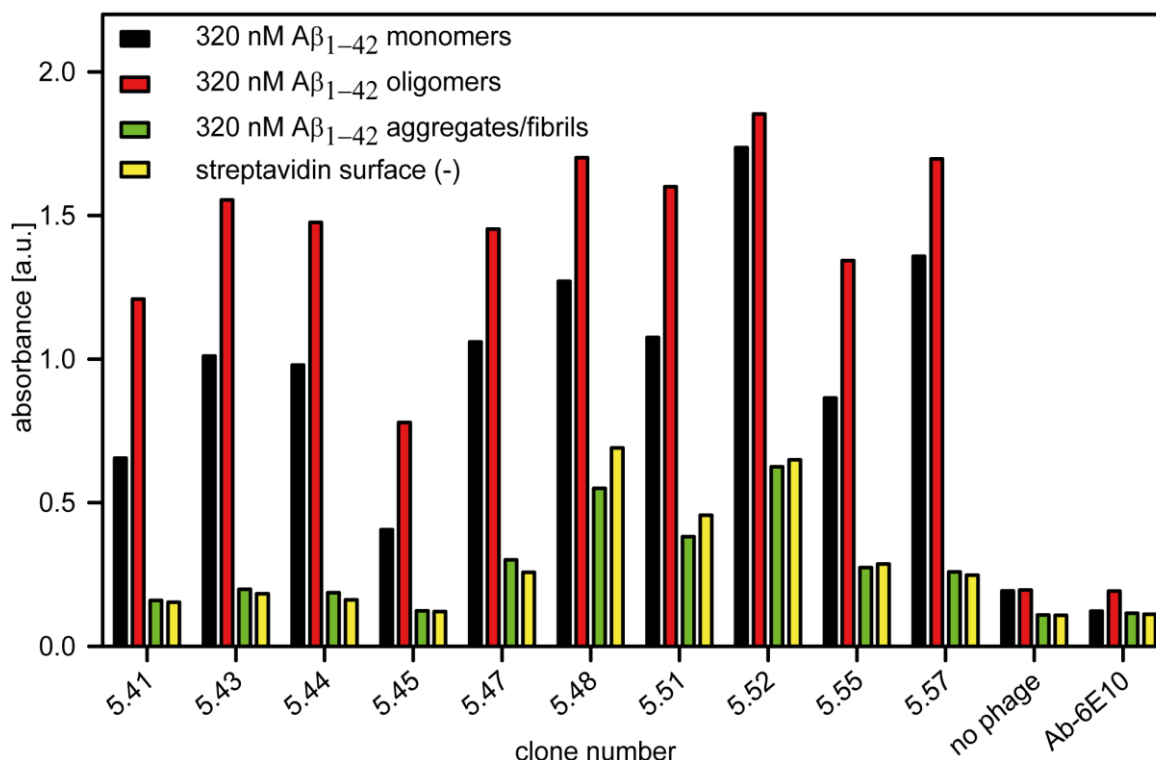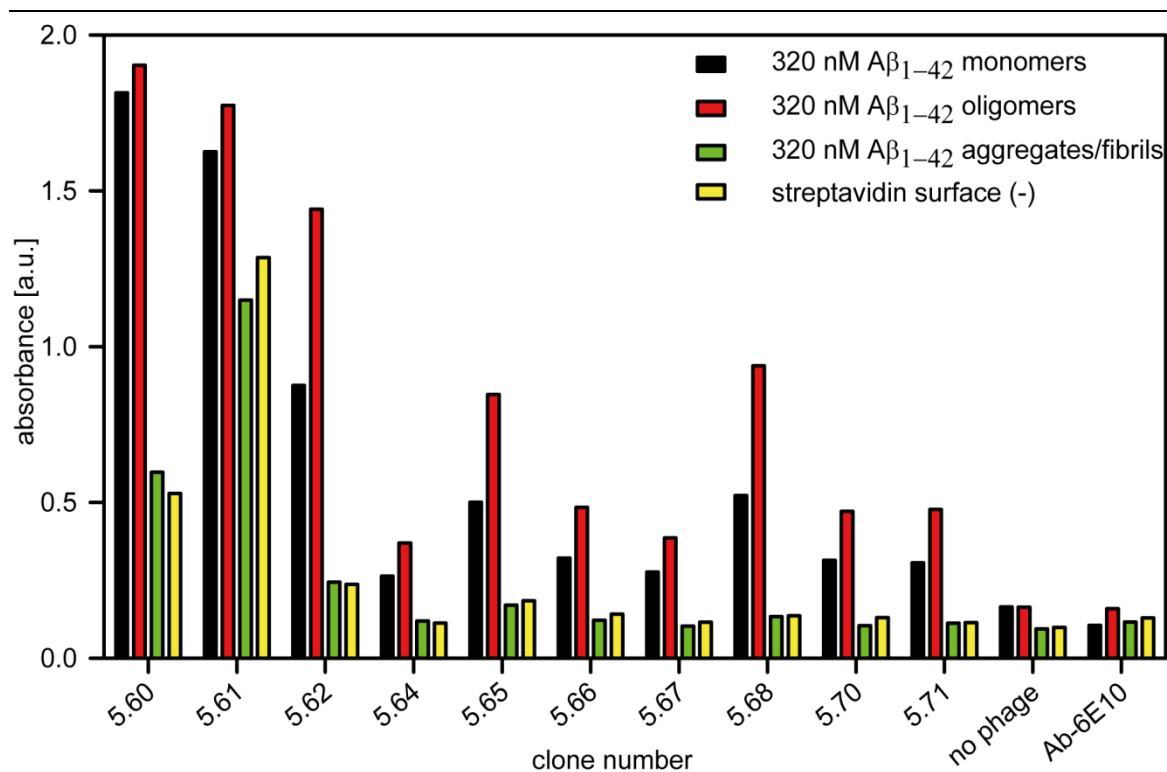
Figure 23: ELISA for relative quantification of binding affinity of single phages from mipd#5 towards different Aβ$_{1-42}$ species - plate A.

The relative binding affinity of single phages from round five (5.41 - 5.48) and six (5.51 - 5.57) to SEC-derived biotinylated Aβ$_{1-42}$ monomers and oligomers as well as DGC-derived biotinylated Aβ$_{1-42}$ fibrils was analyzed. The M13 phage-specific antibody was used for quantification of bound phages. The enzymatic transformation of substrate by antibody-conjugated HRP was measured at 450 nm. The relative absorbance values are plotted. Amplified single phage clones were added to monomeric (black), oligomeric (red) or fibrillar Aβ$_{1-42}$ (green), all immobilized at a concentration of 320 nM. The phages were also added to uncoated wells (yellow). Cross reactivity of the M13 phage-specific antibody was tested in an approach without addition of phages (no phages). In order to verify the immobilization efficiency of different Aβ$_{1-42}$ species, the Aβ-specific antibody 6E10 was added instead of the anti-M13 antibody. The HRP conjugated secondary goat anti-mouse antibody was added to these wells in order to detect bound 6E10.

On plate A, all tested clones showed an increased affinity for monomeric and oligomeric Aβ$_{1-42}$ species compared to Aβ$_{1-42}$ fibrils and uncoated wells. The relative affinity for oligomers was higher than for monomers for all clones. Clone 5.52 exhibited a high affinity for Aβ$_{1-42}$ oligomers and an almost equivalent affinity for Aβ$_{1-42}$ monomers. Clone 5.57 exhibited a considerably higher affinity for Aβ$_{1-42}$ oligomers when compared to monomer affinity. However, clone 5.57 had only a low affinity for Aβ$_{1-42}$ fibrils and uncoated wells. Since the immobilization control experiment indicated an increased immobilization of Aβ$_{1-42}$ oligomers, the affinity

of these single phage clones to monomeric Aβ$_{1-42}$ can be expected to be equivalent or even higher than to Aβ$_{1-42}$ oligomers. The clones 5.52 and 5.57 were chosen later on for synthesis of D-enantiomeric peptides.
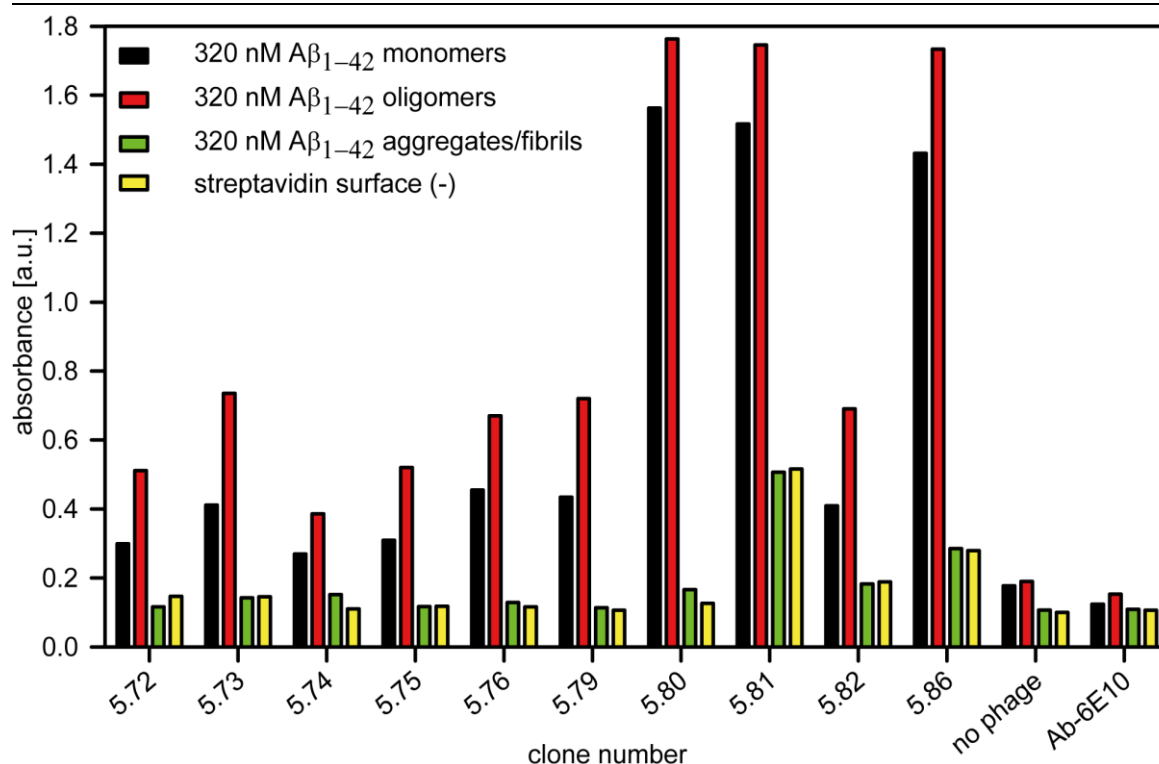

Figure 24: ELISA for relative quantification of binding affinity of single phages of mipd#5 towards different Aβ$_{1-42}$ species - plate B.

The relative binding affinity of single phages from round six (5.60 & 5.61) and five (5.63 - 5.71) to SEC-derived biotinylated Aβ$_{1-42}$ monomers and oligomers as well as DGC-derived biotinylated Aβ$_{1-42}$ fibrils was analyzed. The M13 phage-specific antibody was used for quantification of bound phages. The enzymatic transformation of substrate by antibody-conjugated HRP was measured at 450 nm. The relative absorbance values are plotted. Amplified single phage clones were added to monomeric (black), oligomeric (red) or fibrillar Aβ$_{1-42}$ (green), all immobilized at a concentration of 320 nM. The phages were also added to uncoated wells (yellow). Cross reactivity of the M13 phage-specific antibody was tested in an approach without addition of phages (no phages). In order to verify the immobilization efficiency of different Aβ$_{1-42}$ species, the Aβ-specific antibody 6E10 was added instead of the anti-M13 antibody. The HRP conjugated secondary goat anti-mouse antibody was added to these wells in order to detect bound 6E10.

From plate B, clone 5.60 was chosen for peptide synthesis, because it exhibited the highest affinity for monomeric Aβ$_{1-42}$ of all clones tested. Also, the difference between monomer and oligomer values is small. Considering the different immobilization between Aβ$_{1-42}$ species also on this plate, the affinity to monomeric

Aβ$_{1-42}$ can be expected to be equivalent or higher than to oligomers. Clone 5.61, for example, was not selected, as relative affinities to Aβ$_{1-42}$ fibrils and uncoated wells were high, compared with other clones. Clone 5.67, in contrast, had a low affinity for all species and was therefore also not chosen.

Figure 25: ELISA for relative quantification of binding affinity of single phages of mipd#5 towards different Aβ$_{1-42}$ species - plate C.

The relative binding affinity of single phages from round five (5.72 - 5.76) and six (5.79 – 5.86) to SEC-derived biotinylated Aβ$_{1-42}$ monomers and oligomers as well as DGC-derived biotinylated Aβ$_{1-42}$ fibrils was analyzed. The M13 phage-specific antibody was used for quantification of bound phages. The enzymatic transformation of substrate by antibody-conjugated HRP was measured at 450 nm. The relative absorbance values are plotted. Amplified single phage clones were added to monomeric (black), oligomeric (red) or fibrillar Aβ$_{1-42}$ (green), all immobilized at a concentration of 320 nM. The phages were also added to uncoated wells (yellow). Cross reactivity of the M13 phage-specific antibody was tested in an approach without addition of phages (no phages). In order to verify the immobilization efficiency of different Aβ$_{1-42}$ species, the Aβ-specific antibody 6E10 was added instead of the anti-M13 antibody. The HRP conjugated secondary goat anti-mouse antibody was added to these wells in order to detect bound 6E10.

From plate C the clones 5.80, 5.81 and 5.86 were selected for synthesis of D-enantiomeric peptides. All three clones exhibited high absorbance values for Aβ$_{1-42}$ oligomers and monomers. Additionally, clone 5.80 and 5.86 showed a low
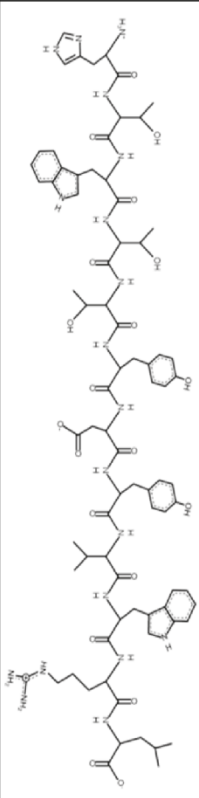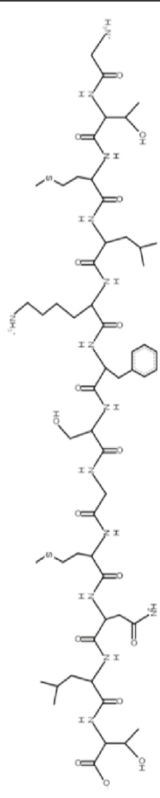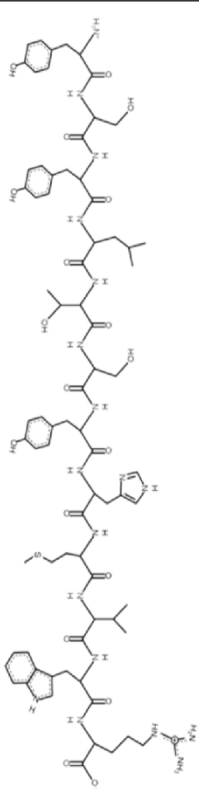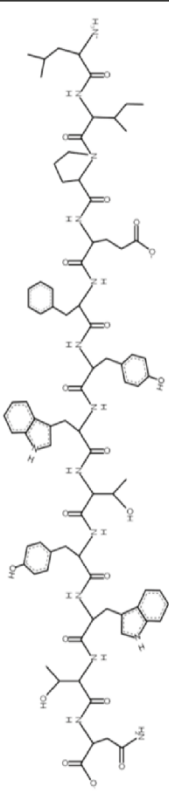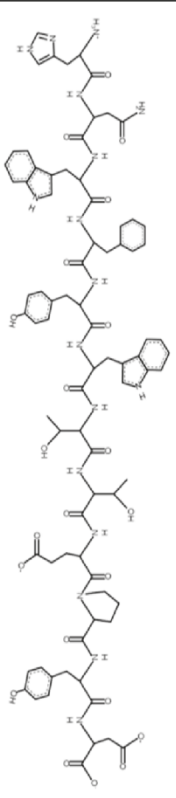
affinity to fibrils and the uncoated wells. As observed before, the immobilization of Aβ$_{1-42}$ oligomers exceeded monomer immobilization.

4.2.4 Sequencing of single phage clones

DNA sequencing results revealed that only a few clones did not have an insert sequence. No consensus sequence was found except for one sequence, HNWFYWTTEPYD, which occurred twice (clones 5.52 and 5.81). The sequence, molecular weight and chemical structure of selected clones are given in Table 12. The synthesized peptides were named MoRu1 – MoRu5, the names were derived from monomeric Aβ species, which they were selected for, and my family name Rudolph followed by a continuing number (1 to 5). MoRu3 was later on renamed Mosd1 (monomer specific d-pepdtide 1).

Table 12: Synthesized D-enantiomeric peptides (mipd#5) with characteristics.

The amino acid sequences in one letter code of the five phage displayed peptides, which were selected for synthesis, are shown below. Additionally plotted are the names, the original clone number, the chemical structure and the molecular weight in Dalton.

Clone number, panning round & name	Sequence [one letter code]	chemical structure	molecular weight [Da]
MoRu1 5.80/R6	HTWTTYDYVWRL		1640.8
MoRu2 5.57/R6	GTMLKFSGMNLT		1299.5
MoRu3 / Mosd1 5.60/R6	YSYLTSYHMVWR		1605.8
MoRu4 5.86/R6	LIPEFYWTYWTN		1632.8
MoRu5 5.52 & 5.81/R6	HNWFYWTTEPYD		1658.7

4.2.5 Amino acid composition and chemical properties of MoRu peptides

The selected peptides differ in their amino acid composition. While MoRu1 and MoRu3–5 include 33 to ~ 42 % amino acids with aromatic side chains, MoRu2 has only ~ 8 %. In contrast, 50 % of the MoRu2 amino acids have an uncharged polar character. The amino acid composition is shown in Figure 26.
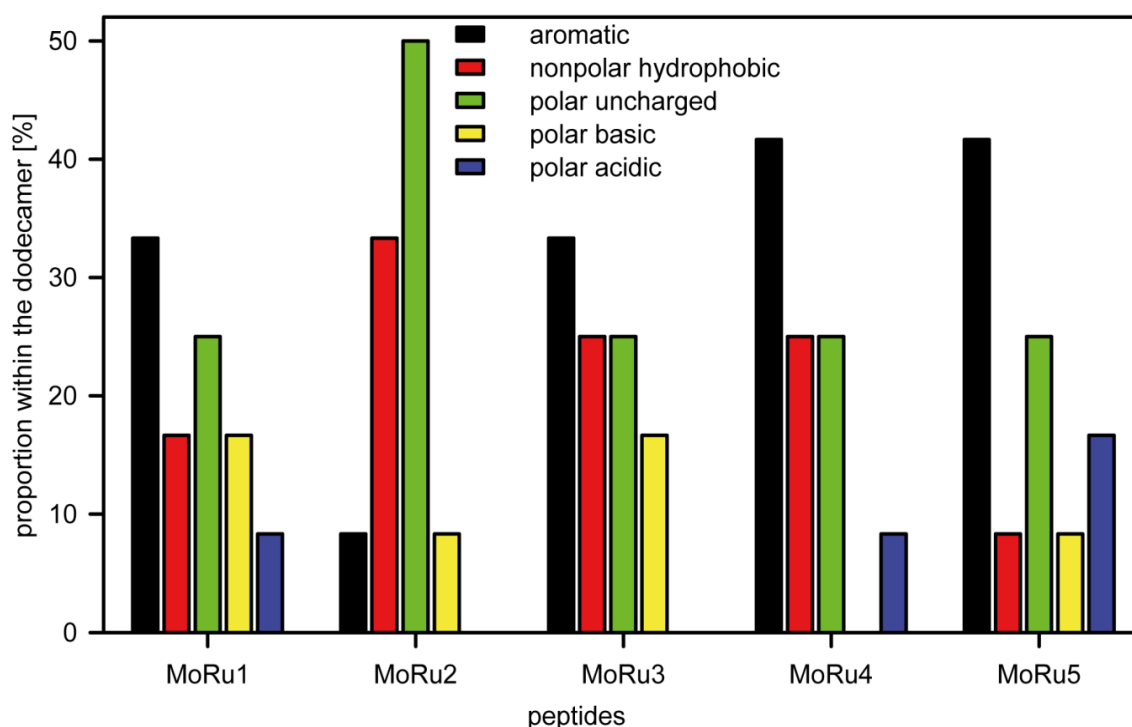
Figure 26: Amino acid composition of MoRu peptides.

The amino acids are grouped according to the chemical character of their side chains: aromatic (black), nonpolar hydrophobic (red), polar charged (green), polar basic (yellow) and polar acidic (blue). The proportions within the peptide dodecamers according to this classification are plotted.

Especially MoRu1 and MoRu3/Mosd1 share similarities. Firstly, they both include 33 % amino acids with aromatic side chains and secondly, they share the motif TXYXXVWR, with X standing for different amino acids.

The isoelectric point (pI), which is the pH value at which a molecule carries no net electrical charge, differs especially from the first three MoRu peptides (MoRu1 pI = 6.74, MoRu2 pI = 8.75, MoRu3 pI = 8.5) to MoRu4 (pI = 4) and MoRu5 (pI = 4.35). The pI is important for solubility. When the molecules have an electrical net charge of zero, they will precipitate.

4.3   Characterization of MoRu peptides

The peptides were tested for their solubility and suitability in established biological assays in order to identify candidates for further experiments.

4.3.1 Solubility of MoRu peptides

Even though MoRu1, 2 and 3 have a pI close to physiological conditions, stock solutions of 1 mM in ddH$_2$O were clear and the peptides were soluble. MoRu4 and MoRu5, however, could not be solved at a concentration of 1 mM in ddH$_2$O. For dissolution, stock solutions needed to be adjusted to 250 µM for MoRu4 and 500 µM for MoRu5, respectively.

In 1x PBS (pH 7.4) only MoRu2 dissolved completely at a concentration of 500 µM. MoRu1 precipitated and MoRu3 appeared turbid, whereas MoRu4 and MoRu5 were clear but viscous. Also mixing and sonication did not solve the problem with solubility, especially for MoRu4 and MoRu5.

In most assays which were performed, the peptides were taken from the stock solution in water and diluted in buffer to concentrations below 100 µM. Thus, solubility problems were circumvented.

4.3.2 ThT assay with MoRu peptides

ThT is a fluorescent dye, which shows a shift in absorbance when bound to β-sheets. Aβ$_{1-42}$ tends to aggregate and form fibrils, which are mainly composed of β-sheet rich structures. Thus, by adding ThT to a solution with predominantly monomeric Aβ$_{1-42}$, aggregation towards β-sheet rich Aβ$_{1-42}$ fibrils can be monitored over time. Peptide compounds, which are able to interfere with Aβ$_{1-42}$ aggregation, will alter ThT fluorescence, when compared to samples incubated without those peptides. This is due to a change in β-sheet content.

In order to perform a ThT assay, HFIP pretreated $A\beta_{1-42}$ was diluted to 10 µM in 1x PBS (pH 7.4) and mixed with 0 or 10 µM of the peptides MoRu1–5 and 10 µM ThT. Each approach was tested in sextuplicates. Peptide only (10 µM) and buffer with ThT served as controls. The measurement was performed at 37 °C in a microplate reader for 20 h with 20 min intervals.

The relative fluorescence values of the buffer were subtracted from of the sample values. Relative fluorescence values at the estimated saturation point of the $A\beta_{1-42}$ control sample were set to 100 %.

The assay was performed seven times with different outcome. Exemplary in Figures 27-31, graphs representing the development of ThT fluorescence in the presence of HFIP pretreated $A\beta_{1-42}$ and MoRu peptides are shown.
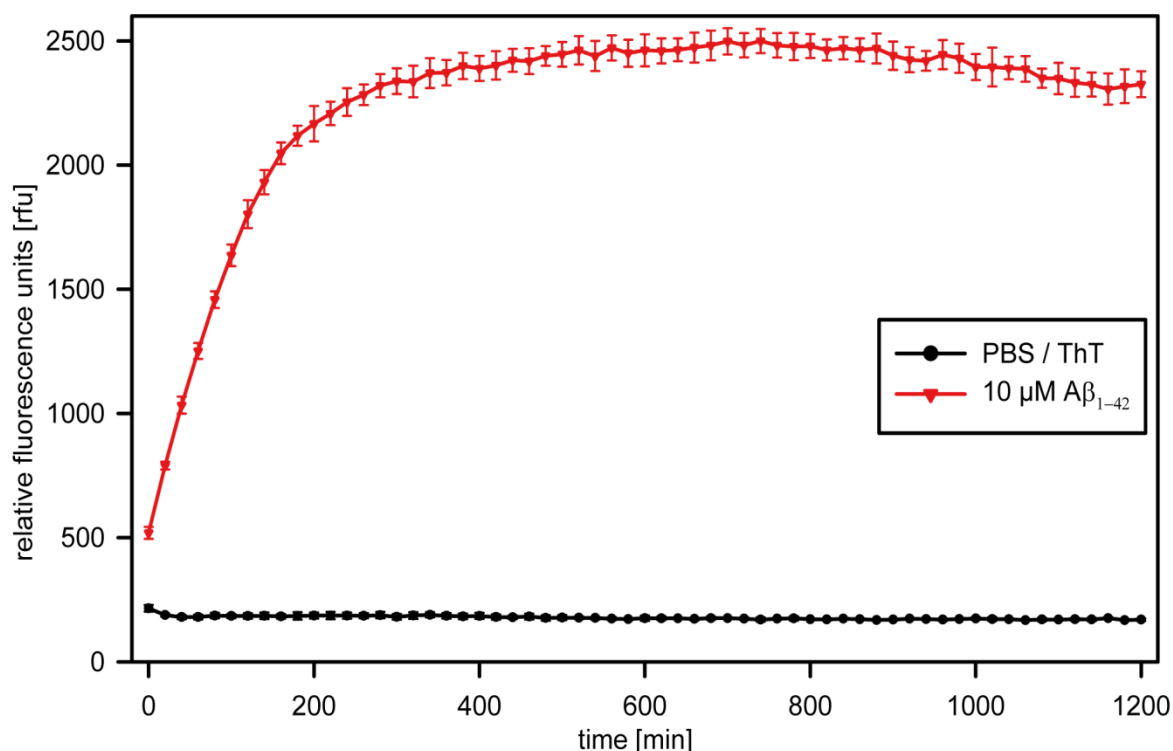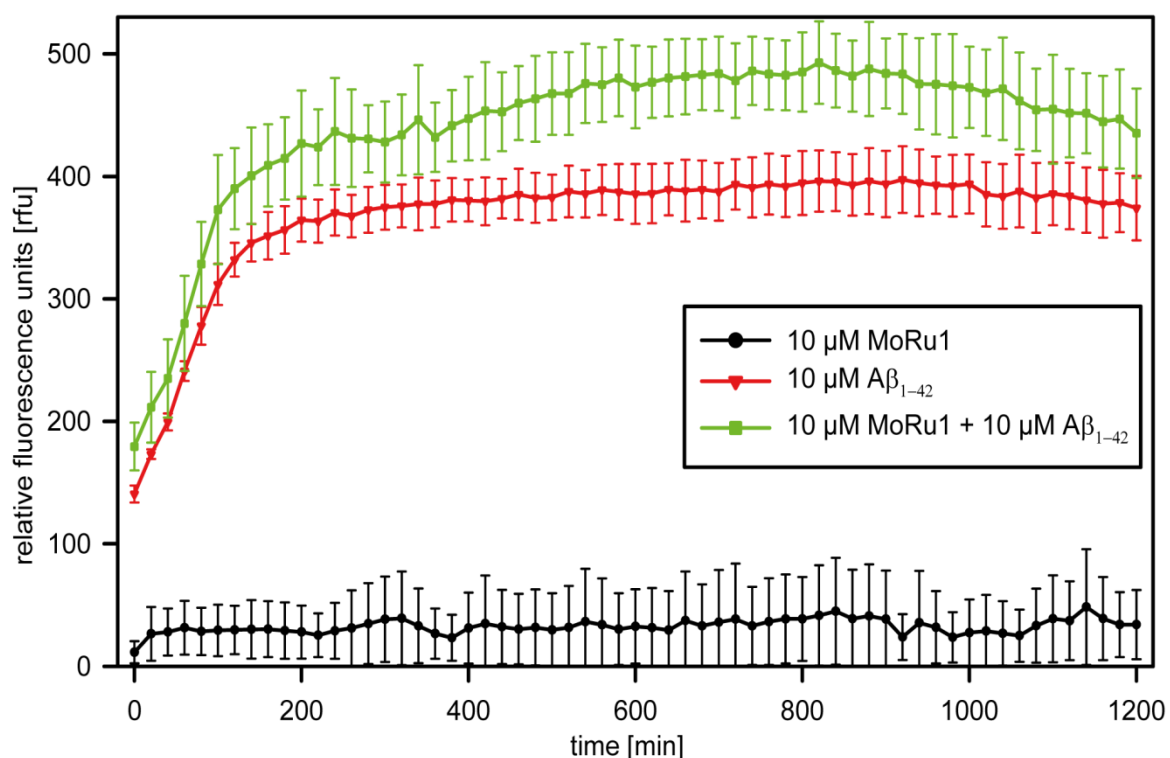

Figure 27: ThT assay - fibrilization of 10 µM $A\beta_{1-42}$.

The fibrilization of 10 µM HFIP pretreated $A\beta_{1-42}$ was analyzed. The fluorescent dye ThT was used for the quantification of β-sheet content. The fluorescence of ThT was measured at 495 nm and the relative fluorescence values were plotted against the time. The fluorescence signals of the buffer (black) and 10 µM $A\beta_{1-42}$ (red) are shown.

Figure 27 shows a typical $A\beta_{1-42}$ aggregation curve in presence of ThT. The buffer components did not increase the relative fluorescence over time. The relative

fluorescence of the Aβ$_{1\text{-}42}$ sample increased logarithmically for approximately 7 h until it reached saturation. During aggregation and conversion of monomeric Aβ$_{1\text{-}42}$ species towards fibrils the content of β-sheets increases. Therefore, ThT binds more β-sheet content and the ThT fluorescence signal increases proportionally to the β-sheet content.

Figure 28: ThT assay - influence of equimolar concentration of MoRu1 on Aβ$_{1\text{-}42}$ fibrilization.

The influence of 10 µM MoRu1 on fibrilization of 10 µM HFIP pretreated Aβ$_{1\text{-}42}$ was analyzed. The fluorescent dye ThT was used for the quantification of β-sheet content. The fluorescence of ThT was measured at 495 nm and the relative fluorescence values were plotted against the time. The fluorescence signals of 10 µM MoRu1 (black), 10 µM Aβ$_{1\text{-}42}$ (red) and equimolar concentrations of MoRu1 and Aβ$_{1\text{-}42}$ (green) are shown.

Figure 28 shows exemplarily, how MoRu1 interferes with Aβ$_{1\text{-}42}$ fibrilization. MoRu1 acts as a fibrilization accelerator. Coincubation of Aβ$_{1\text{-}42}$ and MoRu1 leads to a faster increase in relative fluorescence units. MoRu1 has a direct influence on Aβ$_{1\text{-}42}$ fibrilization, since it shows only limited alterations in fluorescence and low fluorescence values over the whole time when incubated without Aβ$_{1\text{-}42}$.
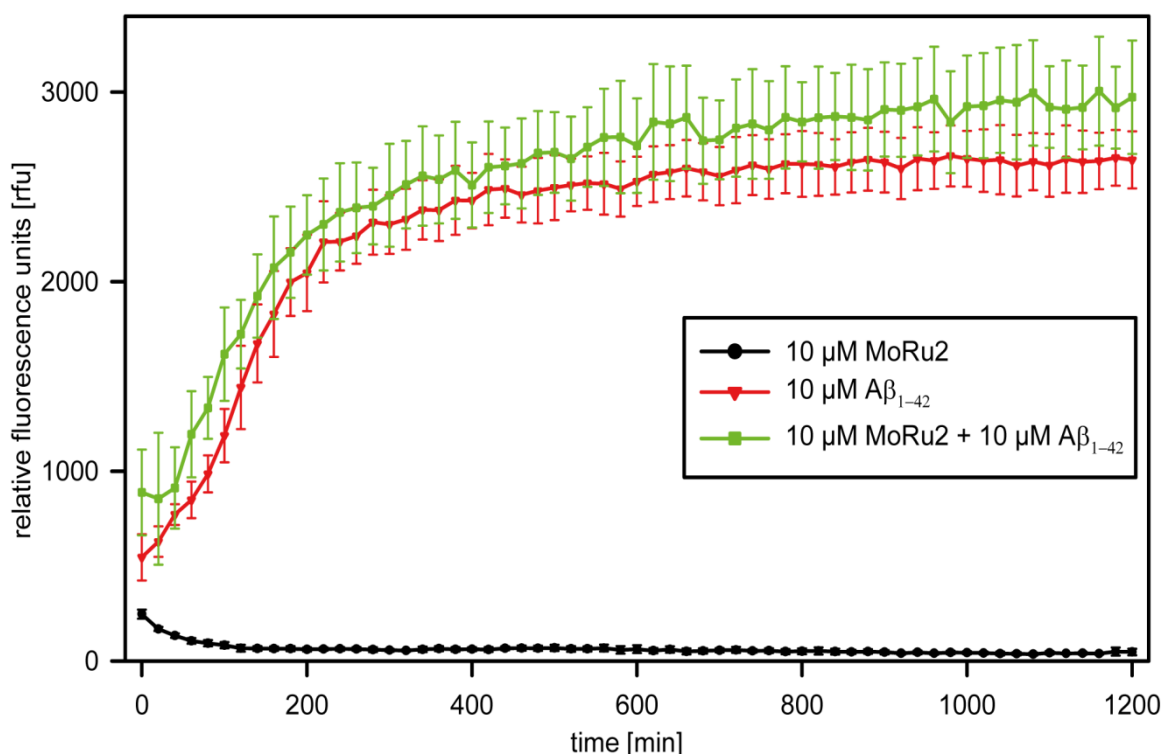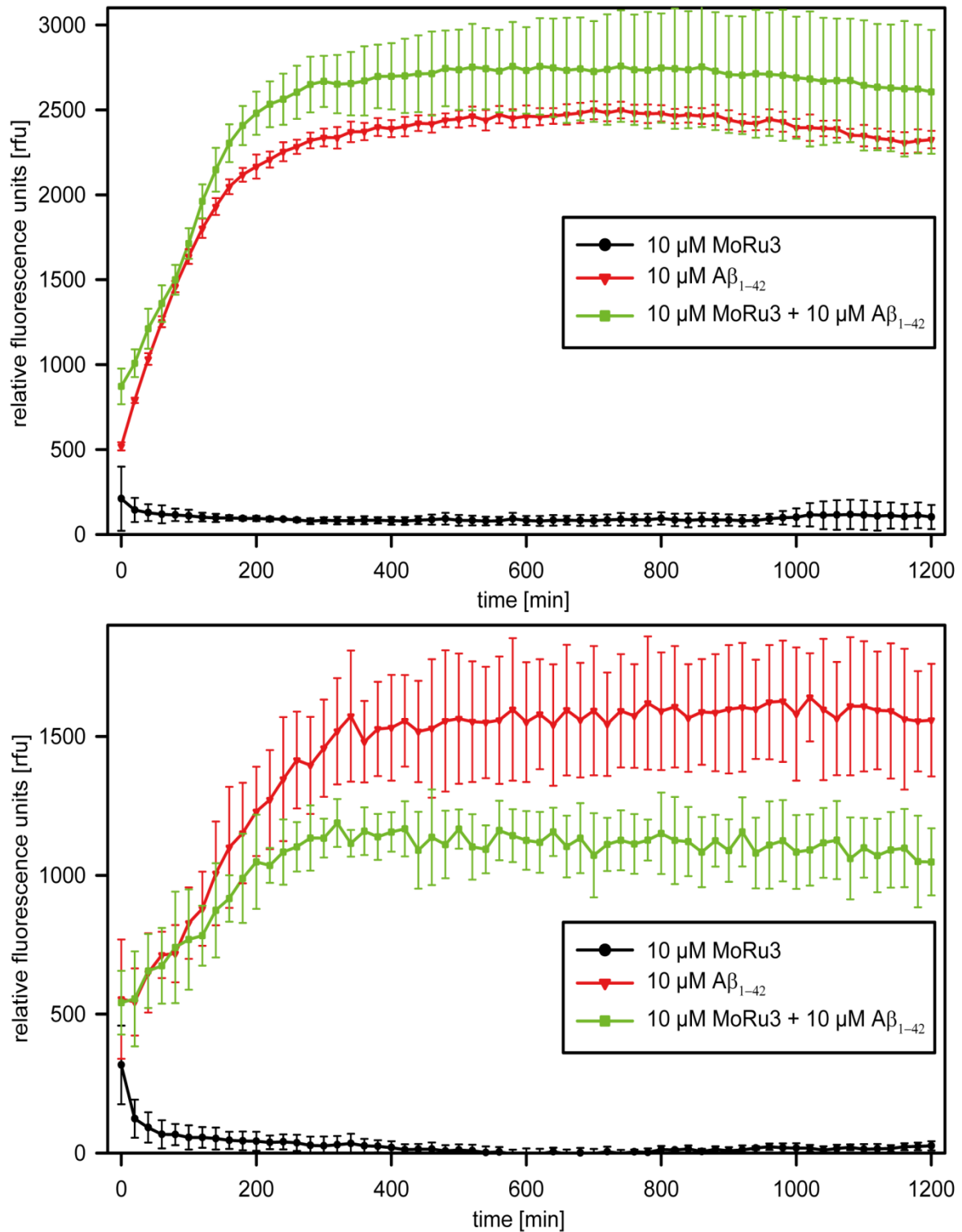
Figure 29: ThT assay - influence of equimolar concentration of MoRu2 on A$\beta_{1\text{-}42}$ fibrilization.

The influence of 10 µM MoRu2 on fibrilization of 10 µM HFIP pretreated A$\beta_{1\text{-}42}$ was analyzed. The fluorescent dye ThT was used for the quantification of β-sheet content. The fluorescence of ThT was measured at 495 nm and the relative fluorescence values were plotted against the time. The fluorescence signals of 10 µM MoRu2 (black), 10 µM A$\beta_{1\text{-}42}$ (red) and equimolar concentrations of MoRu2 and A$\beta_{1\text{-}42}$ (green) are shown.

The influence of MoRu2 on A$\beta_{1\text{-}42}$ aggregation varied a lot. The graph, shown in Figure 29 displays an average result. Other trials with MoRu2 coincubated in equimolar amounts with HFIP pretreated A$\beta_{1\text{-}42}$ showed either a higher increase in fluorescence or decreased fluorescence signals. MoRu2 incubated without A$\beta_{1\text{-}42}$ showed nearly no relative fluorescence over the whole measurement.

MoRu3 has a contradictory impact on A$\beta_{1\text{-}42}$ aggregation as seen in the change of relative fluorescence when added in equimolar amounts to HFIP pretreated A$\beta_{1\text{-}42}$. In Figure 30, two ThT fluorescence time curves are displayed. On the one hand, MoRu3 accelerated and increased ThT fluorescence compared with the sample including only A$\beta_{1\text{-}42}$. On the other hand, MoRu3 decreased fluorescence.

Figure 30: ThT assay - influence of equimolar concentration of MoRu3 on Aβ$_{1-42}$ fibrilization.

The influence of 10 µM MoRu3 on fibrilization of 10 µM HFIP pretreated Aβ$_{1-42}$ was analyzed. The fluorescent dye ThT was used for the quantification of β-sheet content. The fluorescence of ThT was measured at 495 nm and the relative fluorescence values were plotted against the time. The fluorescence signals of 10 µM MoRu3 (black), 10 µM Aβ$_{1-42}$ (red) and equimolar concentrations of MoRu3 and Aβ$_{1-42}$ (green) are shown in both graphs.

MoRu4 and MoRu5 exhibited the same characteristics as MoRu3. In some ThT assays the peptides increased the relative fluorescence. Yet in other trials, the relative fluorescence was decreased (data not shown).

$A\beta_{1-42}$ aggregation shows a logarithmic behavior in the beginning before it enters a stationary phase. The relative fluorescence value at the point in time when this change happens was set to 100 %. This was done in order to analyze the impact of the different compounds at a specific point in time. The percentaged relative fluorescence values of $A\beta_{1-42}$ samples coincubated with the different peptides were calculated based on the 100 % at this point in time. In Figure 31 the average percentages from seven assays are plotted with standard deviation. The averaged saturation point was reached 8 h after the beginning of the experiment. MoRu1 and MoRu2 increased the fluorescence signal to 119 % and 109 %, respectively. Both compounds, therefore, increased the amount of β-sheet content in the sample. MoRu4 with 94 % and MoRu5 with 99 % relative fluorescence units, compared to the separately incubated $A\beta_{1-42}$ (100 %), slightly decreased the production of β-sheet content. MoRu3 led to the strongest decrease of β-sheet content when coincubated with $A\beta_{1-42}$. The relative fluorescence signal exhibited 86 %. As all peptides exhibited only low fluorescence when incubated alone, the effects must be attributed to an interaction with $A\beta_{1-42}$.
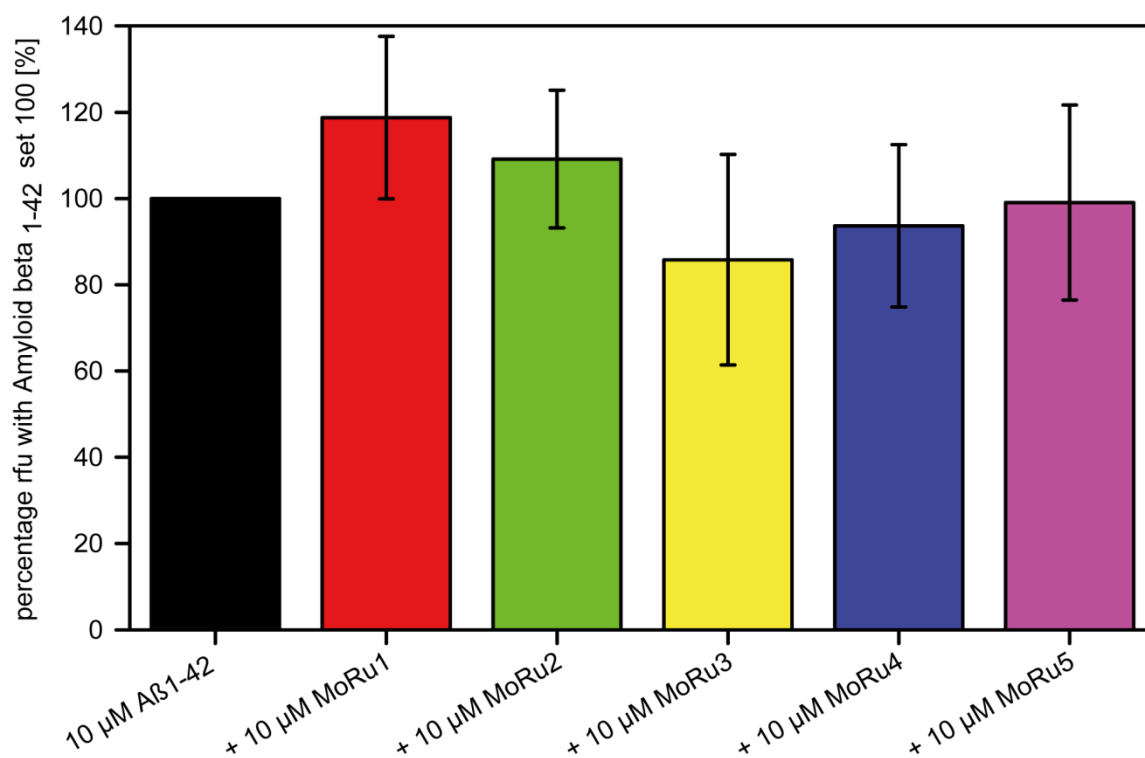
Figure 31: ThT assay - overview of peptide influence on Aβ$_{1-42}$ aggregation.

The averaged percentaged relative fluorescence values of seven independent ThT assays are shown. The relative fluorescence of HFIP pretreated Aβ$_{1-42}$ at the time of the conversion from a logarithmic aggregation phase to a stationary phase was set to 100 %. The influence on the relative fluorescence signal by coincubation with equimolar amounts of MoRu1 (red), MoRu2 (green), MoRu3 (yellow), MoRu 4 (purple) and MoRu5 (magenta) is plotted.

4.3.3 Modulation of Aβ$_{1-42}$ distribution by MoRu peptides

In order to analyze the impact of the selected D-enantiomeric peptides on a variety of preformed Aβ$_{1-42}$ species, the following method was used. Aβ$_{1-42}$ (80 μM) was incubated for 4.5 h at 600 rpm and 21 °C. This incubation method leads to a broad range of species, ranging from monomers and various oligomeric species to HMW aggregates, protofibrils and fibrils. MoRu1, 2, 3 and 5 were added were added at a concentration of 40 μM and coincubated for additional 40 min. Afterwards, the samples were separated via DGC. 14 fractions were taken and analyzed via SDS-PAGE and silver staining. MoRu4 was not tested because of dissolution problems.

$A\beta_{1-42}$ incubated alone is present in all fractions of the gradient (Figure 32; first panel). The largest amounts of $A\beta_{1-42}$ were detected in the first fractions, displaying monomers and low molecular weight oligomers. Also in fractions ten to twelve, which correlate with $A\beta_{1-42}$ protofibrils, fibrils and HMW aggregates, strong signals from $A\beta_{1-42}$ were detected. MoRu1 reduced $A\beta_{1-42}$ content in fractions two to eight and led to an increase of $A\beta_{1-42}$ in fraction 13. Fraction one, ten and eleven were not affected (Figure 32; second panel). MoRu2 exhibited similar characteristics, but reduced $A\beta_{1-42}$ in the first fractions and led to an elevated amount of $A\beta_{1-42}$ in fraction 14 instead of fraction 13, as seen as a stronger band on the SDS gel (Figure 32; third panel). MoRu3 changed $A\beta_{1-42}$ distribution drastically. No $A\beta_{1-42}$ was detected from fraction one to nine. Moreover, there was a reduced amount of $A\beta_{1-42}$ in fractions ten and eleven and an increased $A\beta_{1-42}$ amount in the last fractions (12 to 14) (Figure 32; fourth panel). The peptide MoRu5 showed another pattern. The peptide was not able to modulate $A\beta_{1-42}$ distribution in this concentration and incubation time. $A\beta_{1-42}$ was present in all fractions, though slightly lower amounts were detected in fraction one to nine, when compared to $A\beta_{1-42}$ control (Figure 32; fifth panel).
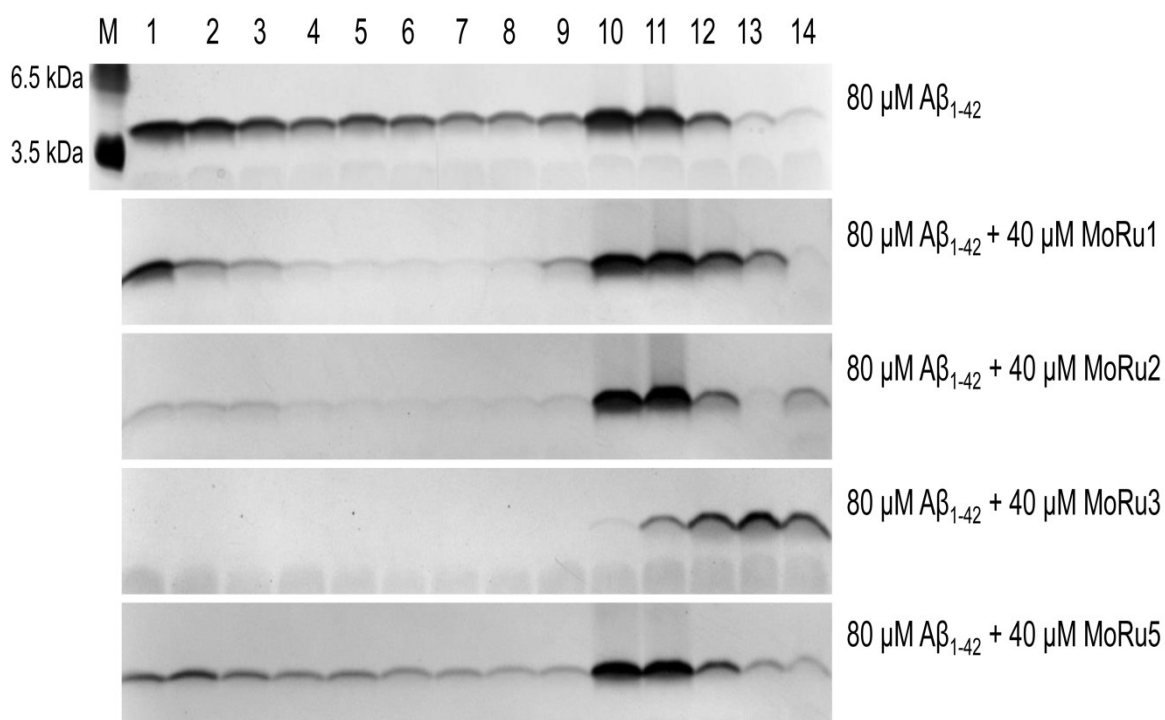
Figure 32: Influence of MoRu peptides on Aβ$_{1-42}$ distribution in an iodixanol gradient.

Silver stained Tris-tricine SDS gels are shown. The protein marker shown in the top panel represents 6.5 and 3.5 kDa, thus the bands within the loaded fractions display Aβ$_{1-42}$ (4.5 kDa). From top to bottom preincubated Aβ$_{1-42}$ without peptide, with MoRu1, MoRu2, MoRu3 and MoRu5 are shown. After preincubation of Aβ$_{1-42}$ (80 µM), the samples were coincubated afterwards for 40 min without and with 40 µM MoRu1/2/3/5. After incubation and DGC, 14 fractions were collected, separated via Tris-tricine SDS-PAGE and silver stained.

In order to analyze the concentration of iodixanol in the gradient stock solutions and the fractions after centrifugation, the relative density was tested with an Abbé refractometer. The freshly prepared iodixanol solutions corresponded with the calculated solutions as shown in Figure 33.

The fractions after centrifugation exhibited a broad range of relative density ranging from 2.4 % Brix in fraction F1 up to 54.5 % Brix in fraction F14 (Figure 33).
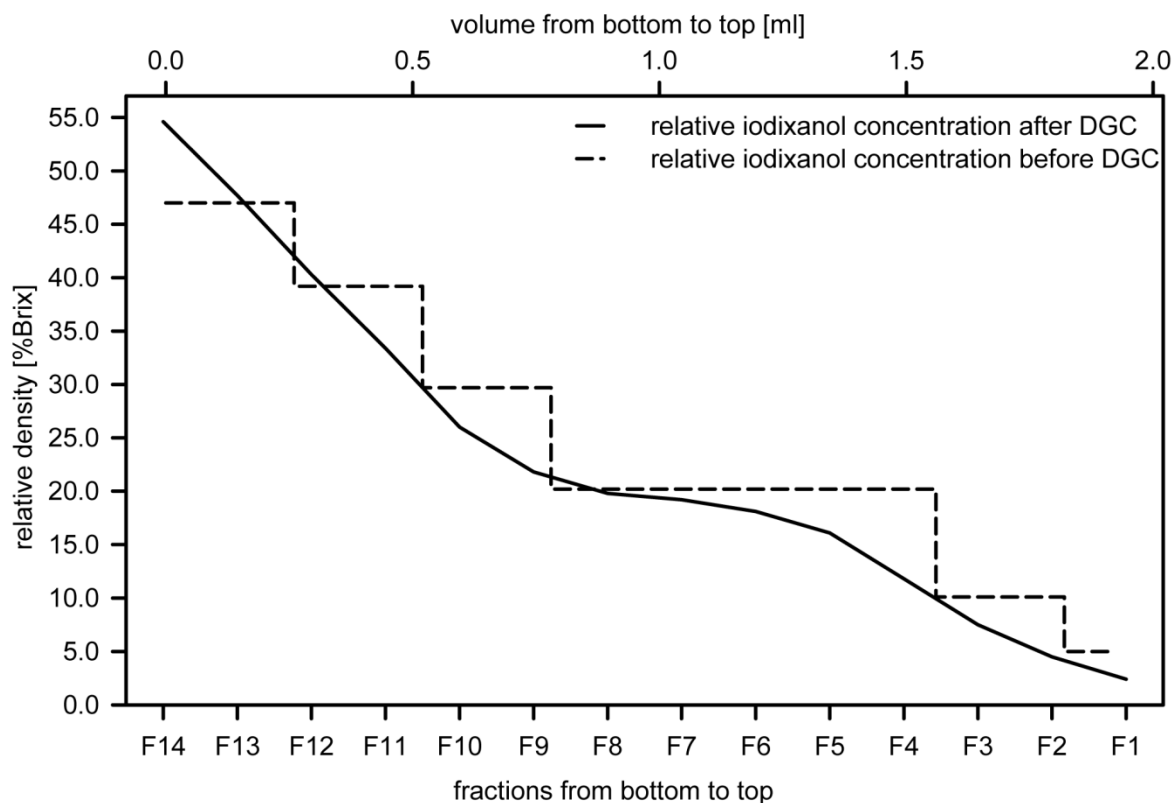
Figure 33: Relative density of iodixanol solutions before and after DGC.

The relative density of iodixanol solutions in 10 mM NaPi (pH 7.4) prior to centrifugation (dashed line) and after centrifugation (solid line) were plotted against the volume in the centrifugation tube and the obtained fractions, respectively.
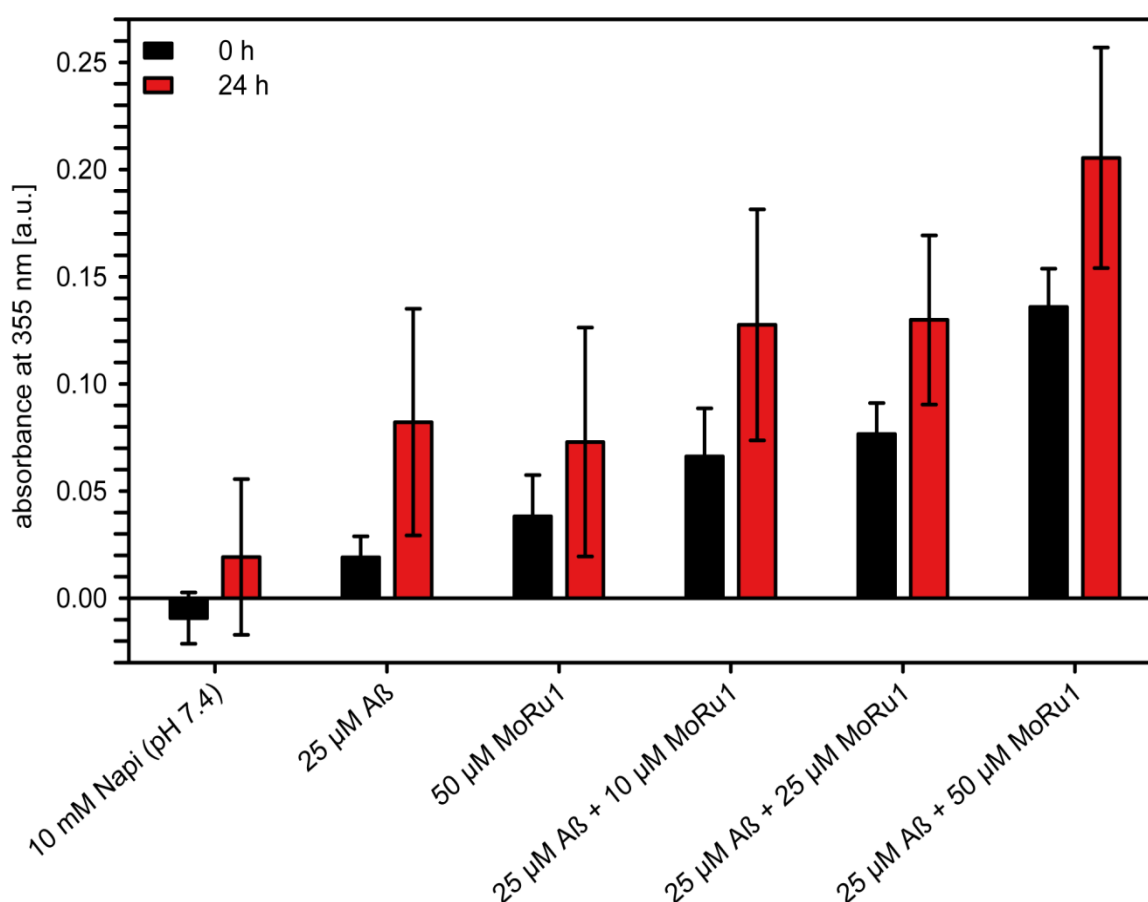
4.3.4 Turbidity assay

In the latter chapter (4.3.3), the distribution modulation assay showed that after 40 min coincubation of $A\beta_{1-42}$ and MoRu3 larger particles had formed (Figure 32, panel 3). In order to verify this observation, a turbidity assay was performed as an additional measure of large particles.

HFIP pretreated $A\beta_{1-42}$ (25 µM) was dissolved in 10 mM NaPi (pH 7.4), containing 0/10/25/50 µM peptide. Samples were mixed and measured at 355 nm directly after preparation (t_0 = 0 h) and after 24 h of incubation at 21 °C (t_1 = 24 h).

The buffer showed no absorbance at time point t_0 and the same was observed after 24 h incubation. Thus, the buffer can be considered particle free. The 25 µM $A\beta_{1-42}$ sample revealed an increase in absorbance signal after 24 h. However, the

values were below 0.1 absorbance units, and thus have to be considered to be below the noise threshold of the spectrophotometer. For all tested MoRu peptides, the controls (buffer and 25 µM Aβ$_{1-42}$) were the same, therefore, both samples will not be discussed further (Figure 34).

The peptide MoRu1 did not lead to values above 0.1 absorbance units. When MoRu1 was incubated with Aβ$_{1-42}$, a concentration dependent increase in absorbance was determined only from 25 to 50 µM MoRu1, but not from 10 to 25 µM. Over time, the absorbance values increased in all measured concentrations up to 0.2 absorbance units (Figure 34).

Figure 34: Turbidity assay - influence of MoRu1 on Aβ$_{1-42}$ aggregate development.

The absorbance units at 355 nm at t_0 0 h (black) and t_1 = 24 h (red) are plotted against the different samples. HFIP pretreated Aβ$_{1-42}$ (25 µM) was dissolved in 10 mM NaPi (pH 7.4) with different concentrations of MoRu1 (0/10/25/50 µM). The samples were mixed and directly measured six times with a spectrophotometer. The samples were incubated at RT for 24 h and measured again for six times. The bars represent mean values of three independent assays with standard errors.

The highest concentration of MoRu2 incubated alone did not lead to values > 0.1 absorbance units, indicating that no particles developed over the 24 h incubation period. All MoRu2 concentrations coincubated with $A\beta_{1-42}$ led to a time dependent increase up to 0.24 absorbance units. However, this increase in absorbance was not concentration dependent (Figure 35).
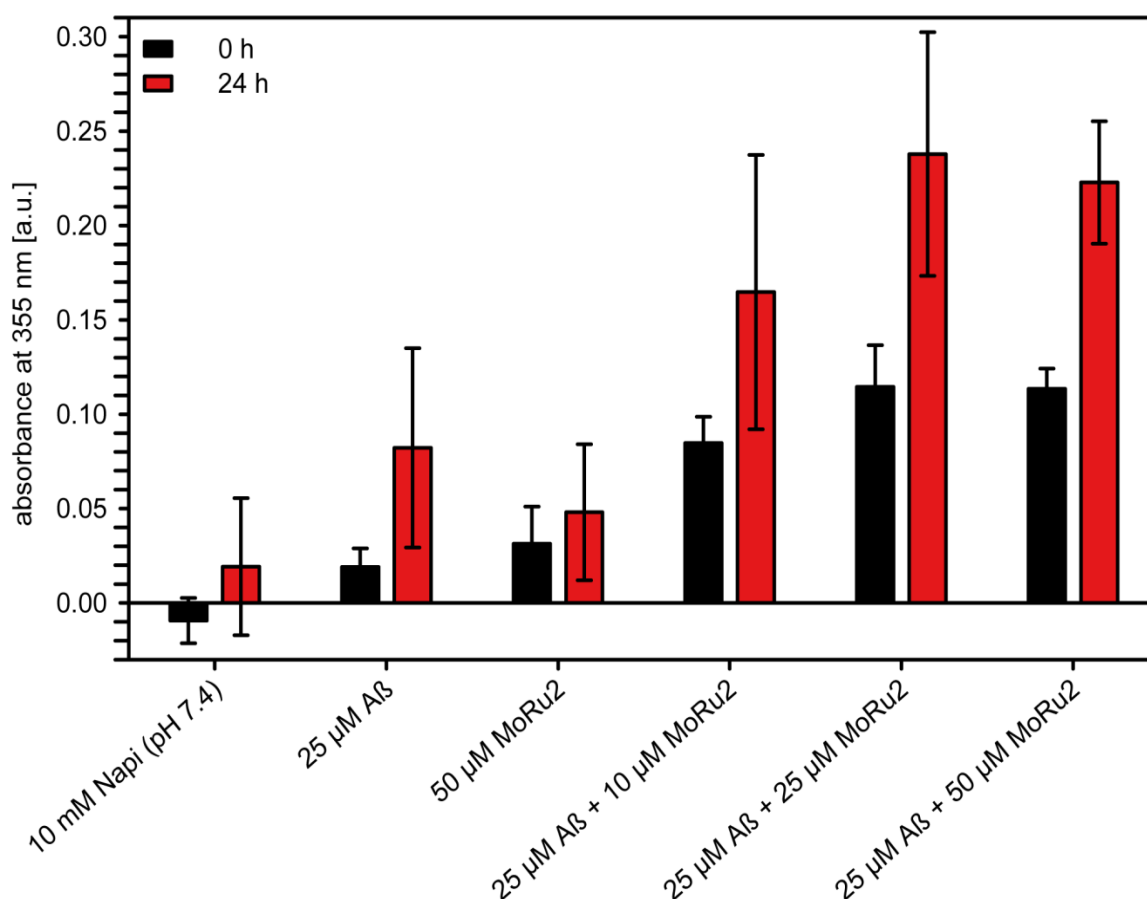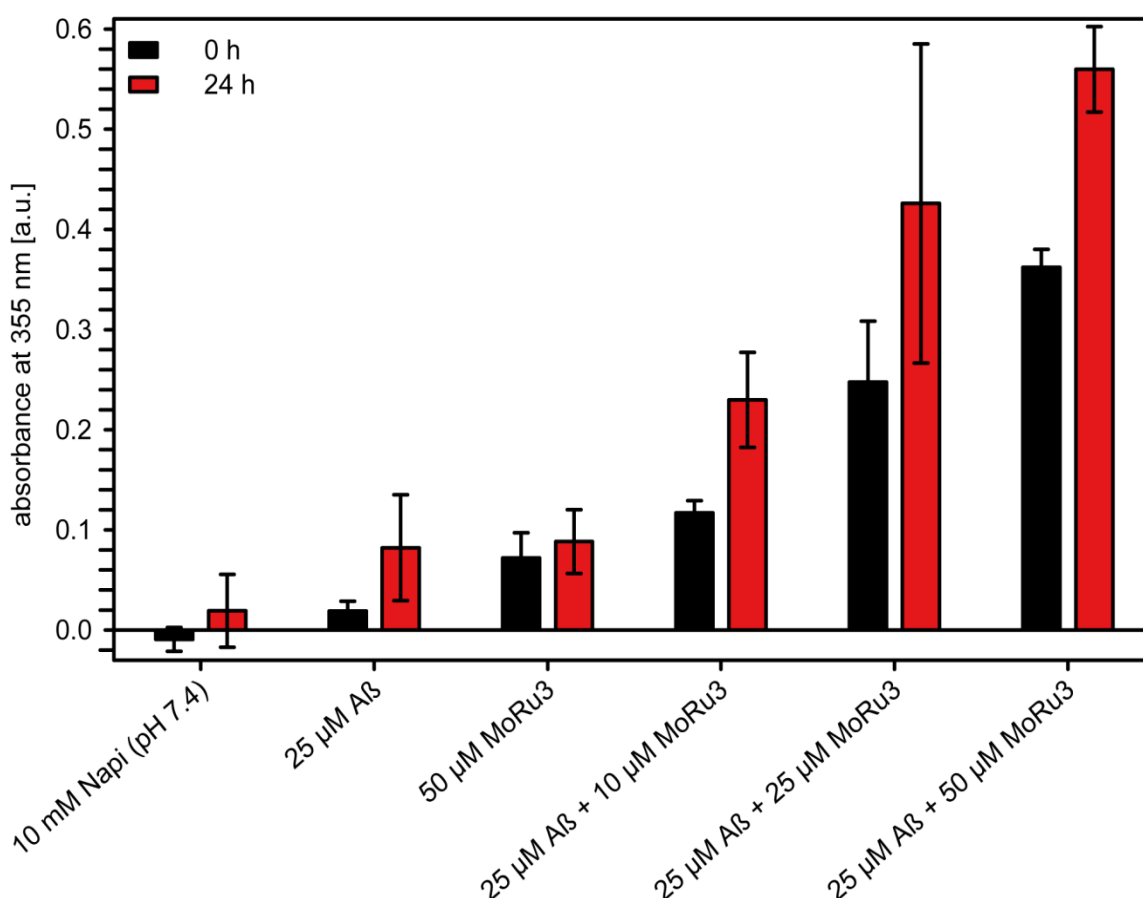

Figure 35: Turbidity assay - influence of MoRu2 on $A\beta_{1-42}$ aggregate development.

The absorbance units at 355 nm at t_0 0 h (black) and t_1 = 24 h (red) are plotted against the different samples. HFIP pretreated $A\beta_{1-42}$ (25 µM) was dissolved in 10 mM NaPi (pH 7.4) with different concentrations of MoRu2 (0/10/25/50 µM). The samples were mixed and directly measured six times with a spectrophotometer. The samples were incubated at RT for 24 h and measured again for six times. The bars represent mean values of three independent assays with standard errors.

The peptide MoRu3, incubated alone at the highest concentration used for coincubation, did not reach values above 0.1 absorbance units after 24 h. Coincubation of MoRu3 with $A\beta_{1-42}$ led to a time and concentration dependent increase in absorbance, indicating a development of large particles over time and with increasing concentration. The values of MoRu3 and $A\beta_{1-42}$ reached 0.55

absorbance units, which are the highest values obtained in this assay. Thus, particle development is clearly shown (Figure 36). The turbidity assay supports the results observed during the Aβ_{1-42} distribution modulation assay for MoRu3.

Figure 36: Turbidity assay - influence of MoRu3 on Aβ_{1-42} aggregate development.

The absorbance units at 355 nm at t_0 0 h (black) and t_1 = 24 h (red) are plotted against the different samples. HFIP pretreated Aβ_{1-42} (25 µM) was dissolved in 10 mM NaPi (pH 7.4) with different concentrations of MoRu3 (0/10/25/50 µM). The samples were mixed and directly measured six times with a spectrophotometer. The samples were incubated at RT for 24 h and measured again for six times. The bars represent mean values of three independent assays with standard errors

Incubation of MoRu4 or MoRu5 resulted in high absorbance values at both timepoints. The peptides are essentially insoluble and aggregate, thus explaining the results of the turbidity assay. Nonetheless, MoRu4 coincubated with Aβ_{1-42} exhibited a time and concentration dependent absorbance increase. However, the large standard errors affect the ability to evaluate whether MoRu4 faciliated Aβ_{1-42} aggregate formation (Figure 37, top panel). The results for MoRu5 coincubated with Aβ_{1-42} correlate with the results of MoRu4 (Figure 37, bottom panel).
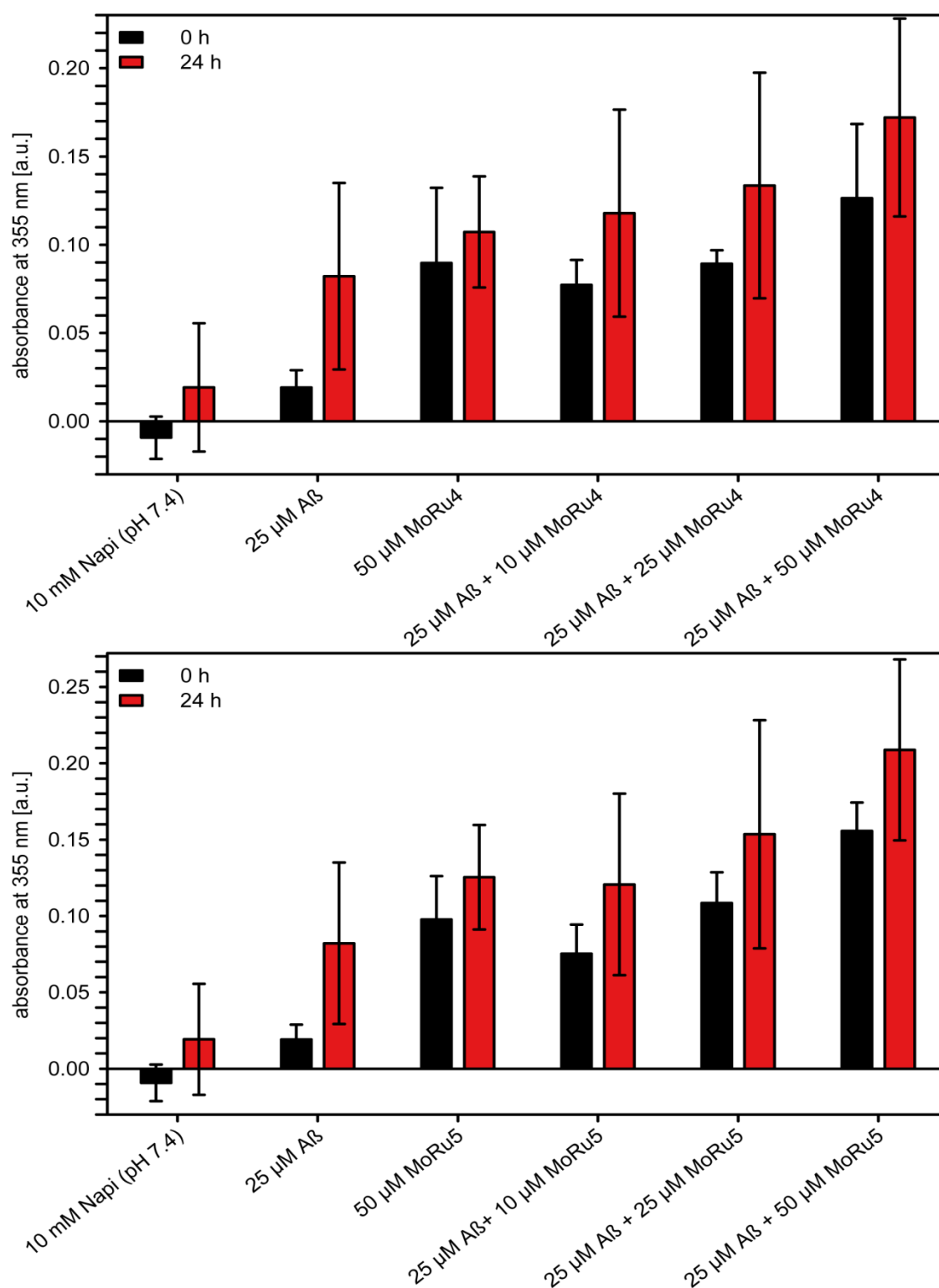
Figure 37: Turbidity assay - influence of MoRu4/5 on Aβ$_{1-42}$ aggregate development.

The absorbance units at 355 nm at t_0 0 h (black) and t_1 = 24 h (red) are plotted against the different samples. HFIP pretreated Aβ$_{1-42}$ (25 µM) was dissolved in 10 mM NaPi (pH 7.4) with different concentrations (0/10/25/50 µM) of MoRu4 (top panel) or MoRu5 (bottom panel). The samples were mixed and directly measured six times with a spectrophotometer. The samples were incubated at RT for 24 h and measured again for six times. The bars represent mean values of three independent assays with standard errors.

4.4 Characterization of MoRu3

The D-enantiomeric peptide MoRu3 shows several beneficial features compared to the other MoRu peptides. This led to the decision to focus on a further characterization of MoRu3.

Firstly, the corresponding phage clone of MoRu3, which was clone 5.60 from panning round 6 of mipd#5, scored one of the highest values for monomer affinity in addition to one of the lowest differences between monomer and oligomer binding values during single phage ELISA (Figure 24). Secondly, in contrast to the remaining MoRu peptides, MoRu3 notably reduced ThT fluorescence when incubated with $A\beta_{1-42}$. This result indicates an interaction with $A\beta_{1-42}$, for example by occupation or concealment of ThT binding sites of $A\beta_{1-42}$ by MoRu3 (Figure 30). Thirdly, MoRu3 was able to abolish $A\beta_{1-42}$ oligomers in a broad range of $A\beta_{1-42}$ species and led to an elevated amount of HMW aggregates as shown by density centrifugation, subsequently followed by SDS-PAGE and silver staining (Figure 32). The other MoRu peptides showed a related, yet, weaker effect on $A\beta_{1-42}$ size distribution, except for MoRu5, which had no effect on $A\beta_{1-42}$ size distribution. Moreover, a strong increase of turbidity in $A\beta_{1-42}$ samples coincubated with MoRu3 showed the formation of large $A\beta_{1-42}$ aggregates (Figure 36). Finally, dissolution of MoRu1, 2 and 3 appeared possible, whereas MoRu4 and MoRu5 exhibit a weak solubility, which makes them not suitable for further applications and experiments.

4.4.1 Modulation of $A\beta_{1-42}$ distribution by MoRu3

As shown before, MoRu3 has an extensive impact on $A\beta_{1-42}$ particle distribution, when coincubated in a molar ratio of 1:2 (40:80 µM; MoRu3:$A\beta_{1-42}$). In order to analyze, whether this effect is concentration dependent and different ratios change the $A\beta_{1-42}$ distribution, MoRu3 was analyzed again. Additionally to the qualitative analysis by SDS-PAGE and silver staining, a quantitative approach with RP-HPLC was performed in order to determine the $A\beta_{1-42}$ concentrations in every fraction.

The method was performed as already described in chapter 4.3.3 but with different concentrations of MoRu3. Preincubated A$\beta_{1\text{-}42}$ (80 µM) was coincubated with increasing concentrations of MoRu3 (0/10/20/40/80 µM) and afterwards separated by DGC. DGC fractions were analyzed by SDS-PAGE and RP-HPLC. The experiments were all performed in triplicates. For RP-HPLC the mean value with standard deviation is plotted.

80 µM A$\beta_{1\text{-}42}$ incubated alone exhibited a broad distribution of A$\beta_{1\text{-}42}$ from fraction 1 to 12 (Figure 38; panel 1). Thus, A$\beta_{1\text{-}42}$ preincubation led to a broad range of different sized species.

Addition of increasing concentrations of MoRu3 shifted the A$\beta_{1\text{-}42}$ distribution from low density fractions to the fractions containing species with higher density and therefore larger in size. This size distribution modulation by MoRu3 was concentration dependent. Particularly, 10 µM MoRu3 had only a weak influence on Aβ species distribution. Yet, this concentration was already sufficient to decrease the A$\beta_{1\text{-}42}$ amount in the first fractions, corresponding to monomers and oligomers and increase the amount of A$\beta_{1\text{-}42}$ in fractions 12 and 13 (Figure 38; panel 2).

Incubation of A$\beta_{1\text{-}42}$ with 20 µM MoRu3 clearly shifted A$\beta_{1\text{-}42}$ towards fractions 12 and 13. At the same time, it reduced the A$\beta_{1\text{-}42}$ amount in earlier fractions, especially fractions 4 to 7 and 9 to 10 (Figure 38; panel 3).

Addition of 40 µM MoRu3 led to a shift of A$\beta_{1\text{-}42}$ species towards HMW aggregates and fibrils in fractions 11 to 13. In parallel, the detected bands in fractions 1 to 9 decreased (Figure 38; panel 4).

At an equimolar ratio, MoRu3 tremendously changed A$\beta_{1\text{-}42}$ size distribution. No A$\beta_{1\text{-}42}$ was detected in fractions 1 to 10 and only a very weak band was observed in fraction 11. In the last fractions (12 to 14) the A$\beta_{1\text{-}42}$ band was enhanced. Thus, all small A$\beta_{1\text{-}42}$ particles like monomers and different oligomer species were converted into HMW aggregates and/or fibrils (Figure 38; panel 5).
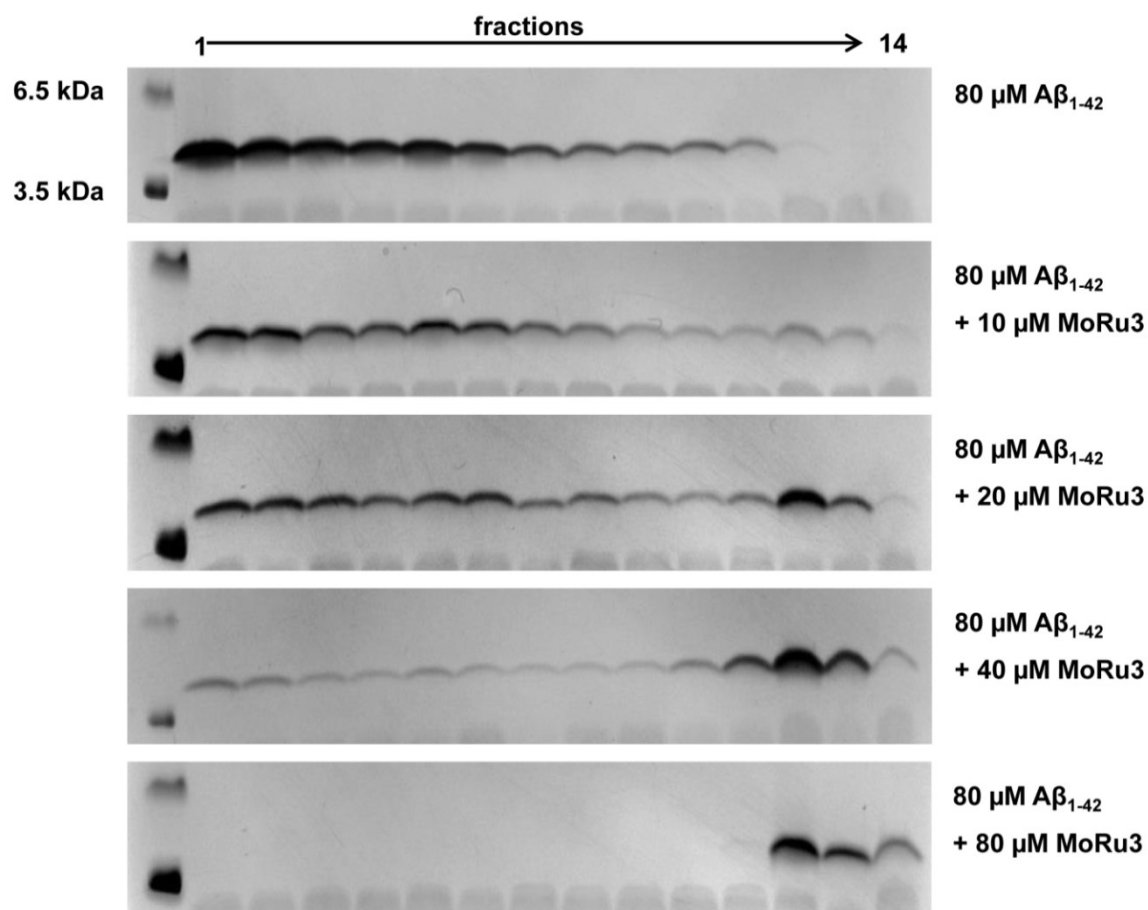
**Figure 38: Influence of different concentrations of MoRu3 on Aβ$_{1-42}$ distribution in an iodixanol gradient.**

Silver stained Tris-tricine SDS gels are shown. The bands in the loaded fractions display Aβ$_{1-42}$ (4.5 kDa). From top to bottom preincubated Aβ$_{1-42}$ with 0/10/20/40/80 µM MoRu3 are shown. Preincubated Aβ$_{1-42}$ (80 µM) was mixed with the samples and coincubated for additional 40 min. After DGC, 14 fractions were collected separated by Tris-tricine SDS-PAGE. Afterwads, gels were silver stained.

In order to verify and quantify the results from SDS-PAGE, samples from each fraction were analyzed by RP-HPLC with a Zorbax 300SB-C8 column. The isocratic run with a mobile phase of aqueous acetonitrile (30 % (v/v)) and TFA (0.1 % (v/v)) and elevated column temperature (80 °C) was used to denature Aβ$_{1-42}$ and separate it from other components, especially iodixanol.

For each fraction, measurements from three independent experiments were averaged and the error bars display the standard deviation. The results correspond to the outcome of SDS-PAGE analysis. Samples from 80 µM Aβ$_{1-42}$ incubated without MoRu3, show that Aβ$_{1-42}$ concentrations constantly decreased

from fraction 1 to 14. Fraction 15, representing the pellet, also includes small amounts of $A\beta_{1-42}$. In a concentration dependent manner, addition of MoRu3 led to a decrease of $A\beta_{1-42}$ concentration in the first fractions and elevated concentrations in fractions 11 to 14. Especially in fraction 12, the concentration of $A\beta_{1-42}$ increased strongly compared to $A\beta_{1-42}$, which was not treated with MoRu3 (Figure 39).
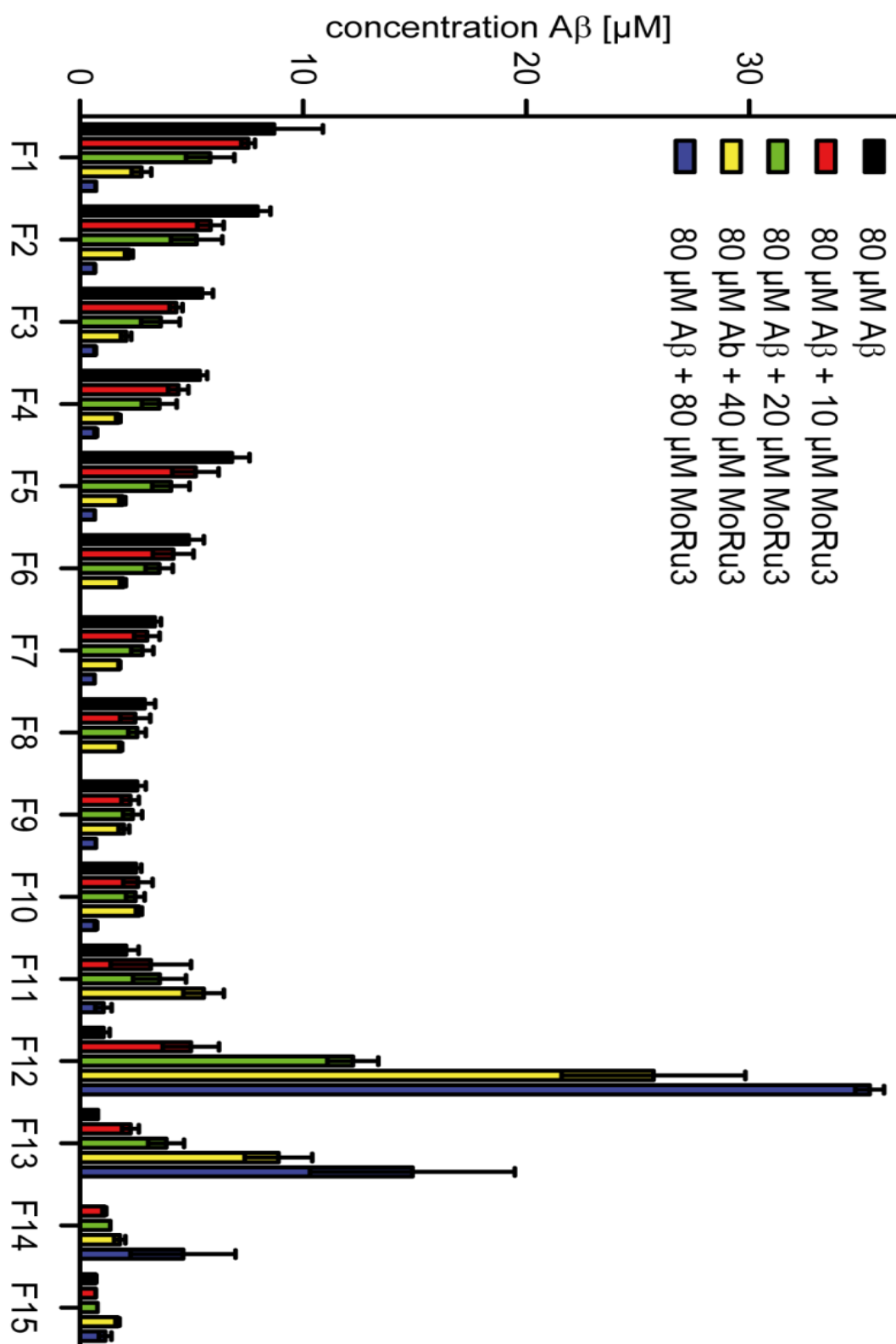
Figure 39: Quantitive determination of Aβ$_{1-42}$ concentrations via RP-HPLC.

The concentration of Aβ$_{1-42}$ is plotted against the DGC fractions (F1-F14). Aβ$_{1-42}$ (80 μM) was preincubated and subsequently coincubated for 40 min with 0 μM (black), 10 μM (red), 20 μM (green), 40 μM (yellow) and 80 μM MoRu3 (blue). The samples were separated by DGC. The obtained fractions were and loaded onto a Zorbax 300SB-C8 column for RP-HPLC.

4.4.2 Impact of MoRu3 on Aβ$_{1-42}$ aggregation shown by TEM

The latter experiments indicate that coincubation of Aβ$_{1-42}$ with MoRu3 leads to a modulation of Aβ$_{1-42}$ aggregation towards HMW aggregates. Aβ$_{1-42}$ was incubated with and without MoRu3 in an equimolar ratio (10 µM) for 24 h at RT in order to analyze the formed Aβ$_{1-42}$ species. Subsequently, the samples were stained with uranyl acetate and photographed via TEM.

Aβ$_{1-42}$ incubated without MoRu3 developed large aggregates and fibrils (Figure 40; left panel). Coincubation with an equimolar concentration of MoRu3 led to the formation of large aggregates (Figure 40; right panel).
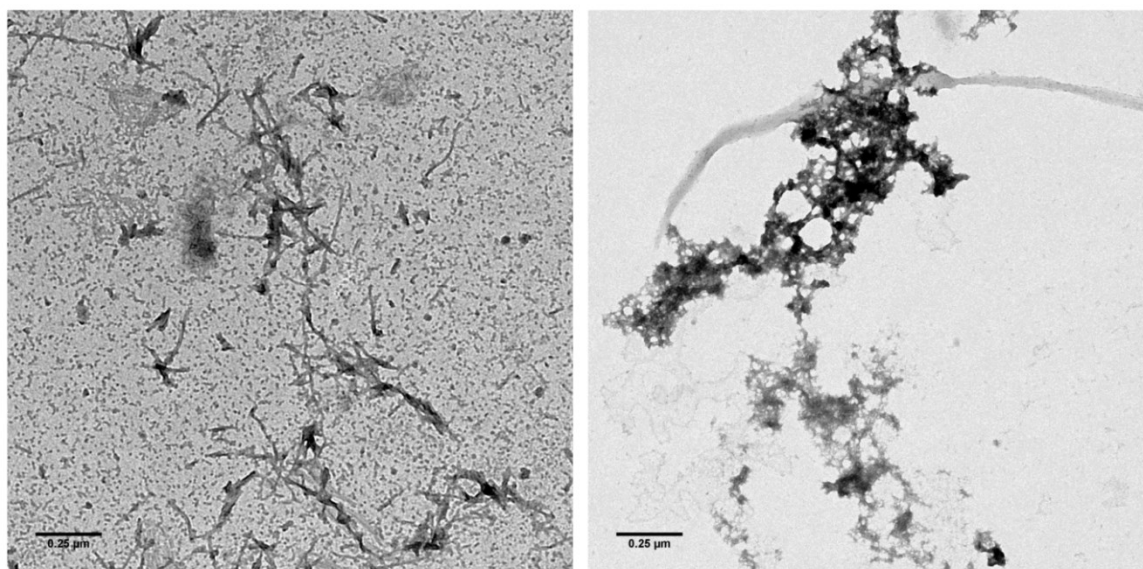
Figure 40: TEM pictures of 10 µM Aβ$_{1-42}$ incubated with and without 10 µM MoRu3.

The left picture shows 10 µM Aβ$_{1-42}$. The right picture shows 10 µM Aβ$_{1-42}$ incubated with 10 µM MoRu3. HFIP-pretreated Aβ$_{1-42}$ (10 µM) was incubated with 0 or 10 µM MoRu3 for 24 h at 25 °C. The samples were spotted on formvar/carbon copper grids and stained with an aqueous solution of 1 % uranyl acetate and analyzed by TEM (Libra120; 120 kV). Scale bars represent 0.25 µm.

## 4.4.3 Influence of MoRu peptides on Aβ$_{1-42}$ mediated cell toxicity

In order to analyze the impact of the broad range Aβ$_{1-42}$ species preparation on PC-12 cells, cell viability was measured via MTT reduction assay. Additionally,

MoRu1, 2 and 3 were tested, whether they are able to compensate or abrogate $A\beta_{1-42}$ induced cell toxicity.

For this purpose, PC-12 cells were grown adherently in a 96-well microtiter plate. HFIP pretreated $A\beta_{1-42}$, previously incubated to gain a broad range of differently sized species, was added in a final concentration of 1 µM. The peptides MoRu1, 2 and 3 were tested for their influence on PC-12 viability and after coincubation with $A\beta_{1-42}$.

Untreated cells (medium) were defined as 100 % viable and the values of all other approaches were normalized to untreated cells. Treatment with 0.1 % TritonX-100 was used as positive control for cell toxicity and reduced the amount of viable cells to 1.5 %. The above mentioned $A\beta_{1-42}$ preparation decreased cell viability to 45 % (Figure 41).

MoRu1 was toxic to PC-12 cells in a concentration of 1 µM. Only 57 % of the treated cells survived incubation with MoRu1. Additionally, MoRu1 was not able to prevent $A\beta_{1-42}$ induced cell death in both tested concentrations (0.5 µM and 1 µM), after coincubation with the toxic $A\beta_{1-42}$ preparation.This assay demonstrates once more, that MoRu1 is not suitable for further research (Figure 41).
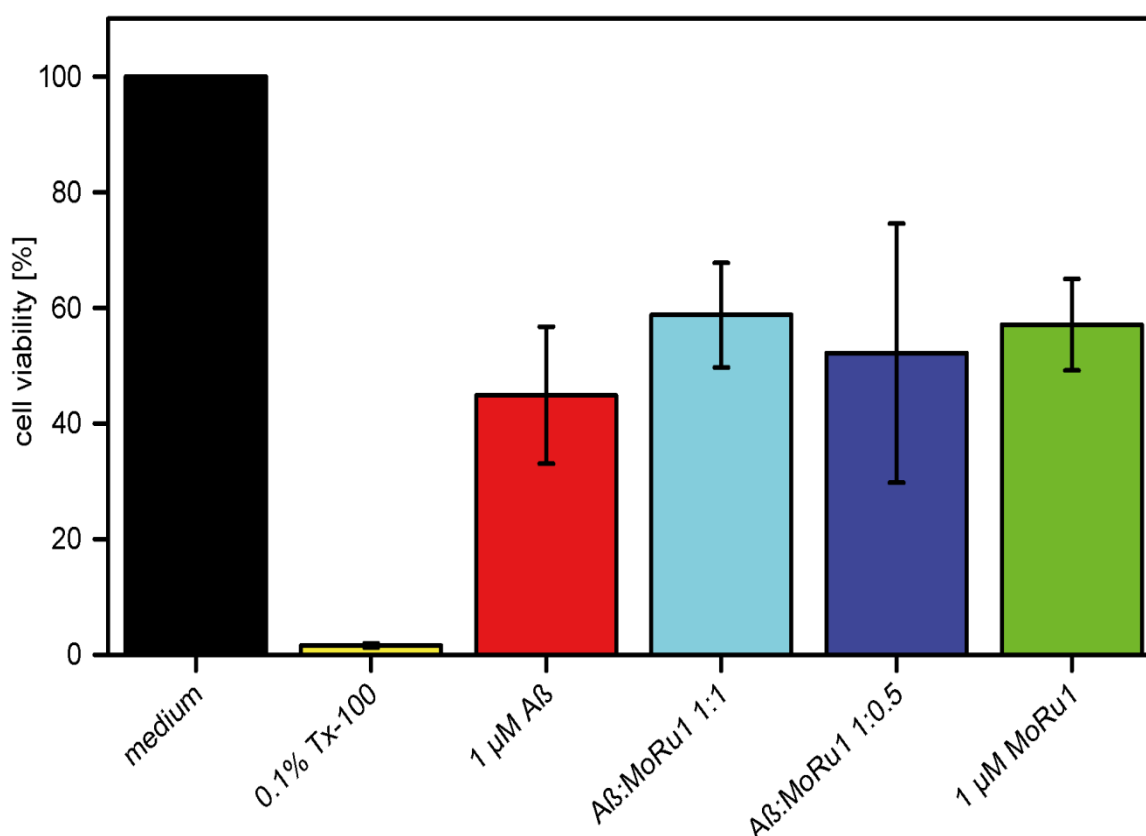
Figure 41: MTT reduction assay - Influence of MoRu1 on Aβ$_{1-42}$ induced cell toxicity.

The cell viability of PC-12 cells (in percent) is plotted against different treatment conditions. Adherently grown PC-12 cells were incubated 24 h with medium (black) or 0.1 % TritonX-100 (yellow). Cells incubated for 24 h with 1 μM Aβ$_{1-42}$ (red), 1 μM Aβ$_{1-42}$ and 1 μM MoRu1 (light blue) or 1 μM Aβ$_{1-42}$ and 0.5 μM MoRu1 (purple) were tested as well as 1 μM MoRu1 (green). Viability was tested by subsequent incubation with MTT substrate followed by solubilization of formed formazan crystals. Absorbance was measured at 570 nm. Untreated cells (medium) were defined 100 % viable and values of all other approaches were normalized according to untreated cells.

MoRu2, in contrast to MoRu1, was not toxic to PC-12 cells, since 99.9 % of the treated cells survived treatment. Moreover, MoRu2 reduced Aβ$_{1-42}$ induced cytotoxicity in a concentration dependent manner. When coincubated in equimolar concentrations with Aβ$_{1-42}$, 75 % of the cells survived. With half of the MoRu2 concentration Aβ$_{1-42,}$ 67 % of the cells survived (Figure 42).
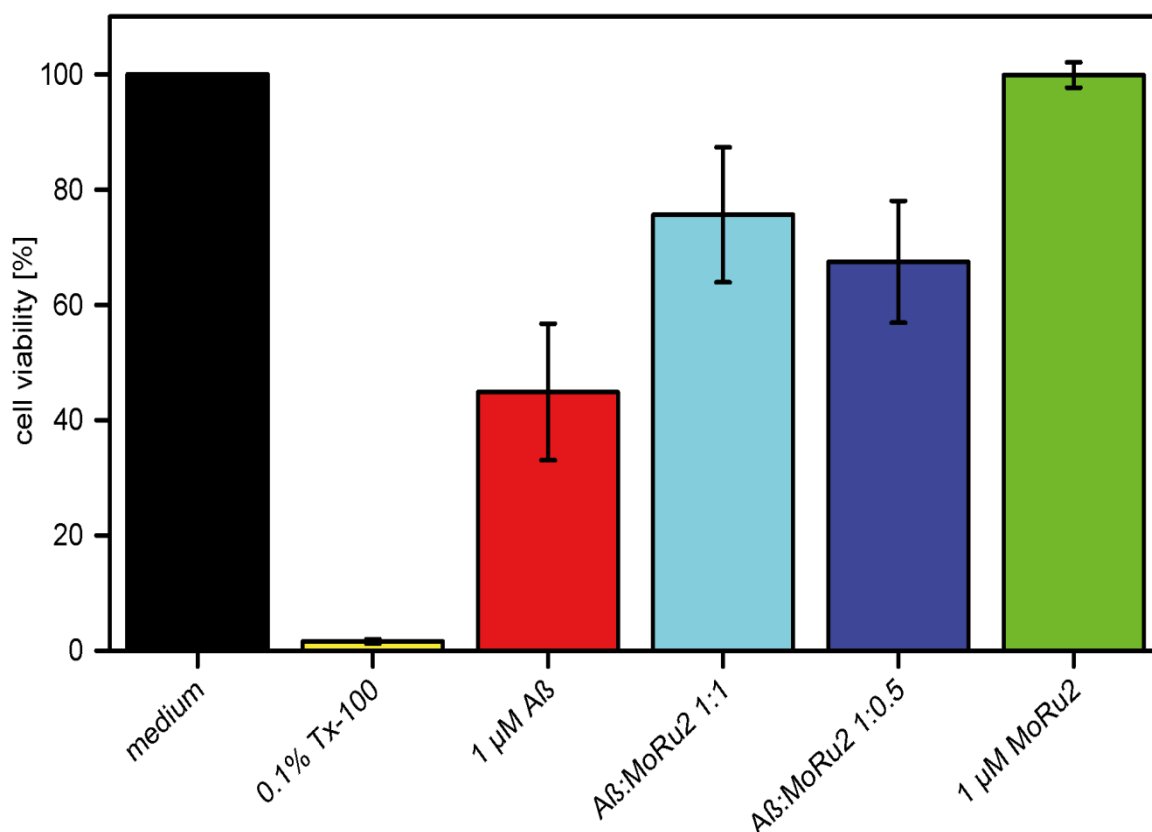
Figure 42: MTT reduction assay - Influence of MoRu2 on Aβ$_{1-42}$ induced cell toxicity.

The cell viability of PC-12 cells (in percent) is plotted against different treatment conditions. Adherently grown PC-12 cells were incubated 24 h with medium (black) or 0.1 % TritonX-100 (yellow). Cells incubated for 24 h with 1 μM Aβ$_{1-42}$ (red), 1 μM Aβ$_{1-42}$ and 1 μM MoRu2 (light blue) or 1 μM Aβ$_{1-42}$ and 0.5 μM MoRu2 (purple) were tested as well as 1 μM MoRu2 (green). Viability was tested by subsequent incubation with MTT substrate followed by solubilization of formed formazan crystals. Absorbance was measured at 570 nm. Untreated cells (medium) were defined 100 % viable and values of all other approaches were normalized according to untreated cells.

MoRu3 exhibits similar characteristics as MoRu2 in this assay. The peptide itself is not toxic to PC-12 cells. Aβ$_{1-42}$ induced cytotoxicity was decreased in a concentration dependent manner when Aβ$_{1-42}$ was coincubated with MoRu3. In a 1:1 ratio, 86 % of the cells survived Aβ$_{1-42}$ treatment. In a lower concentration of MoRu3, 66 % of the cells survived (see Figure 43).
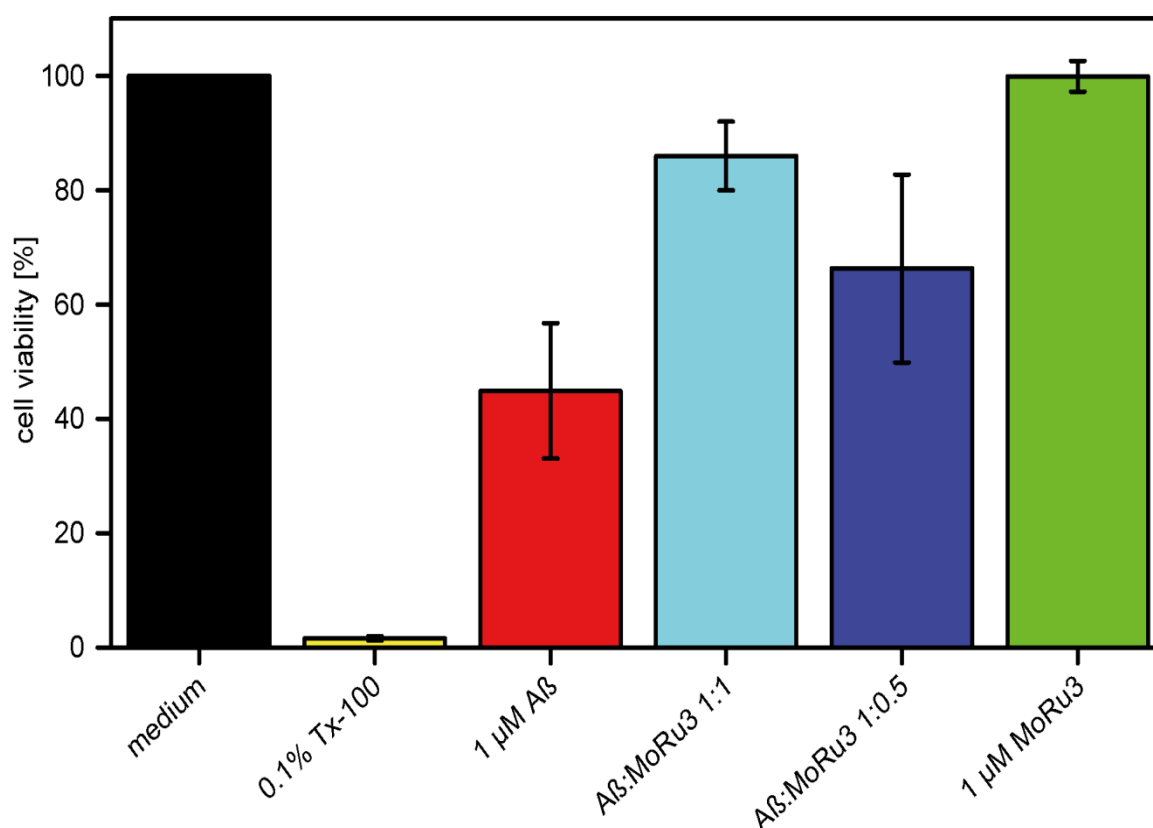
Figure 43: MTT reduction assay - Influence of MoRu3 on Aβ$_{1\text{-}42}$ induced cell toxicity.

The cell viability of PC-12 cells (in percent) is plotted against different treatment conditions. Adherently grown PC-12 cells were incubated 24 h with medium (black) or 0.1 % TritonX-100 (yellow). Cells incubated for 24 h with 1 μM Aβ$_{1\text{-}42}$ (red), 1 μM Aβ$_{1\text{-}42}$ and 1 μM MoRu3 (light blue) or 1 μM Aβ$_{1\text{-}42}$ and 0.5 μM MoRu3 (purple) were tested as well as 1 μM MoRu3 (green). Viability was tested by subsequent incubation with MTT substrate followed by solubilization of formed formazan crystals. Absorbance was measured at 570 nm. Untreated cells (medium) were defined 100 % viable and values of all other approaches were normalized according to untreated cells

4.4.4 Influence of MoRu3 on the phenotype of murine neuroblastoma cells

The murine neuroblastoma cell line Neuro-2a is a model for neuronal cells, and thus an ideal cell line to study AD symptoms. Neuro-2a cells, stably transfected with human APP695, can mimic neuronal cells that express APP and its cleavage products, such as toxic Aβ. Therefore, they are suitable for analyzing the impact of potential therapeutic compounds on Aβ in an environment that resembles a pathological phenotype in neuronal cells.

Untreated Neuro-2a cells appear accumulated and polygonal with many protrusions connecting the cells (Figure 44; left panel). The influence of MoRu3 (10 or 100 µM) on wild-type Neuro-2a cells was tested and the phenotype was analyzed by microscopy. Both concentrations slightly altered the overall phenotype of Neuro-2a cells. The cells did accumulate and develop protrusions to connect with each other. However, more protrusions were observed when compared to untreated cells, and the cells appeared to be more rounded (Figure 44; middle and right panel).
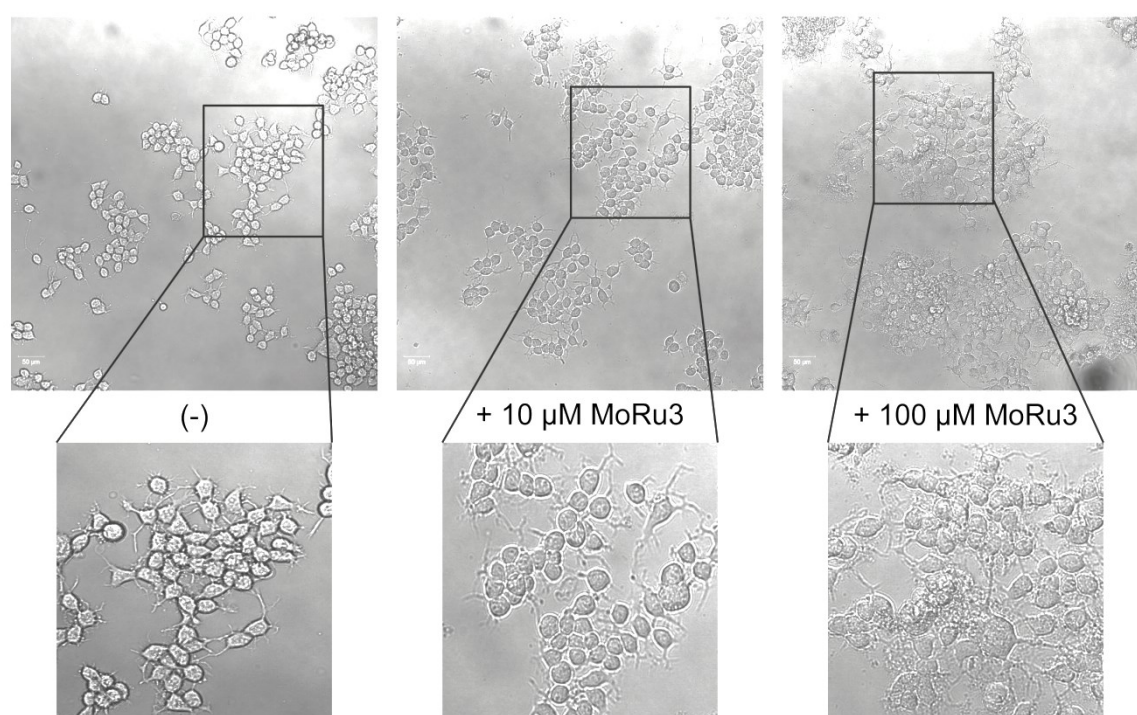

Figure 44: Micrographs of wild-type Neuro-2a cells treated with or without MoRu3.

Micrographs of wild-type murine neuroblastoma cells (Neuro-2a) are shown. The left panel shows untreated wild-type Neuro-2a cells. In the middle and the right panel wild-type Neuro-2a cells were treated with 10 µM MoRu3 (middle) or 100 µM MoRu3 (right). The cells were grown in 24-well microtiter plates for 24 h and incubated afterwards with 0/10/100 µM MoRu3 for additional 24 h. Cell viability and morphology were analyzed with a laser scanning microscope (LSM 710). Scale bars represent 50 µm.

Neuro-2a cells stably transfected with human APP695, develop a pathological phenotype (Figure 45; left panel). The cells are rounder and isolated when compared with wild-type Neuro-2a cells. In addition, the protrusions are observed to be shorter and fewer. The presence of MoRu3 reversed the pathological phenotype observed in transfected Neuro-2a cells (Figure 45; middle and right

panel). After incubation with MoRu3 at different concentrations (10 and 100 µM), the cells matched closely the phenotype of wild-type Neuro-2a cells. The growth rate was also elevated. The cells developed branched connections between each other, accumulated in number and became polygonal. The impact of MoRu3 on APP-transfected Neuro-2a cells is likely to be concentration dependent, as a higher MoRu3 concentration increased the number of protrusions.
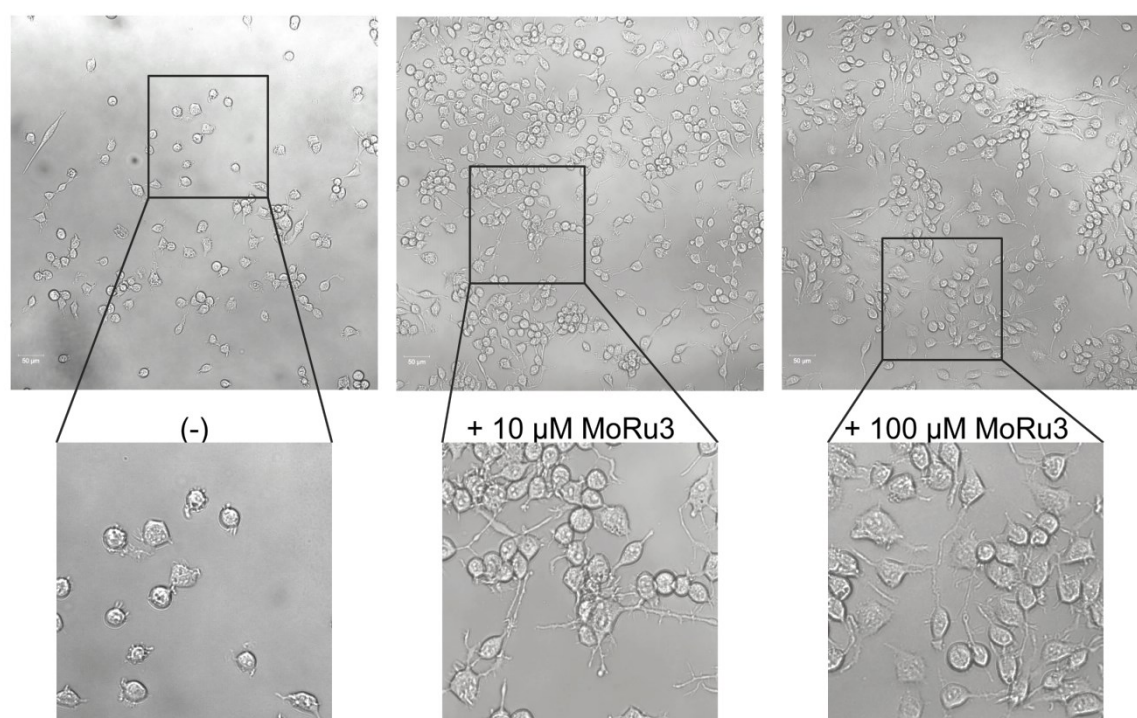

Figure 45: Micrographs of Neuro-2a cells, stably transfected with human APP695, treated with or without MoRu3.

Micrographs of Neuro-2a cells stably transfected with human APP695. The left panel shows untreated Neuro-2a/huAPP695 cells. In the middle and the right panel Neuro-2a/huAPP695 cells treated with 10 µM MoRu3 (middle) or 100 µM MoRu3 (right) are shown. The cells were grown in 24-well microtiter plates for 24 h and incubated afterwards with 0/10/100 µM MoRu3 for additional 24 h. Cell viability and morphology were analyzed with a laser scanning microscope (LSM 710). Scale bars represent 50 µm.

4.4.5 Influence of MoRu3 on γ-secretase activity in APP-transfected Neuro-2a cells

In order to test whether MoRu3 has an influence on γ-secretase activity, APP-transfected Neuro-2a cells were incubated with 0, 10 and 100 µM of MoRu3. DAPT, a known γ-secretase inhibitor, was used as control. Additionally, DMSO, which served as dissolvent for DAPT, was tested. After 24 h, cells were lysed, proteins were separated via Tris-tricine SDS-PAGE, blotted onto a PVDF membrane and the signal for the γ-secretase substrate APP C-terminal fragment β (APP CTFβ) was detected via enhanced chemoluminsence.

When γ-secretase activity is restricted, APP CTFβ accumulates in the cells, since it is no further cleaved. Upon treating the cells with DAPT, the 15 kDa APP CTFβ fragment is detected by Western blot (Figure 46, lane 2). Neither DMSO (Figure 46, lane 1) nor 10 or 100 µM MoRu3 (Figure 46, lane 3 and 4) induced a detectable accumulation of CTFβ. The β-actin control at 55 kDa showed, that equal amounts of total protein were loaded (Figure 46).
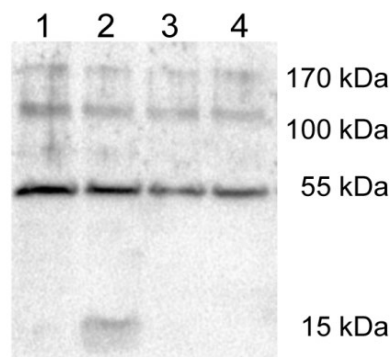
Figure 46: Western blot of human APP695-transfected Neuro-2a cell lysates towards APP C-terminal fragment β (CTFβ).

Detection of CTFβ and β-actin by enhanced chemoluminescence on a Western blot of human APP695-transfected Neuro-2a cell lysates. Human APP695-transfected Neuro-2a cells were incubated with DMSO (lane 1), DAPT (lane 2), 10 µM MoRu3 (lane 3) or 100 µM MoRu3 (lane 4). The cells were harvested, lysed and proteins were separated by Tris-tricine SDS-PAGE and subsequently blotted to a PVDF membrane. CTFβ was detected with an anti-APP-CTF antibody. Binding of HRP-conjugated secondary antibody was detected by transformation of ECL substrate.

4.5 Repetition of mirror image phage display #5 with an optimized elution procedure (mipd#6)

The latter mirror image phage display (mipd#5) led to promising peptides of which MoRu3 exhibited its therapeutic potential in several *in vitro* assays. However, since the elution procedure during the panning rounds of mipd#1-5 might have led to the loss of several specifically monomeric $A\beta_{1-42}$ binding phages, the procedure of the so far most promising mirror image phage display, #5, was repeated with another elution procedure.

The protocol of mipd#5 (Chapter 3.1) was revised in two steps. Firstly, the iodixanol gradient for separation of $A\beta_{1-42}$ fibrils and HMW aggregates was changed from layers of 30/24/18/12/6 and 3 % iodixanol (mipd#5) to layers of 50/40/30/20/10 and 5 % iodixanol (mipd#6) in order to achieve a broad separation of HMW $A\beta_{1-42}$ species. The second modification was to neutralize the eluted phage solution after panning in a fresh reaction tube instead of the well which presents immobilized monomeric $A\beta_{1-42}$.

4.5.1 Enrichment ELISA

As in the enrichment ELISAs conducted before, the affinity of amplified phage pools from each panning round to different $A\beta_{1-42}$ species was analyzed in order to gain information about which round has the highest $A\beta_{1-42}$ monomer specificity.

Biotinylated $A\beta_{1-42}$ monomers as well as mixed $A\beta_{1-42}$ oligomers and fibrils were produced as in the panning rounds and immobilized to streptavidin coated wells in duplicates for each panning round and the naïve phage library at concentrations of 320 nM. The mixture of $A\beta_{1-42}$ oligomers and fibrils resembles the counterselection during panning rounds and should adjust the immobilization efficiency between different $A\beta_{1-42}$ species. Streptavidin coated wells without immobilized $A\beta_{1-42}$ served as control for unspecific binding of phages to the wells or streptavidin.

In order to assess potential cross-reactivity of the M13 phage-specific antibody with $A\beta_{1-42}$ or the surface, control wells were incubated with buffer instead of phages. The M13 phage-specific antibody was added and substrate

transformation by HRP conjugated to the antibody was measured. Furthermore, in order to test immobilization efficiency, $A\beta_{1-42}$ monomers and mixed $A\beta_{1-42}$ oligomers and fibrils were immobilized to streptavidin coated wells and detected with the Aβ-specific antibody 6E10. Subsequently, 6E10 was detected with a HRP conjugated goat anti mouse antibody and the values of substrate transformation by HRP were measured at 450 nm (Figure 47).

The affinity of phages towards $A\beta_{1-42}$ increased from the naïve library (R0) to panning round four (R4). The signal for monomeric $A\beta_{1-42}$ increased stronger than the signal for aggregated $A\beta_{1-42}$ (i.e. $A\beta_{1-42}$ oligomers and fibrils). Additionally, the binding of phages to the streptavidin surface increased from round two to four in every round. In round five the values for surface binding remained stable and decreased again in round six. Compared with wells immobilized with $A\beta_{1-42,}$ the values were considerably lower.

The controls showed that the M13 phage-specific antibody in this enrichment ELISA did not cross react with $A\beta_{1-42}$. Furthermore, the efficiency of $A\beta_{1-42}$ immobilization was low, therefore the results have to be considered carefully.

Regarding the overall values and the signal-to-noise ratio between binding to monomeric $A\beta_{1-42}$ and $A\beta_{1-42}$ oligomers and fibrils, single phage clones from round three to six were amplified. The DNA of these clones was sequenced and the single phage clones were tested in an additional ELISA.
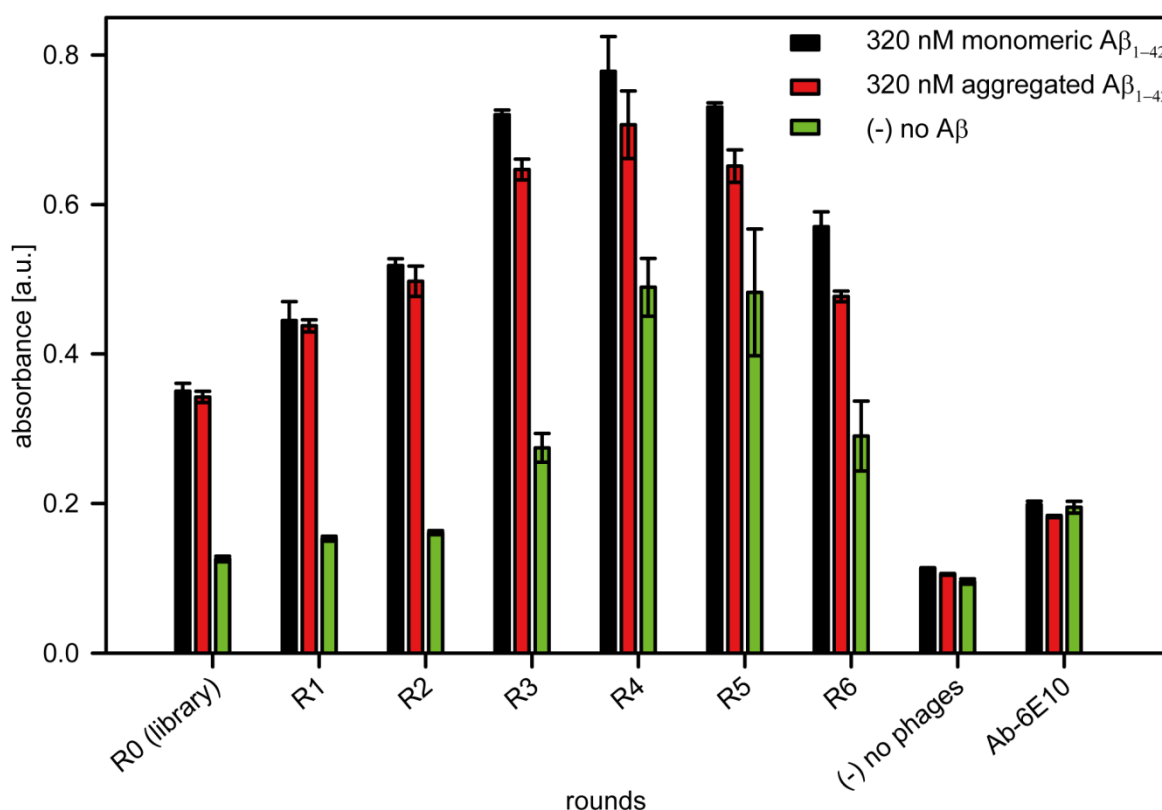
Figure 47: ELISA for relative quantification of binding affinity of phage pools from mipd#6 towards different Aβ1-42 species after six panning rounds.

The relative binding affinity of phages from the dodecameric library to SEC-derived biotinylated monomeric $Aβ_{1-42}$ and aggregated $Aβ_{1-42}$ (SEC-derived oligomers and DGC-derived fibrils) was analyzed. The M13 phage-specific antibody was used for quantification of bound phages. The enzymatic transformation of substrate by the antibody-conjugated HRP was measured at 450 nm. The relative absorbance values are plotted. Amplified phages from round one to six (R1–R6) as well as phages from the naïve library (R0) were added to monomeric (black) and aggregated (red) $Aβ_{1-42}$, both immobilized at a concentration of 320 nM. The phages were also added to wells only coated with streptavidin (green). Cross reactivity of the M13 phage-specific antibody was additionally tested (no phages). Moreover, the immobilization efficiency of $Aβ_{1-42}$ was analyzed with the Aβ-specific antibody 6E10.

4.5.2 Sequencing of single phage clones

Clones from round three to round six were sequenced. In total, the DNA of 272 single phage clones was extracted and sent in for sequencing. Several sequences occurred repeatedly. Two sequences were found in 39 and 28 clones, respectively. One sequence occurred four times, four sequences occurred three

times and nine sequences were found two times (Table 13).

Table 13: Amino acid sequences of single phage clones from mipd#6.

Amino acid sequences obtained from the corresponding DNA of single phage clones from mipd#6. The amino acid sequence in one letter code is given together with the frequency of occurrence.

amino acid sequence	frequency
VHWDFRQWWQPS	39
DWSSWVYRDPQT	28
FSWSMVMPWPTA	4
HNWSWEWWYNPN	3
STLHFYTAFLNK	3
STWSILHGWWTN	3
VVSPDMNLLLTN	3
EHWDFRQWWQPS	2
FSHSHHTWFTWN	2
HFWSWTSLSMTR	2
HLSWYWEKYLTS	2
HTWTHWFSWNVP	2
LSMNITTVHRWH	2
VHWDFRQWWQQS	2
YNVARPMSQIPT	2
YSFHFEMNMGNY	2

Additionally, several clones that occurred once, shared similarities in their amino acid sequence with the more frequent clones. Thereby, aromatic amino acids (Phenylalanine/Phe/F; Tryptophan/Trp/W and Tyrosine/Tyr/Y) and the basic amino acid Histidin (His/H) were found repeatedly.

4.5.3 Single phage ELISA

All clones from mipd#6 that had a sequence which occurred more than once were tested in a single phage ELISA. Additionally, solitary occuring clones which resemble these sequences were tested. Moreover, several clones with a unique but special sequence (e.g. many charged amino acids or only small uncharged amino acids) were tested as well. The single phage clones that bear the DNA sequence of the peptides MoRu1/2/3 and MoRu5 (mipd#5) were also tested again

in order to compare the outcome of both mirror image phage displays (Table 14).

Table 14: Selected clones for single phage ELISA.

Single phage clones tested by ELISA. The clone number of each clone tested is listed together with its amino acid sequence and the selection criteria. For frequently occurring sequences, one clone was selected and tested.

clone number	amino acid sequence	selection criteria
>6.167	VHWDFRQWWQPS	frequency (39x)
>6.262	DWSSWVYRDPQT	frequency (28x)
>6.135	FSWSMVMPWPTA	frequency (4x)
>6.216	HNWSWEWWYNPN	frequency (3x)
>6.249	STLHFYTAFLNK	frequency (3x)
>6.246	STWSILHGWWTN	frequency (3x)
>6.159	VVSPDMNLLLTN	frequency (3x)
>6.217	EHWDFRQWWQPS	frequency (2x) and related to 6.167
>6.247	FSHSHHTWFTWN	frequency (2x)
>6.227	HFWSWTSLSMTR	frequency (2x)
>6.239	HLSWYWEKYLTS	frequency (2x)
>6.242	HTWTHWFSWNVP	frequency (2x)
>6.245	LSMNITTVHRWH	frequency (2x)
>6.141	VHWDFRQWWQQS	frequency (2x) and related to 6.167
>6.84	YNVARPMSQIPT	frequency (2x)
>6.113	YSFHFEMNMGNY	frequency (2x)
>6.31	RTSEEFHTDRWP	sequence starting with an positively charged amino acid
>6.197	EHWDFGQWWQQS	related to 6.167
>6.255	GQWDFRQWWQPC	related to 6.167
>6.139	DWSSRVYRDPQT	related to 6.262
>6.240	ERSQWGHRDPQS	related to 6.167
>6.257	DRSKGDHRITQM	related to 6.262
>6.29	EDLKLPLEDWRP	six charged amino acids
>6.121	IHGHYGLSLVNE	occurred 2x with slightly different amino acid composition
>6.190	DLRFSSLWKLSH	occured 2x with slightly different amino acid composition
>6.142	GSQSLLSNMQNT	many hydrophilic + no aromatic amino acids
>6.74	SLKLLNGTSTQT	many hydrophilic + no aromatic amino acids
>6.85	NTWCAEDDVNLA	only one aromatic amino acid + a core of acidic amino acids
>5.80	HTWTTYDYVWRL	MoRu1 (mipd#5)
>5.57	GTMLKFSGMNLT	MoRu2 (mipd#5)
>5.60	YSYLTSYHMVWR	MoRu3 (mipd#5)
>5.81	HNWFYWTTEPYD	MoRu5 (mipd#5)

The ELISA was conducted as described for mipd#6 in Chapter 3.1.4. A new batch 6E10 antibody was used for this assay and Aβ_{1-42} oligomers and fibrils were mixed

as in the enrichment ELISA of mipd#6 in order to reflect the conditions during the panning procedure. Additionally, the anaylsis of raw data was revised as follows. Firstly, the anti M13 phage specific antibody yielded no cross reactivity with neither any of the immobilized $A\beta_{1-42}$ species nor the plastic surface and was therefore subtracted as background from the according values of the phage clones. Secondly, the 6E10 signal for $A\beta_{1-42}$ immobilization efficiency showed that oligomers and fibrils were immobilized in a higher amount to the surface compared with monomeric $A\beta_{1-42}$. Therefore, the values for $A\beta_{1-42}$ oligomers and fibrils were normalized to the values of $A\beta_{1-42}$ monomer binding.
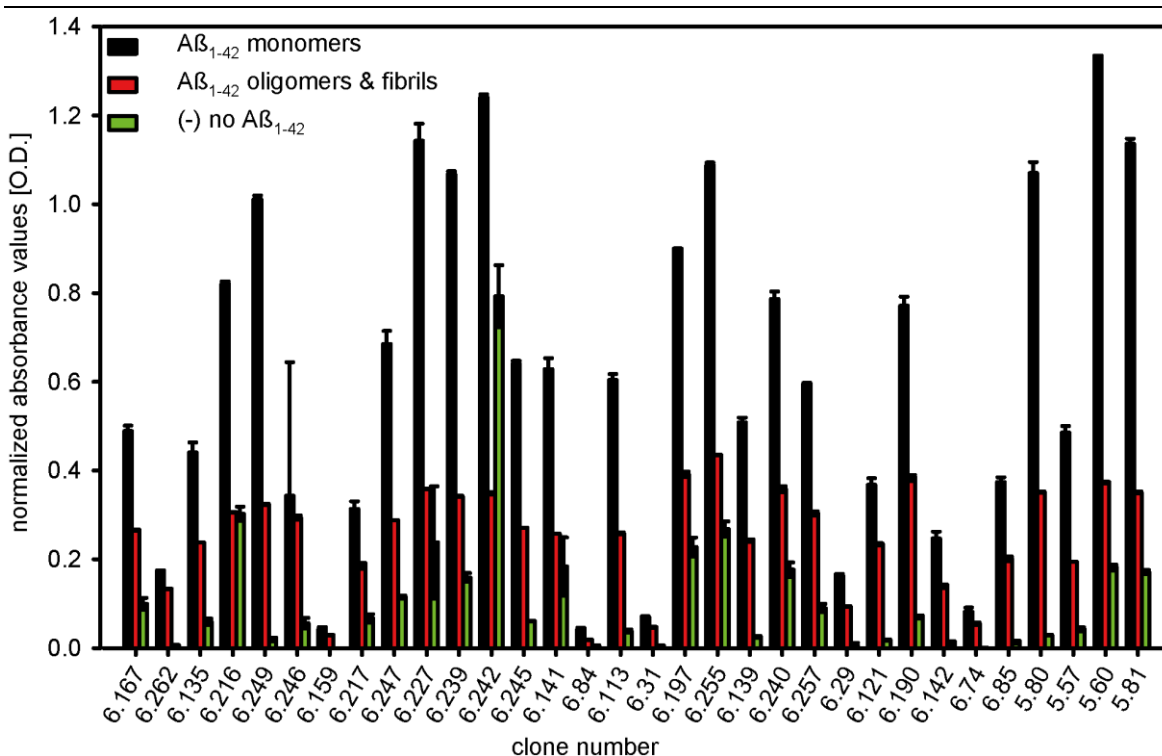
Figure 48: ELISA for relative quantification of binding affinity of single phage clones towards different $A\beta_{1-42}$ species.

The relative binding affinity of single phages from mipd#6 (6.xx) and mipd#5 (5.xx) to SEC-derived biotinylated $A\beta_{1-42}$ monomers and a mixture of SEC-derived biotinylated $A\beta_{1-42}$ oligomers and DGC-derived biotinylated $A\beta_{1-42}$ fibrils was analyzed. The M13 phage-specific antibody was used for quantification of bound phages. The enzymatic transformation of substrate by the antibody-conjugated HRP was measured at 450 nm. The relative absorbance values are plotted. Amplified single phage clones were added to monomeric (black) or oligomeric/fibrillar $A\beta_{1-42}$ (red), immobilized at a concentration of 320 nM. The phages were also added to uncoated wells (green). Values of the M13 phage-specific antibody against $A\beta_{1-42}$ and uncoated wells were subtracted as background from the values obtained for phages. Immobilization efficiency was analyzed by the antibody 6E10. The values for oligomeric/fibrillary $A\beta_{1-42}$ were normalized to to monomeric $A\beta_{1-42}$.

The normalized absorbance values show that all clones tested had a higher affinity for monomeric $A\beta_{1-42}$ compared to oligomeric/fibrillar $A\beta_{1-42}$. Moreover, most clones had a low affinity for the uncoated surface. Interestingly, MoRu3 (clone 5.60) exhibited the highest values for monomeric $A\beta_{1-42}$ of all clones tested and also the highest $A\beta_{1-42}$ monomer specificity as deduced by the ratio of values for $A\beta_{1-42}$ monomer binding and oligomeric/fibrillary $A\beta_{1-42}$. Most of the clones from mipd#6 (clones 6.xx) have a lower overall affinity for $A\beta_{1-42}$ compared with clone 5.60 and also the specificity to monomeric $A\beta_{1-42}$ is lower.

5. Discussion

AD is the most common type of dementia and accounts for the majority of deaths caused by dementia. Aβ oligomers are supposed to be the main pathogenic agents. Numerous publications indicate that oligomeric Aβ species are neurotoxic. However, Aβ monomers do have a physiological role and even a neuroprotective effect.

For AD, neither a reliable *pre mortem* diagnostic tool nor curative therapies are available until now. Several promising therapy approaches, such as targeting Aβ clearance, immunotherapy, or modulation of secretases have failed.

A novel approach is the modulation of toxic Aβ species towards non-toxic aggregates and the stabilization of monomers. Mirror image phage display is a suitable method to obtain small D-enantiomeric peptide compounds that specifically bind to, stabilize and modulate Aβ molecules. By refining the standard mirror image phage display the specificity for distinct species of $Aβ_{1-42}$ can be increased.

5.1 A mirror image phage display for identification of monomer specific $Aβ_{1-42}$ binding peptides

The objective of this thesis was to identify binding partners for monomeric $Aβ_{1-42}$ by mirror image phage display. The first approach was to repeat a mirror image phage display protocol that resulted in the isolation of the D-enantiomeric peptide D3 [180].

D3 is a dodecameric, D-enantiomeric peptide that was identified during a mirror image phage display targeting monomeric and small oligomeric $Aβ_{1-42}$ species. In order to assure the monomeric state, the concentration of biotinylated $Aβ_{1-42}$ was very low (2 nM) [180]. The selected peptide D3 was shown to have a high therapeutic impact and improves cognition in AD mice. D3 also reduces Aβ-related inflammation in Alzheimer transgenic mice, disaggregates Aβ plaques *in vivo* and

fibrils *in vitro* and reduces aggregate formation and cell toxicity induced by Aβ. Furthermore, D3 has a plaque staining capability [179, 180, 188]. Moreover, D3 did not cause inflammation in mice brains even after long term infusion, suggesting that the peptide is medically save to administer [189].

In order to find peptides that resemble the beneficial characteristics of D3 or even show improved efficiency, the protocol that was used for the identification of D3 was repeated with slightly changed parameters (mipd#1; Chapter 4.1).
Interestingly, the single phage clones did not specifically bind $Aβ_{1-42}$, but bound preferentially to the streptavidin surface. The different streptavidin surfaces used in both mirror image phage displays may explain this observation. Another possible explanation is that phages with a high affinity for streptavidin were the major species selected and amplified [190, 191]. In some cases, the inserted sequence can interfere with the M13 phage infection and secretion, leading to a decrease in amplification. Thus, target specific phage clones may be lost because of an excess of unspecific clones with a higher amplification rate [159].

In order to reduce plastic or streptavidin binding phages, additional blocking steps and a competition step with biotin were included into the panning procedure (mipd#2). However, these steps did not dramatically improve selection when compared with the earlier results, since plastic and streptavidin binding phages occurred again. In order to avoid a streptavidin coated surface, amine coupling was used to immobilize $Aβ_{1-42}$ to the plate (mipd#3). However, this approach did not result in $Aβ_{1-42}$ monomer specific phages either. Sequencing of single phage clones from the heptameric phage library led to a consensus sequence (LPPNPTK), which was found in the majority of clones. This sequence strongly resembles a known BSA binding motif [192].

In mipd#4, streptavidin-biotin coupling was used again and counterselecitve agents, an increasing stringency during the washing steps and a biotin competition step were implemented into panning procedure.
This approach led to promising results. The binding of phages to the plastic surface was significantly reduced and single phage clones exhibited an increased affinity for small $Aβ_{1-42}$ species (monomers and oligomers) whereas affinities for $Aβ_{1-42}$ fibrils decreased compared to earlier conducted mirror image phage display approaches. The amino acid sequences from four single phage clones were

produced as D-enantiomeric peptides (SRM1-4) for further analysis. These peptides did not solve in the buffer systems used for characterization experiments and were therefore not analyzed further.

A novel approach (mipd#5) was developed that should overcome the aforementioned problems (Chapter 3.1.1 & 4.2). In order to reduce plastic-, streptavidin- and BSA binding phages, six panning rounds were conducted, which all differed in their composition of surface and blocking. Additionally, a competition step with biotin was included to eliminate phages that share their binding site to streptavidin with biotin. Furthermore, the number of washing steps from one round to the next was increased. The most important alteration, however, was to introduce an increasing competition with different $A\beta_{1-42}$ species. $A\beta_{1-42}$ oligomers and $A\beta_{1-42}$ fibrils without a biotin tag were added to the sample in increasing concentrations to deplete phages, which bind to those species. Thus, phages which specifically bind to monomeric $A\beta_{1-42}$, should have been selected.

The task was to identify binding partners that target monomeric $A\beta_{1-42}$, which is thought to have a physiological neuroprotective function. An extremely high affinity for this species would probably inhibit its beneficial function. However, a highly specific ligand could stabilize the monomeric state and promote disaggregation of toxic oligomers under an equilibrium reaction, thereby leading to a reduced load of toxic oligomers [140].

The enrichment ELISA indicated an increase in affinity to $A\beta_{1-42}$ monomers and oligomers over the six panning rounds (Chapter 4.2.2). The affinity for $A\beta_{1-42}$ oligomers increased only slightly over the six panning rounds, whereas the affinity for $A\beta_{1-42}$ monomers showed a higher increase. Additionally, binding of phages to $A\beta_{1-42}$ fibrils and HMW aggregates and to the surface remained low. The outcome of the single phage ELISA revealed several clones, which preferentially bind to $A\beta_{1-42}$ monomers and small oligomeric species, rather than to $A\beta_{1-42}$ fibrils or to the surface of the well, indicating a specificity for small $A\beta_{1-42}$ species (Chapter 4.2.3).

Six phage clones (two clones sharing the same sequence) were identified that specifically bind to very small $A\beta_{1-42}$ species such as monomers. All phage clones analyzed in the single phage ELISA showed also an affinity to $A\beta_{1-42}$ oligomers which was higher than the corresponding $A\beta_{1-42}$ monomer affinity. Yet, the

differences were minor and the strong signal for oligomeric $A\beta_{1-42}$ species can be attributed to several reasons described in the following paragraph.

The anti-M13 antibody was observed to cross-react non-specifically with oligomeric $A\beta_{1-42}$ species in this experiment (Figures 22 to 25 in Chapters 4.2.2 & 4.2.3). Therefore, the antibody might have bound to $A\beta_{1-42}$ instead of the phages which are its initial target. However, there is no reported observation of this performance in the literature. One reason might be the usage of an old batch of antibody since this cross reaction did not appear in mipd#6 where another batch was used.

Another possibility is that the phages bind to a structural epitope that appears in $A\beta_{1-42}$ monomers and oligomers but is concealed in fibrillary structures of $A\beta_{1-42}$ [58, 131, 193-195]. Since $A\beta_{1-42}$ oligomers could provide more binding sites and M13 phages express five copies of pⅢ, which presents the inserted sequence, binding to $A\beta_{1-42}$ oligomers can be stronger due to avidity effects, since it exceeds the 1:1 binding ratio expected for monomers [159].

The observation of strong signals for the $A\beta_{1-42}$ oligomer species could also originate from varying immobilization efficiencies of the different $A\beta_{1-42}$ species to the surface. Control experiments with the $A\beta$ specific antibody 6E10 showed that more $A\beta_{1-42}$ oligomers were immobilized than monomers and fibrils (Figures 22 to 25 in Sections 4.2.2 & 4.2.3).

Furthermore, one has to consider the following points when analyzing the ELISA results.

Krishnan *et al*. [196] claimed that the phage protein pⅢ bears a general amyloid interaction motif, which preferentially binds to fibrillar $A\beta$ [196]. This leads to the assumption that phages which present $A\beta_{1-42}$ monomer targeting sequences could be removed during the competition step due to the affinity of the phage itself to $A\beta_{1-42}$ fibrils. Krishnans observation can explain why some phages which strongly bind $A\beta_{1-42}$ monomers (and are therefore not removed during the competition step) still show a residual affinity to $A\beta_{1-42}$ fibrils.

Moreover, gp3, to which the randomized sequences are fused, plays a critical role for phage infection. Infection rate and secretion from the bacterial host can be significantly affected by the displayed peptide. This can lead to an altered amplification efficiency and loss of putative $A\beta_{1-42}$ binding phages [159].

Additionally, neutralizing the pH in the well after elution (mipd#1-5) enabled phages to instantly re-bind to the target $A\beta_{1-42}$, thus the applied elution protocol might have led to the collection of mostly weak and/or slow binding phages.

Nonetheless, taking into account all given explanations, the corresponding sequences, synthesized as D-enantiomeric peptides MoRu1 to MoRu5 were characterized and MoRu3/Mosd1 exhibited its therapeutic potential in several assays.

5.2 Chemical characteristics of the selected peptides

The amino acid sequences of the tested single phage clones of mipd#5 shared no predominant consensus sequence among each other, probably because of a mistake during the elution procedure. Therefore, even though the eluted phages were removed from the well immediately after neutralizing the eluate, the phages have had the possibility to bind again to the target peptide (monomeric $A\beta_{1-42}$) and were not eluted thoroughly. Another possibility is the aforementioned loss of specifically binding phages due to the affinity of phages themselves for fibrillar $A\beta_{1-42}$.

Yet two of the six selected single phage clones had an identical sequence (HNWFYWTTEPYD). Moreover, two other clones shared the amino acid motif TXYXXVWR (X for different amino acids) and were later on synthesized as MoRu1 and MoRu3 (see chapter 4.2.4).

The high content of aromatic amino acids in these two peptides could contribute largely to an anti amyloidogenic effect by interaction with the region 16-23 of $A\beta_{1-42}$ which contains two aromatic residues itself [197, 198].

Dissolving the peptides MoRu4 and MoRu5 to a concentration of 1 mM was not possible in water or 1x PBS. The peptides precipitated or had a gel like appearance and were not suitable for most of the assays conducted. MoRu1 to MoRu3 solved well in water up to 1 mM and also in lower concentrations in PBS and sodium phosphate buffer. As the performed assays were executed with concentrations far below these margins, this was not a problem. BLI and SPR

measurements with MoRu1 to MoRu3, performed later on by Tamar Ziehm, showed that, especially MoRu3, does aggregate when used in a concentration above 100 µM in different buffers, even when solubility enhancinig chemicals were added.

Determination of binding affinity via SPR and BLI is restricted to substances with known molecular weight. Since MoRu3 aggregates have a higher molecular weight than monomers and the number of MoRu3 entities in such an aggregate is not known, received curves can hardly be fitted by the adjacent software and values of binding affinity cannot be determined.

5.3   Changes in Aβ derived ThT fluorescence by MoRu peptides

ThT is a fluorescent dye widely used to monitor amyloid peptide aggregation. The absorbance wavelength of the dye shifts when it is bound to β-sheets. The detected fluorescence is directly proportional to β-sheet content. Aβ tends to aggregate and thereby develops β-sheet rich fibrils. As ThT does not interact with unstructured Aβ monomers and oligomers and also not with amorphous aggregates, an increase in ThT fluorescence is due to developing fibrils. Thus, ThT can be used to analyze Aβ fibrilization and the influence of compounds on the fibrilization process [199, 200].

Predominantly monomeric $Aβ_{1-42}$ was used for coincubation with each of the MoRu peptides in order to monitor their influence on $Aβ_{1-42}$ fibrilization at 37 °C. The ability for fibrilization was reassured with samples of $Aβ_{1-42}$, which were not incubated with the peptides. The resulting fibrilization behavior (Chapter 4.3.2, Figure 27) resembles already published data [201-203]. The tested peptides, however, had differential influence on $Aβ_{1-42}$ fibrilization. MoRu1 and MoRu2 increased the ThT signal slightly, indicating an increased amount of fibrillar $Aβ_{1-42}$ in the sample (Chapter 4.3.2, Figure 28 & 29), whereas MoRu4 and 5 decreased the signal slightly. The impact of MoRu3 on the fibrilization process is higher than of the other peptides. MoRu3 was able to reduce ThT fluorescence to 86 % compared with the $Aβ_{1-42}$ sample which was incubated without peptide. It needs to be mentioned that, especially in case of MoRu3, MoRu4 and MoRu5, the values

differed considerably (Chapter 4.3.2, Figure 30). The given values represent the mean value of all measurements taken.

Yet, the impact of MoRu3 on the fibrilization of $A\beta_{1-42}$ could be due to its proposed mode of action, described later. MoRu3, as shown in several experiments, is able to reduce the oligomeric species of $A\beta_{1-42}$, leading to amorphous aggregates, which are not detected by ThT fluorescence. As $A\beta_{1-42}$ oligomers are part of the aggregation towards fibrils, the conversion of oligomers to ThT negative amorphous aggregates subducts the oligomers from the pool out of which $A\beta_{1-42}$ fibrils are produced. Also other molecules with aromatic residues exhibit such an influence on $A\beta$ fibril derived ThT fluorescence, like D3, resveratrol and other phenolic compounds [177, 204-206].

5.4   Modulation of $A\beta_{1-42}$ distribution by MoRu peptides

Preincubation of $A\beta_{1-42}$ leads to a broad range of $A\beta_{1-42}$ species ranging from monomers to fibrils. The effect of MoRu peptides on this $A\beta_{1-42}$ mixture was tested via DGC subsequently followed by SDS PAGE and silver staining.

First of all, this incubation method allows production of a reproducible broad range of $A\beta_{1-42}$ species in a short time, which makes this method useful for further experiments in which different $A\beta_{1-42}$ species are required.

This mixture of $A\beta_{1-42}$ species is modulated by the newly identified peptides MoRu1, 2 and 3. Yet, MoRu5 has only little influence on the mixture and MoRu4 was excluded from this assay due to solubility problems (Chapter 4.3.3, Figure 32).

MoRu1 and MoRu2 alter the $A\beta_{1-42}$ composition towards species which resemble protofibrils or large oligomers and thereby reduce monomeric and small oligomeric $A\beta_{1-42}$ species in fractions with lower density. MoRu3, however, abolishes all small $A\beta_{1-42}$ species and enhances the amount of $A\beta_{1-42}$ in fractions that most probably contain fibrils and large amorphous aggregates, which are not toxic (Chapters 4.3.3, 4.3.4 and 4.4.1). The $A\beta_{1-42}$ species in fractions four to six, which are also abolished by MoRu3, are proven to be toxic and accord to globular proteins with a

s-value of approximately 7 S, tested in a calibration run. AFM and modeling revealed that these species are $A\beta_{1-42}$ oligomers with a size of 66 to 150 kDa [177].

This outcome underlines our hypothesized mode of action for MoRu3. MoRu3 binds $A\beta_{1-42}$ monomers and modulates the dynamic equilibrium of $A\beta_{1-42}$ species towards not toxic amorphous aggregates as seen in TEM (Chapter 4.4.2) and turbidity assay (Chapter 4.3.4), thereby reducing the amount of toxic oligomers (Chapter 4.4.1) [177, 204, 205, 207, 208]. A comparable outcome was published for the D3 peptide. D3 also abolished toxic $A\beta_{1-42}$ species and led to the development of amorphous aggregates as shown by TEM [177].

5.5 MoRu3 abolishes $A\beta_{1-42}$ induced cell toxicity

The outcome of preliminary experiments led to the selection of MoRu3 for further investigation.

The produced mixture of $A\beta_{1-42}$ species was tested for its toxicity to PC-12 cells. The cell culture experiments showed an impact of the $A\beta_{1-42}$ mixture on the cell viability, reducing it to 45 %. This result indicates the presence of toxic $A\beta_{1-42}$ species as shown before.

According to our experiments, MoRu3, which itself is not toxic for PC-12 cells, is able to reduce the cytotoxic effect of $A\beta_{1-42}$ in a concentration dependent manner (Chapter 4.4.3, Figure 43). The ability to bind $A\beta_{1-42}$ monomers and prevent their aggregation towards toxic species and the conversion of already formed toxic $A\beta_{1-42}$ oligomers to not toxic species is an explanation for this experimental outcome. Also other compounds, which consist of aromates or include aromatic side chains were reported to reduce $A\beta$ induced cellular toxicity [198, 208, 209].

5.6 MoRu3 reverses a pathological phenotype in Neuro-2a cells stably transfected with human APP695

Neuro-2a cells are mouse derived neuroblastoma cells, which share similarities with neurons. Therefore, the cells are a suitable model for investigation of the impact of compounds on neuronlike cells.

MoRu3 did not alter the physiological phenotype of wild-type Neuro-2a cells and can be considered safe to be used in this model system. The MoRu3 treated cells have a wild-type phenotype, they grow protrusions and accumulate. Also, they develop a shape which resembles the polygonal appearance of wild-type Neuro-2a cells (Chapter 4.4.4, Figure 44).

Neuro-2a cells stably transfected with the human APP695 exhibit a pathological phenotype. The cells grow slower and are more rounded. Also, they have fewer and shorter protrusions than wild-type Neuro-2a cells. Thus, the cells are less connected with each other. When MoRu3 was added, the cells reconstitute the physiological phenotype of wild-type Neuro-2a cells (Chapter 4.4.4, Figure 45).

The pathological phenotype is most probably induced by the expression of APP and the production of its cleavage products, particularly Aβ and its aggregation products [210]. This pathological phenotype is reversed to a wild-type phenotype by MoRu3. This result is likely to be due to its capability to modulate toxic $A\beta_{1-42}$ species, as already shown in previous experiments.

5.7 MoRu3 has no effect on γ-secretase activity

A therapeutically active compound should show no side effects when delivered *in vivo*. Even though MoRu3 should modulate the Aβ aggregation pathway, it needs to be assured that the compound does not interfere with other physiological pathways.

It is known that first generation γ-secretase inhibitors (GSIs) interfere with the Notch signaling pathway [136, 211, 212]. The cleaved Notch intracellular domain interacts with transcription factors in the nucleus, which are involved in the

expression of genes that control cell fate. γ-secretases are not only involved in APP cleavage but also Notch is a γ-secretase substrate.Therefore, non-specific inhibitors can lead to severe side effects like gastrointestinal bleeding and immunosuppression, due to interference with Notch signaling pathways [213].

Even though our hypothesized mode of action for MoRu3 lacks a connection to APP cleavage and γ-secretase modulation, the influence was tested in human APP695 expressing Neuro-2a cells. MoRu3 did not inhibit γ-secretases, as no accumulation of the γ-secretase substrate APP C-terminal fragment β (APP CTFβ) was detected. Whereas, the established inhibitor DAPT led to detection of APP CTFβ in Western blots (Chapter 4.4.5).

5.8   MoRu3 – a hypothesis for its mode of action

We were able to show that the D-enantiomeric peptide MoRu3, identified by a competitive mirror image phage display for monomeric $A\beta_{1-42}$, can modulate the size distribution of $A\beta_{1-42}$ and withdraw or modulate toxic oligomers. The emerging species following treatment with MoRu3 are large, not toxic, amorphous $A\beta_{1-42}$ aggregates.

Over the last few years, several research groups have identified aromatic residues within the Aβ peptide that are involved in Aβ aggregation. Cukalevski *et al.* [202] reported, that the aromatic residue phenylalanine 19 (Phe19) in Aβ is crucial for aggregation [202]. Substitution of phenylalanine 19 with leucine (Leu) reduced aggregation dramatically. Since phenylalanine and leucine have the same hydrophobicity and van der Waals volume, wild-type Aβ has the same net charge and hydrogen bonding capacity as Aβ with a Phe19Leu substitution. Therefore steric hindrance and aromatic stacking appear to be crucial for nucleation. Thus, this specific Aβ region is a suitable target for therapeutic compounds [202, 214]. Esler *et al.* [215] showed by nuclear magnetic resonance (NMR) that Aβ with a point mutation (Phe19Thr) in this hydrophobic core region was incompetent of plaque formation and less structured than wild-type Aβ [215].

It was already shown that interaction with this region can prevent the assembly of monomeric Aβ into toxic oligomers or fibrils, for example by galantamine or

cyclic D, L-α-peptides that bear aromatic residues [198, 216, 217]. The compounds may interact with aromatic residues in the hydrophobic core of Aβ (Aβ$_{16-20}$ with the amino acid sequence KLVFF), which is important for self-recognition, formation of a β-sheet structure and aggregation. The compounds might inhibit aggregation by disrupting π-stacking of the aromatic residues within the KLVFF motif [218-220].

For compounds with especially phenolic residues, Porat *et al.* [221] hypothesized an aromatic interaction between the inhibitor molecule and aromatic residues of the amyloidogenic sequence. Those could direct the inhibitory compound to the amyloidogenic core and facilitate interaction, thus, leading to an interference with further assembly [221]. Additionally, Tjernberg and colleagues [153] showed that short D-peptides containing a phenylalanine residue can bind to Aβ and prevent fibril assembly [153].

Comparing these results with the results for MoRu3/Mosd1, we hypothesize that the mode of action could be as follows:
MoRu3 (YSYLTSYHMVWR; also named Mosd1; [222]) includes four aromatic residues, that are likely to interact with the hydrophobic core of Aβ (Aβ$_{16-20}$) via aromatic interactions, therefore hampering π-stacking. As this core region of Aβ is known to be involved in further aggregation of Aβ, an interaction with this region can lead to off-pathway aggregation towards large, not toxic, amorphous aggregates of Aβ. The binding epitope is accessible already in monomers but could be additionally accessible in oligomers but not in fibrillar Aβ since the epitope is concealed inside the structured fibril, thus allowing a specific interaction with Aβ, prior to the formation of toxic aggregates [223]. Additionally, specific binding of MoRu3/Mosd1 to monomeric Aβ$_{1-42}$ can remove these species from the dynamic equilibrium of Aβ$_{1-42}$ assamblies, leading to a gradual disaggregation of toxic Aβ$_{1-42}$ oligomers to monomers due to an altered equilibrium [140].

5.9   Repetition of mipd#5 with an optimized elution procedure yielded $A\beta_{1-42}$ monomer specific phage clones

Mipd#5 yielded peptide sequences that have an increased affinity for monomeric $A\beta_{1-42}$. One peptide, namely MoRu3/Mosd1, led to promising results in several biological assays, leading to the assumption, that the peptide is able to reduce the amount of toxic $A\beta_{1-42}$ species and stabilizes $A\beta_{1-42}$ monomers.

Nevertheless, since the elution procedure during mipd#5 was suboptimal, the procedure was repeated with another elution protocol in mipd#6. The sixth mirror image phage display (mipd#6) was expected to yield highly $A\beta_{1-42}$ monomer specific phages since more phages with a high affinity for the target should have been eluted by this procedure and consensus sequences were expected to be found.

The DNA of obtained single phages was sequenced and several corresponding amino acid sequences occurred repeatedly in different single phage clones. Moreover, additional to the repeatedly occurring sequences, closely related sequences occurred. Therefore, consensus sequences were found indeed. Interestingly, most sequences had an amino acid composition that resembled the amino acid composition of the MoRu peptides from mipd#5. Aromatic amino acids for example occurred repeatedly as well as histidines.

For each repeatedly occurring sequence, one phage clone was chosen for ELISA experiments. Additionally, sequences which occurred only once but aligned well with repeatedly occurring sequences were tested. Moreover, clones with a peculiar sequence (e.g. lots of charged amino acid residues or consisting of only uncharged, small polar amino acids) were tested. Furthermore, since the ELISA procedure was optimized, clones from MoRu1, 2, 3 and 5 were tested as well in order to be able to compare the outcome with mipd#5 results.

The combination of $A\beta_{1-42}$ oligomers and fibrils in the optimized ELISA procedure allowed an enhanced comparability of binding affinities of single phage clones to different $A\beta_{1-42}$ species. Oligomers and fibrils were immobilized more efficiently than $A\beta_{1-42}$ monomers, and both exceeded the 6E10 signal of uncoated wells. Therefore, it was necessary to normalize the signals. Additionally, the anti M13

phage specific antibody did not cross react with any coated or uncoated surface and was therefore subtracted as background and did not have to be considered as possible influence on affinities.

Interestingly, MoRu3 did not only exhibit the strongest affinity for $A\beta_{1-42}$ monomers as shown by the highest values in single phage ELISA, but also showed the highest specificity deduced by the ratio of $A\beta_{1-42}$ monomer signal to $A\beta_{1-42}$ oligomer/fibril signal. We therefore conclude that MoRu3/Mosd1 indeed is a very specific and strongly binding $A\beta_{1-42}$ monomer ligand.

The phages which displayed repeatedly occurring sequences did not bind that strongly and specifically to monomeric $A\beta_{1-42}$. Therefore, repeatedly occurring sequences do not always represent the best ligand.

However, several clones from mipd#6 showed high binding affinities to $A\beta_{1-42}$ monomers (e.g. 6.227, 6.239, 6.242, 6.255) and/or $A\beta_{1-42}$ monomer specificity (e.g. 6.227, 6.239, 6.242, 6.249, 6.255) as well and should therefore be analyzed in more detail.

5.10 Outlook

The work presented in this thesis concludes that the identified small D-enantiomeric peptide MoRu3/Mosd1 is suitable as a compound towards causative therapy for AD. The results show that MoRu3 abolishes toxic $A\beta_{1-42}$ oligomers *in vitro* and reconstitute cell viability and physiological phenotypes.

Currently, the mode of action of MoRu3 can only be speculated, as described before. However, with additional experiments, including species-specific kinetic studies via BLI or SPR, specificity for distinct $A\beta_{1-42}$ species can be investigated. Regarding the binding site of MoRu3 to $A\beta_{1-42}$, epitope mapping with different, overlapping parts of the $A\beta_{1-42}$ sequence should provide information.

Although MoRu3 has been shown to be effective in *in vitro* studies, its impact on $A\beta_{1-42}$ aggregation has to be tested in animal models. This will give information about the effects on pathological hallmarks of AD, such as cognitive deficits, anxiety, neuron death and $A\beta$ deposition in the brain. Furthermore, its blood-brain-

barrier penetration capability, the impact on inflammation and overall compatibility in animals has to be investigated in order to analyze possible adverse side-effects. Moreover, pharmacokinetic and pharmacodynamic characteristics should be examined.

Additionally, MoRu3 could be optimized regarding bioavailability, impact on AD symptomes and half-life in the body by rational drug design or further screening with a library of compounds, derived from MoRu3, by peptide microarrays or another phage display. The combination of MoRu3 with distinct molecules, which are known to interfere with $A\beta$ aggregation or increase bioavailability, may improve its therapeutic impact [224-226].

Finally, when MoRu3 or derivatives are proven to exhibit striking therapeutic features in AD, the substance could be tested against other amyloidogenic peptides, because these peptides frequently share related aggregation patterns and core regions [227].

The last mirror image phage display (mipd#6) in this work led to further sequences that exhibit strong $A\beta_{1-42}$ monomer specificity even though the MoRu3 clone from mipd#5 was shown to exceed their binding abilities. Nevertheless, several clones from mipd#6 (e.g. 6.227, 6.239 or 6.197) had a promising specificity to monomeric $A\beta_{1-42}$ and therefore characterization of the corresponding D-peptides could lead to new $A\beta_{1-42}$ monomer ligands with therapeutic effects.

Zusammenfassung

Die Alzheimer´sche Demenz (AD) ist die häufigste neurodegenrerative Erkrankung weltweit. Sie zählt zu den Amyloidosen, Krankheiten bei denen es zu einer unnatürlichen Ansammlung und Speicherung von fehlgefaltetem Protein kommt. Diese toxischen Aggregate sind die Auslöser der krankheitstypischen Symptome.

In AD wird dem Peptid Amyloid beta (Aβ) eine wichtige Rolle im Krankheitsverlauf zugesprochen. Während monomerem Aβ eine neuroprotektive Rolle attestiert wird, aggregiert es im Fall von AD. Schon Aβ-Oligomere wirken nachweislich neurotoxisch. Aus diesem Grund wird gezielt nach Substanzen gesucht, welche die toxischen Spezies modulieren können ohne dabei monomeres Aβ oder physiologische Abläufe in den Zellen zu beeinflussen.

In der vorliegenden Arbeit wurde zunächst ein Verfahren zur Identifizierung $Aβ_{1-42}$-Monomer spezifischer und therapeutisch wirksamer Liganden optimiert. Die identifizierten Moleküle wurden im Nachhinein auf ihren Einfluss auf die $Aβ_{1-42}$ Aggregation und Toxizität hin charakterisiert.

Das angewandte Verfahren des Spiegelbild-Phagen-Display wurde dabei um einen kompetitiven Ansatz erweitert, der es ermöglicht aus der großen, rekombinanten Bibliothek der von den Phagen präsentierten Peptide, spezifische Liganden für monomeres $Aβ_{1-42}$ zu identifizieren. Die dabei erhaltenen Sequenzen wurden als D-enantiomere Peptide synthetisiert.

Die MoRu1 bis MoRu5 benannten Peptide wurden in verschiedenen experimentellen Ansätzen getestet, um ihren Einfluss auf $Aβ_{1-42}$ Toxizität und Aggregation zu analysieren. Mittels ThT-Assay, TEM und Versuchen die den Einfluss der Peptide auf eine Mischung verschiedener $Aβ_{1-42}$ Spezies untersuchen, konnte festgestellt werden, dass das Peptid MoRu3, auch Mosd1 genannt, die $Aβ_{1-42}$ Aggregation beeinflusst und die toxischen $Aβ_{1-42}$ Oligomere zu nicht-toxischen amorphen Aggregaten umwandeln kann. Darauf folgende Zellkulturexperimente konnten bestätigen, dass die entstandene Mischung aus MoRu3 und hochmolekularen $Aβ_{1-42}$ Aggregaten eine deutlich verringerte Zelltoxizität zur Folge hat.

Des Weiteren konnte für MoRu3 in einem Zellmodell, welches humanes Amyloid Vorläuferprotein (amyloid precursor protein; APP) exprimiert und in welchem auch das Abbauprodukt Aβ entsteht, gezeigt werden, dass es nicht nur bereits vorhandene toxische Aβ Spezies in nicht-toxische umwandeln kann, sondern auch die Entstehung toxischer Spezies verhindert, ohne dabei die in die APP-Spaltung und in zelluläre Signalwegen involvierte γ-Sekretase zu inhibieren.

Die optimierte, kompetitive Methode hat das Potential zukünftige Medikamenten-Screens spezifischer zu gestalten. Das vorhandene therapeutische Potential, sowie der Wirkmechanismus von MoRu3 hingegen sollen zukünftig noch detaillierter analysiert werden.

Summary

Alzheimer´s dementia (AD) is the most common neurodegenerative disease worldwide. It belongs to the group of amyloidoses. These diseases are characterized by an unnatural accumulation and storage of misfolded proteins. In AD, the amyloid beta peptide (Aβ) plays an important role in disease progression.

While monomeric Aβ was shown to exhibit neuroprotective functions, the presence of oligomers was found to exhibit verifiable neurotoxicity. Thus, researchers have been screening for compounds that interfere with the toxicity of Aβ oligomers without affecting Aβ monomers or physiological pathways.

In the present work, a technique was successfully optimized that facilitated the identification of $A\beta_{1-42}$ monomer specific and therapeutically active ligands. Hence, selected ligands were characterized regarding their influence on $A\beta_{1-42}$ aggregation and toxicity.

The applied mirror image phage display was extended by a competitive approach, which enabled identification of specific ligands for monomeric $A\beta_{1-42}$. The identified sequences were synthesized as D-enantiomeric peptides. The derived peptides MoRu1 to MoRu5 were tested via the ThT assay, TEM and an approach, which allows the testing of the influence of peptides on a broad range of $A\beta_{1-42}$ species, in order to analyze their influence on $A\beta_{1-42}$ toxicity and aggregation. MoRu3, also named Mosd1, was shown to modulate $A\beta_{1-42}$ aggregation and to convert toxic $A\beta_{1-42}$ oligomers into nontoxic amorphous aggregates. Cell culture experiments confirmed that the generated mixture of MoRu3 and $A\beta_{1-42}$ is considerably less toxic than the $A\beta_{1-42}$ mixture itself. In addition, in another cell culture experiment with cells expressing human amyloid precursor protein (APP) and subsequently Aβ, MoRu3 was shown to convert already existing toxic Aβ species into not toxic species and to prevent the development of toxic $A\beta_{1-42}$ species without inhibiting γ-secretase, which is involved in APP cleavage and cellular signaling pathways.

The optimized mirror image phage display has the potential to increase the specificity of future drug screens. The existing therapeutic potential on the one

hand, as well as the mode of action of MoRu3 on the other hand, need to be analyzed in more detail in the future.

Appendix

List of abbreviations

%Brix	value for relative mass density
°C	degree Celsius
22G	wire diameter of cannulae (22G = 0.643 mm)
3D	three-dimensional space
α	Greek small letter alpha (a)
A	Ampere
a.u.	absorbance unit
Ach	acetylcholine
AD	Alzheimer´s disease
ADDL	Aβ-derived diffusible ligand
ADI	Alzheimer´s Disease International
AICD	APP intracellular domain
AMP	antimicrobial peptide
APOE	Apolipoprotein E
APP	amyloid precursor protein
APS	ammonium persulfate
Aβ	amyloid beta
Aβ*56	56 kDa soluble amyloid beta assembly
β	Greek small letter beta (b)
BACE-1	beta-secretase 1
BCA	bicinchoninic acid
Bio-	Biotin
BSA	bovine serum albumin fraction Ⅴ
cDNA	complementary DNA
CJD	Creutzfeldt-Jakob disease
CO_2	carbon dioxide
CSF	cerebrospinal fluid
CTF	C-terminal fragment
Cu^{1+}	cuprous ion
Cu^{2+}	cupric ion
D-	Latin: *dexter*, „right", stereodescriptor for Fischer projection of stereoisomers
D. melanogaster	*Drosophila melanogaster*
DAPT	N-[N-(3,5-difluoro-phenacetyl)-L-alanyl]-S-phenylglycine t-butyl ester

dd	double distilled
DGC	density gradient centrifugation
DIE	insulin-degrading enzyme
DMEM	Dulbecco´s modified Eagle medium
DMF	N,N–dimethylformamide
DMSO	dimethyl sulfoxide
DNA	deoxyribonucleic acid
E. coli	*Escherichia coli*
e.g.	Latin: *exempli gratia*, for example
EDTA	ethylenediaminetetraacetic acid
ELISA	enzyme-linked immunosorbent assay
et al.	Latin: *et alii*, and others
FAD	familial Alzheimer´s disease
FBS	fetal bovine serum
FDA	Food and Drug Administration
FPLC	fast protein liquid chromatography
FTD	frontotemporal dementia
γ	Greek small letter gamma (g)
gp41	glycoprotein 41
G-protein	guanosine nucleotide-binding protein
H	heavy chain
h	hours
H_2O	water
H_2SO_4	sulfuric acid
HCl	hydrochloric acid
HFIP	1,1,1,3,3,3-Hexafluoro-2-propanol
HIV	human immunodeficiency virus
HMW	high molecular weight
HRP	horse radish peroxidase
i.e.	Latin: *id est*, that is
IC_{50}	half maximal inhibitory concentration
IgG	immunoglobulin G
IPTG	isopropyl-β-D-1-thiogalactopyranoside
KAI1	cluster of differentiation 82 protein
KCl	potassium chloride
kDa	kilo Dalton
kV	kiloVolt
L	light chain
L-	Latin: *laevus*, „left", stereodescriptor for Fischer projection of stereoisomers
LB	lysogeny broth
LRP1	low density lipoprotein receptor-related protein 1

LTP	long term potentiation
μ	Greek small letter my (m)
μg	microgramm
μl	microliter
μm	micrometer
μM	microMolar
M	molarity
mA	milliAmpere
MALDI-TOF-MS	matrix-associated laser desorption/ionization time of flight mass spectrometry
mAU	milli absorbance unit
MCI	mild cognitive impairment
MHC II	major histocompatibility complex class 2
min	minutes
ml	milliliter
mm	millimeter
mM	milliMolar
MMP	matrix-metalloprotease
MMSE	mini-mental state examination
MoRu	proper noun for selected peptides
MRI	magnetic resonance imaging
mRNA	messenger ribonucleic acid
MTT	3-(4,5-dimethythiazol-2-yl)-2,5-diphenyltetrazolium bromide
NaCl	sodium chloride
NAD(P)H	reduced form of nicotinamide adenine dinucleotide phosphate
$NaHCO_3$	sodium bicarbonate
NaP_i	sodium phosphate
NEP	neutral endopeptidase or neprilysin
NFT	neurofibrillary tangles
ng	nanogramm
NLS	nuclear localization sequence
nM	nanoMolar
Nm	nanometer
NMDA	N-methyl-D-aspartate
NMR	nuclear magnetic resonance
NPY	neuropeptide Y
O.D.	optical density
π	Greek small letter pi (p)
p	Italian: *piccolo*, „small", a unit prefix
p.a.	Latin: *pro analysi*, analytically pure
p75	p75 neurotrophin receptor

pIII, pVI, pVIII	M13 phage proteins
PAGE	polyacrylamide gel electrophoresis
PBS	phosphate buffered saline
PDAPP	transgenic mice with minigene encoding the $APP_{717 \rightarrow F}$ mutation associated with familial AD under control of a platelet-derived growth factor-β promoter
PEG	polyethylene glycol
PET	positron emission tomography
pfu	plaque forming unit
pH	decimal logarithm of the reciprocal of the hydrogen ion activity in a solution
pI	isoelectric point
PiB	Pittsburgh compound B
pM	picoMolar
PSEN	Presenilin
PTFE	polytetrafluoroethylene
PVDF	polyvinylidene fluoride
RAGE	receptor for advanced glycation endproducts
rfu	relative fluorescence units
RP-HPLC	reversed phase - high-performance liquid chromatography
rpm	revolutions per minute
RT	room temperature
sAPPα/β	soluble APP alpha / beta
scFv	single-chain variable fragment
SDS	sodium dodecyl sulfate
SEC	size exclusion chromatography
sFIDA	surface-fluorescence intensity distribution analysis
Tau	protein Tau
TBS	Tris buffered saline
TE	Tris EDTA
TEM	transmission electron microscopy
TEMED	N,N,N′,N′-tetramethylethane-1,2-diamine
Tet	tetracycline
TFA	2,2,2-triflouroacetic acid
TGF-β	transforming growth factor beta
ThT	Thioflavin T
TMB	3,3′, 5,5′-tetramethylbenzidine
tricine	N-(2-hydroxy-1,1-bis(hydroxymethyl)ethyl)-glycine
Tris	2-amino-2-hydroxymethyl-propane-1,3-diol
V	Volt
v / v	volume per volume
w / v	weight per volume
WHO	World Health Organization

x g	multiples of g (relative centrifugal force)
X-Gal	5-bromo-4-chloro-3-indolyl-β-D-galactopyranoside

One and three letter amino acid code

A	Ala	alanine
C	Cys	cysteine
D	Asp	aspartic acid
E	Glu	glutamic acid
F	Phe	phenylalanine
G	Gly	glycine
H	His	histidine
I	Ile	isoleucine
K	Lys	lysine
L	Leu	leucine
M	Met	methionine
N	Asn	asparagine
P	Pro	proline
Q	Gln	glutamine
R	Arg	arginine
S	Ser	serine
T	Thr	threonine
V	Val	valine
W	Trp	tryptophan
Y	Tyr	tyrosine

Publications and poster presentations

Publications

Rudolph S., Klein A.N., Tusche M., Schlosser C., Funke S.A., Kutzsche J. and Willbold D.; *"Competitive mirror image phage display yielded a peptide that modulates amyloid beta aggregation and decreases its toxicity."*; submitted (2015).

Poster presentations

Rudolph S., Kutzsche J., Klein A.N., Frenzel D., Schlosser C., Tusche M. and Willbold D.; *Characterization of D-enantiomeric peptides binding to monomeric amyloid beta (1-42) identified by a competitive mirror image phage display.* Alzheimer´s Association International Conference (AAIC); Copenhagen; 07/2014

Reference list

1. Organization, W.H., *Dementia: A Public Health Priority*. 2012: World Health Organization.

2. Querfurth, H.W. and F.M. LaFerla, *Alzheimer's disease.* N Engl J Med, 2010. 362(4): p. 329-44.

3. Ferri, C.P., et al., *Global prevalence of dementia: a Delphi consensus study.* Lancet, 2005. 366(9503): p. 2112-7.

4. Ritchie, K. and S. Lovestone, *The dementias.* Lancet, 2002. 360(9347): p. 1759-66.

5. Selkoe, D.J., *Translating cell biology into therapeutic advances in Alzheimer's disease.* Nature, 1999. 399(6738 Suppl): p. A23-31.

6. Golde, T.E., C.B. Eckman, and S.G. Younkin, *Biochemical detection of Abeta isoforms: implications for pathogenesis, diagnosis, and treatment of Alzheimer's disease.* Biochim Biophys Acta, 2000. 1502(1): p. 172-87.

7. Masters, C.L., et al., *Amyloid plaque core protein in Alzheimer disease and Down syndrome.* Proc Natl Acad Sci U S A, 1985. 82(12): p. 4245-9.

8. Obulesu, M., R. Venu, and R. Somashekhar, *Tau mediated neurodegeneration: an insight into Alzheimer's disease pathology.* Neurochem Res, 2011. 36(8): p. 1329-35.

9. Trojanowski, J.Q., et al., *Microtubule-stabilising drugs for therapy of Alzheimer's disease and other neurodegenerative disorders with axonal transport impairments.* Expert Opin Pharmacother, 2005. 6(5): p. 683-6.

10. Xu, S., et al., *Characterization of tau fibrillization in vitro.* Alzheimers Dement, 2010. 6(2): p. 110-7.

11. Testi, S., et al., *A novel PSEN1 mutation in a patient with sporadic early-onset Alzheimer's disease and prominent cerebellar ataxia.* J Alzheimers Dis, 2014. 41(3): p. 709-14.

12. Avramopoulos, D., *Genetics of Alzheimer's disease: recent advances.* Genome Med, 2009. 1(3): p. 34.

13. Kim, D.H., et al., *Genetic markers for diagnosis and pathogenesis of Alzheimer's disease.* Gene, 2014. 545(2): p. 185-93.

14. Huang, Y., *Roles of apolipoprotein E4 (ApoE4) in the pathogenesis of Alzheimer's disease: lessons from ApoE mouse models.* Biochem Soc Trans, 2011. 39(4): p. 924-32.

15. Ridge, P.G., M.T. Ebbert, and J.S. Kauwe, *Genetics of Alzheimer's disease.* Biomed Res Int, 2013. 2013: p. 254954.

16. Bickel, H., *[Need for nursing care by the elderly: results of a population based retrospective longitudinal study].* Gesundheitswesen, 1996. 58(1 Suppl): p. 56-62.

17.   Berr, C., J. Wancata, and K. Ritchie, *Prevalence of dementia in the elderly in Europe.* Eur Neuropsychopharmacol, 2005. 15(4): p. 463-71.

18.   Goedert, M. and M.G. Spillantini, *A century of Alzheimer's disease.* Science, 2006. 314(5800): p. 777-81.

19.   Alzheimer, A., et al., *An English translation of Alzheimer's 1907 paper, "Uber eine eigenartige Erkankung der Hirnrinde".* Clin Anat, 1995. 8(6): p. 429-31.

20.   Bauer, J., *[Clinical diagnosis and therapeutic possibilities for dementia of the Alzheimer type].* Fortschr Neurol Psychiatr, 1994. 62(11): p. 417-32.

21.   Thal, D.R., et al., *Phases of A beta-deposition in the human brain and its relevance for the development of AD.* Neurology, 2002. 58(12): p. 1791-800.

22.   Kang, J., et al., *The precursor of Alzheimer's disease amyloid A4 protein resembles a cell-surface receptor.* Nature, 1987. 325(6106): p. 733-6.

23.   Selkoe, D.J., et al., *Beta-amyloid precursor protein of Alzheimer disease occurs as 110- to 135-kilodalton membrane-associated proteins in neural and nonneural tissues.* Proc Natl Acad Sci U S A, 1988. 85(19): p. 7341-5.

24.   Dawkins, E. and D.H. Small, *Insights into the physiological function of the beta-amyloid precursor protein: beyond Alzheimer's disease.* J Neurochem, 2014. 129(5): p. 756-69.

25.   Quitschke, W.W. and D. Goldgaber, *The amyloid beta-protein precursor promoter. A region essential for transcriptional activity contains a nuclear factor binding domain.* J Biol Chem, 1992. 267(24): p. 17362-8.

26.   Zheng, H., et al., *beta-Amyloid precursor protein-deficient mice show reactive gliosis and decreased locomotor activity.* Cell, 1995. 81(4): p. 525-31.

27.   Luo, L., T. Tully, and K. White, *Human amyloid precursor protein ameliorates behavioral deficit of flies deleted for Appl gene.* Neuron, 1992. 9(4): p. 595-605.

28.   Rossjohn, J., et al., *Crystal structure of the N-terminal, growth factor-like domain of Alzheimer amyloid precursor protein.* Nat Struct Biol, 1999. 6(4): p. 327-31.

29.   Murayama, Y., et al., *Cell surface receptor function of amyloid precursor protein that activates Ser/Thr kinases.* Gerontology, 1996. 42 Suppl 1: p. 2-11.

30.   Clarris, H.J., et al., *Expression of the amyloid protein precursor of Alzheimer's disease in the developing rat olfactory system.* Brain Res Dev Brain Res, 1995. 88(1): p. 87-95.

31.   Masliah, E., et al., *Amyloid precursor protein is localized in growing neurites of neonatal rat brain.* Brain Res, 1992. 593(2): p. 323-8.

32.   Masliah, E., et al., *Localization of amyloid precursor protein in GAP43-immunoreactive aberrant sprouting neurites in Alzheimer's disease.* Brain Res, 1992. 574(1-2): p. 312-6.

33.   Salbaum, J.M. and F.H. Ruddle, *Embryonic expression pattern of amyloid protein precursor suggests a role in differentiation of specific subsets of neurons.* J Exp Zool, 1994. 269(2): p. 116-27.

34.   Beher, D., et al., *Regulation of amyloid protein precursor (APP) binding to collagen and mapping of the binding sites on APP and collagen type I.* J Biol Chem, 1996. 271(3): p. 1613-20.

35.   Clarris, H.J., et al., *Identification of heparin-binding domains in the amyloid precursor protein of Alzheimer's disease by deletion mutagenesis and peptide mapping.* J Neurochem, 1997. 68(3): p. 1164-72.

36.   Dahms, S.O., et al., *Structure and biochemical analysis of the heparin-induced E1 dimer of the amyloid precursor protein.* Proc Natl Acad Sci U S A, 2010. 107(12): p. 5381-6.

37.   Soba, P., et al., *Homo- and heterodimerization of APP family members promotes intercellular adhesion.* EMBO J, 2005. 24(20): p. 3624-34.

38.   Wang, Z., et al., *Presynaptic and postsynaptic interaction of the amyloid precursor protein promotes peripheral and central synaptogenesis.* J Neurosci, 2009. 29(35): p. 10788-801.

39.   Shigematsu, K., P.L. McGeer, and E.G. McGeer, *Localization of amyloid precursor protein in selective postsynaptic densities of rat cortical neurons.* Brain Res, 1992. 592(1-2): p. 353-7.

40.   Cousins, S.L., et al., *Amyloid precursor protein 695 associates with assembled NR2A- and NR2B-containing NMDA receptors to result in the enhancement of their cell surface delivery.* J Neurochem, 2009. 111(6): p. 1501-13.

41.   Hoe, H.S., et al., *The effects of amyloid precursor protein on postsynaptic composition and activity.* J Biol Chem, 2009. 284(13): p. 8495-506.

42.   Lee, K.J., et al., *Beta amyloid-independent role of amyloid precursor protein in generation and maintenance of dendritic spines.* Neuroscience, 2010. 169(1): p. 344-56.

43.   Nishimoto, I., et al., *Alzheimer amyloid protein precursor complexes with brain GTP-binding protein G(o).* Nature, 1993. 362(6415): p. 75-9.

44.   Ramaker, J.M., T.L. Swanson, and P.F. Copenhaver, *Amyloid precursor proteins interact with the heterotrimeric G protein Go in the control of neuronal migration.* J Neurosci, 2013. 33(24): p. 10165-81.

45.   Reinhard, C., et al., *Soluble amyloid-beta precursor protein binds its cell surface receptor in a cooperative fashion with glypican and syndecan proteoglycans.* J Cell Sci, 2013. 126(Pt 21): p. 4856-61.

46.   Zheng, H. and E.H. Koo, *The amyloid precursor protein: beyond amyloid.* Mol Neurodegener, 2006. 1: p. 5.

47.   Turner, P.R., et al., *Roles of amyloid precursor protein and its fragments in regulating neural activity, plasticity and memory.* Prog Neurobiol, 2003. 70(1): p. 1-32.

48.   Muller, T., et al., *The amyloid precursor protein intracellular domain (AICD) as modulator of gene expression, apoptosis, and cytoskeletal dynamics-relevance for Alzheimer's disease.* Prog Neurobiol, 2008. 85(4): p. 393-406.

49.   De Strooper, B., *Proteases and proteolysis in Alzheimer disease: a multifactorial view on the disease process.* Physiol Rev, 2010. 90(2): p. 465-94.

50.   Munter, L.M., et al., *Model peptides uncover the role of the beta-secretase transmembrane sequence in metal ion mediated oligomerization.* J Am Chem Soc, 2013. 135(51): p. 19354-61.

51.   Chasseigneaux, S. and B. Allinquant, *Functions of Abeta, sAPPalpha and sAPPbeta : similarities and differences.* J Neurochem, 2012. 120 Suppl 1: p. 99-108.

52.   Olsson, F., et al., *Characterization of intermediate steps in amyloid beta (Abeta) production under near-native conditions.* J Biol Chem, 2014. 289(3): p. 1540-50.

53.   Wilcock, D.M. and W.S. Griffin, *Down's syndrome, neuroinflammation, and Alzheimer neuropathogenesis.* J Neuroinflammation, 2013. 10: p. 84.

54.   Nilsberth, C., et al., *The 'Arctic' APP mutation (E693G) causes Alzheimer's disease by enhanced Abeta protofibril formation.* Nat Neurosci, 2001. 4(9): p. 887-93.

55.   Van Dam, D. and P.P. De Deyn, *Drug discovery in dementia: the role of rodent models.* Nat Rev Drug Discov, 2006. 5(11): p. 956-70.

56.   Coles, M., et al., *Solution structure of amyloid beta-peptide(1-40) in a water-micelle environment. Is the membrane-spanning domain where we think it is?* Biochemistry, 1998. 37(31): p. 11064-77.

57.   Lazo, N.D., et al., *On the nucleation of amyloid beta-protein monomer folding.* Protein Sci, 2005. 14(6): p. 1581-96.

58.   Zhang, S., et al., *The Alzheimer's peptide a beta adopts a collapsed coil structure in water.* J Struct Biol, 2000. 130(2-3): p. 130-41.

59.   Soscia, S.J., et al., *The Alzheimer's disease-associated amyloid beta-protein is an antimicrobial peptide.* PLoS One, 2010. 5(3): p. e9505.

60.   Barucker, C., et al., *Nuclear translocation uncovers the amyloid peptide Abeta42 as a regulator of gene transcription.* J Biol Chem, 2014. 289(29): p. 20182-91.

61.   Liu, W.M. and X.A. Zhang, *KAI1/CD82, a tumor metastasis suppressor.* Cancer Lett, 2006. 240(2): p. 183-94.

62.   Giuffrida, M.L., et al., *Beta-amyloid monomers are neuroprotective.* J Neurosci, 2009. 29(34): p. 10582-7.

63.   Giuffrida, M.L., et al., *Beta-amyloid monomer and insulin/IGF-1 signaling in Alzheimer's disease.* Mol Neurobiol, 2012. 46(3): p. 605-13.

64.   Toneff, T., et al., *Beta-amyloid peptides undergo regulated co-secretion with neuropeptide and catecholamine neurotransmitters.* Peptides, 2013. 46: p. 126-35.

65.   Zilka, N., M. Korenova, and M. Novak, *Misfolded tau protein and disease modifying pathways in transgenic rodent models of human tauopathies.* Acta Neuropathol, 2009. 118(1): p. 71-86.

66.   Mendieta, J., et al., *Phosphorylation modulates the alpha-helical structure and polymerization of a peptide from the third tau microtubule-binding repeat.* Biochim Biophys Acta, 2005. 1721(1-3): p. 16-26.

67.   Ballatore, C., et al., *Discovery of brain-penetrant, orally bioavailable aminothienopyridazine inhibitors of tau aggregation.* J Med Chem, 2010. 53(9): p. 3739-47.

68.   Peterson, D.W., et al., *A soluble oligomer of tau associated with fiber formation analyzed by NMR.* Biochemistry, 2008. 47(28): p. 7393-404.

69.   von Bergen, M., et al., *Assembly of tau protein into Alzheimer paired helical filaments depends on a local sequence motif ((306)VQIVYK(311)) forming beta structure.* Proc Natl Acad Sci U S A, 2000. 97(10): p. 5129-34.

70.   Hardy, J.A. and G.A. Higgins, *Alzheimer's disease: the amyloid cascade hypothesis.* Science, 1992. 256(5054): p. 184-5.

71.   McLean, C.A., et al., *Soluble pool of Abeta amyloid as a determinant of severity of neurodegeneration in Alzheimer's disease.* Ann Neurol, 1999. 46(6): p. 860-6.

72.   Cizas, P., et al., *Size-dependent neurotoxicity of beta-amyloid oligomers.* Arch Biochem Biophys, 2010. 496(2): p. 84-92.

73.   Haass, C. and D.J. Selkoe, *Soluble protein oligomers in neurodegeneration: lessons from the Alzheimer's amyloid beta-peptide.* Nat Rev Mol Cell Biol, 2007. 8(2): p. 101-12.

74.   Mori, H., et al., *Mass spectrometry of purified amyloid beta protein in Alzheimer's disease.* J Biol Chem, 1992. 267(24): p. 17082-6.

75.   Jawhar, S., O. Wirths, and T.A. Bayer, *Pyroglutamate amyloid-beta (Abeta): a hatchet man in Alzheimer disease.* J Biol Chem, 2011. 286(45): p. 38825-32.

76.   Jawhar, S., et al., *Overexpression of glutaminyl cyclase, the enzyme responsible for pyroglutamate A{beta} formation, induces behavioral deficits, and glutaminyl cyclase knock-out rescues the behavioral phenotype in 5XFAD mice.* J Biol Chem, 2011. 286(6): p. 4454-60.

77.   Nussbaum, J.M., et al., *Prion-like behaviour and tau-dependent cytotoxicity of pyroglutamylated amyloid-beta.* Nature, 2012. 485(7400): p. 651-5.

78.   Finder, V.H. and R. Glockshuber, *Amyloid-beta aggregation.* Neurodegener Dis, 2007. 4(1): p. 13-27.

79.   Lesne, S., et al., *A specific amyloid-beta protein assembly in the brain impairs memory.* Nature, 2006. 440(7082): p. 352-7.

80.   Blennow, K., M.J. de Leon, and H. Zetterberg, *Alzheimer's disease.* Lancet, 2006. 368(9533): p. 387-403.

81.   Jin, M., et al., *Soluble amyloid beta-protein dimers isolated from Alzheimer cortex directly induce Tau hyperphosphorylation and neuritic degeneration.* Proc Natl Acad Sci U S A, 2011. 108(14): p. 5819-24.

82.   Shankar, G.M., et al., *Amyloid-beta protein dimers isolated directly from Alzheimer's brains impair synaptic plasticity and memory.* Nat Med, 2008. 14(8): p. 837-42.

83.   Townsend, M., et al., *Effects of secreted oligomers of amyloid beta-protein on hippocampal synaptic plasticity: a potent role for trimers.* J Physiol, 2006. 572(Pt 2): p. 477-92.

84.   Lambert, M.P., et al., *Diffusible, nonfibrillar ligands derived from Abeta1-42 are potent central nervous system neurotoxins.* Proc Natl Acad Sci U S A, 1998. 95(11): p. 6448-53.

85.   Stine, W.B., Jr., et al., *In vitro characterization of conditions for amyloid-beta peptide oligomerization and fibrillogenesis.* J Biol Chem, 2003. 278(13): p. 11612-22.

86.   Zahs, K.R. and K.H. Ashe, *beta-Amyloid oligomers in aging and Alzheimer's disease.* Front Aging Neurosci, 2013. 5: p. 28.

87.   Connelly, L., et al., *Atomic force microscopy and MD simulations reveal pore-like structures of all-D-enantiomer of Alzheimer's beta-amyloid peptide: relevance to the ion channel mechanism of AD pathology.* J Phys Chem B, 2012. 116(5): p. 1728-35.

88.   Lal, R., H. Lin, and A.P. Quist, *Amyloid beta ion channel: 3D structure and relevance to amyloid channel paradigm.* Biochim Biophys Acta, 2007. 1768(8): p. 1966-75.

89.   Paranjape, G.S., et al., *Amyloid-beta(1-42) protofibrils formed in modified artificial cerebrospinal fluid bind and activate microglia.* J Neuroimmune Pharmacol, 2013. 8(1): p. 312-22.

90. Ye, C.P., D.J. Selkoe, and D.M. Hartley, *Protofibrils of amyloid beta-protein inhibit specific K+ currents in neocortical cultures.* Neurobiol Dis, 2003. 13(3): p. 177-90.

91. Wegiel, J., et al., *The role of microglial cells and astrocytes in fibrillar plaque evolution in transgenic APP(SW) mice.* Neurobiol Aging, 2001. 22(1): p. 49-61.

92. Butterfield, D.A., et al., *Evidence of oxidative damage in Alzheimer's disease brain: central role for amyloid beta-peptide.* Trends Mol Med, 2001. 7(12): p. 548-54.

93. Cappai, R. and A.R. White, *Amyloid beta.* Int J Biochem Cell Biol, 1999. 31(9): p. 885-9.

94. Hensley, K., et al., *A model for beta-amyloid aggregation and neurotoxicity based on free radical generation by the peptide: relevance to Alzheimer disease.* Proc Natl Acad Sci U S A, 1994. 91(8): p. 3270-4.

95. Vickers, J.C., et al., *The cause of neuronal degeneration in Alzheimer's disease.* Prog Neurobiol, 2000. 60(2): p. 139-65.

96. Yan, S.D., et al., *RAGE and amyloid-beta peptide neurotoxicity in Alzheimer's disease.* Nature, 1996. 382(6593): p. 685-91.

97. Fossati, S., J. Ghiso, and A. Rostagno, *Insights into caspase-mediated apoptotic pathways induced by amyloid-beta in cerebral microvascular endothelial cells.* Neurodegener Dis, 2012. 10(1-4): p. 324-8.

98. Sotthibundhu, A., et al., *Beta-amyloid(1-42) induces neuronal death through the p75 neurotrophin receptor.* J Neurosci, 2008. 28(15): p. 3941-6.

99. De Felice, F.G., M.V. Lourenco, and S.T. Ferreira, *How does brain insulin resistance develop in Alzheimer's disease?* Alzheimers Dement, 2014. 10(1 Suppl): p. S26-32.

100. de la Monte, S.M. and J.R. Wands, *Alzheimer's disease is type 3 diabetes-evidence reviewed.* J Diabetes Sci Technol, 2008. 2(6): p. 1101-13.

101. Zhao, W.Q., et al., *Amyloid beta oligomers induce impairment of neuronal insulin receptors.* FASEB J, 2008. 22(1): p. 246-60.

102. Burgmans, S., et al., *Amyloid-beta interacts with blood-brain barrier function in dementia: a systematic review.* J Alzheimers Dis, 2013. 35(4): p. 859-73.

103. Folstein, M.F., S.E. Folstein, and P.R. McHugh, *"Mini-mental state". A practical method for grading the cognitive state of patients for the clinician.* J Psychiatr Res, 1975. 12(3): p. 189-98.

104. Hoozemans, J.J., et al., *Neuroinflammation in Alzheimer's disease wanes with age.* J Neuroinflammation, 2011. 8: p. 171.

105. Ma, Y., et al., *Predictive accuracy of amyloid imaging for progression from mild cognitive impairment to Alzheimer disease with different lengths of follow-up: a systematic review.* Medicine (Baltimore), 2014. 93(27): p. e150.

106.   Matveev, S.V., et al., *A distinct subfraction of Abeta is responsible for the high-affinity Pittsburgh compound B-binding site in Alzheimer's disease brain.* J Neurochem, 2014. 131(3): p. 356-68.

107.   Funke, S.A., et al., *Single particle detection of Abeta aggregates associated with Alzheimer's disease.* Biochem Biophys Res Commun, 2007. 364(4): p. 902-7.

108.   Funke, S.A., et al., *Single-particle detection system for Abeta aggregates: adaptation of surface-fluorescence intensity distribution analysis to laser scanning microscopy.* Rejuvenation Res, 2010. 13(2-3): p. 206-9.

109.   Wang-Dietrich, L., et al., *The amyloid-beta oligomer count in cerebrospinal fluid is a biomarker for Alzheimer's disease.* J Alzheimers Dis, 2013. 34(4): p. 985-94.

110.   www.alzheimer.de. *Behandlung.* [Web Page] 2014   August 12th 2014]; www.alzheimer.de/alzheimer/behandlung.html].

111.   Anand, R., K.D. Gill, and A.A. Mahdi, *Therapeutics of Alzheimer's disease: Past, present and future.* Neuropharmacology, 2014. 76 Pt A: p. 27-50.

112.   Butterfield, D.A. and C.B. Pocernich, *The glutamatergic system and Alzheimer's disease: therapeutic implications.* CNS Drugs, 2003. 17(9): p. 641-52.

113.   Revett, T.J., et al., *Glutamate system, amyloid ss peptides and tau protein: functional interrelationships and relevance to Alzheimer disease pathology.* J Psychiatry Neurosci, 2013. 38(1): p. 6-23.

114.   Gilling, K.E., et al., *Potency, voltage-dependency, agonist concentration-dependency, blocking kinetics and partial untrapping of the uncompetitive N-methyl-D-aspartate (NMDA) channel blocker memantine at human NMDA (GluN1/GluN2A) receptors.* Neuropharmacology, 2009. 56(5): p. 866-75.

115.   Parsons, C.G., et al., *Memantine and cholinesterase inhibitors: complementary mechanisms in the treatment of Alzheimer's disease.* Neurotox Res, 2013. 24(3): p. 358-69.

116.   Drever, B.D., G. Riedel, and B. Platt, *The cholinergic system and hippocampal plasticity.* Behav Brain Res, 2011. 221(2): p. 505-14.

117.   Hofrichter, J., et al., *Reduced Alzheimer's disease pathology by St. John's Wort treatment is independent of hyperforin and facilitated by ABCC1 and microglia activation in mice.* Curr Alzheimer Res, 2013. 10(10): p. 1057-69.

118.   Ono, K., et al., *Effects of grape seed-derived polyphenols on amyloid beta-protein self-assembly and cytotoxicity.* J Biol Chem, 2008. 283(47): p. 32176-87.

119.   Lemere, C.A. and E. Masliah, *Can Alzheimer disease be prevented by amyloid-beta immunotherapy?* Nat Rev Neurol, 2010. 6(2): p. 108-19.

120. Schenk, D., et al., *Immunization with amyloid-beta attenuates Alzheimer-disease-like pathology in the PDAPP mouse.* Nature, 1999. 400(6740): p. 173-7.

121. Panza, F., et al., *Is there still any hope for amyloid-based immunotherapy for Alzheimer's disease?* Current Opinion in Psychiatry, 2014. 27(2): p. 128-137 10.1097/YCO.0000000000000041.

122. Doody, R.S., et al., *Phase 3 trials of solanezumab and bapineuzumab for Alzheimer's disease.* N Engl J Med, 2014. 370(15): p. 1460.

123. Doody, R.S., et al., *Phase 3 trials of solanezumab for mild-to-moderate Alzheimer's disease.* N Engl J Med, 2014. 370(4): p. 311-21.

124. Salloway, S., R. Sperling, and H.R. Brashear, *Phase 3 trials of solanezumab and bapineuzumab for Alzheimer's disease.* N Engl J Med, 2014. 370(15): p. 1460.

125. Salloway, S., et al., *Two phase 3 trials of bapineuzumab in mild-to-moderate Alzheimer's disease.* N Engl J Med, 2014. 370(4): p. 322-33.

126. Cedernaes, J., H.B. Schioth, and C. Benedict, *Efficacy of antibody-based therapies to treat Alzheimer's disease: Just a matter of timing?* Exp Gerontol, 2014. 57: p. 104-6.

127. Matsubara, E., et al., *Disease modifying therapies for Alzheimer's disease targeting Abeta oligomers: implications for therapeutic mechanisms.* Biomed Res Int, 2013. 2013: p. 984041.

128. Meli, G., et al., *Direct in vivo intracellular selection of conformation-sensitive antibody domains targeting Alzheimer's amyloid-beta oligomers.* J Mol Biol, 2009. 387(3): p. 584-606.

129. Tse, E., et al., *Intracellular antibody capture technology: application to selection of intracellular antibodies recognising the BCR-ABL oncogenic protein.* J Mol Biol, 2002. 317(1): p. 85-94.

130. Gebauer, M. and A. Skerra, *Engineered protein scaffolds as next-generation antibody therapeutics.* Curr Opin Chem Biol, 2009. 13(3): p. 245-55.

131. Hoyer, W., et al., *Stabilization of a beta-hairpin in monomeric Alzheimer's amyloid-beta peptide inhibits amyloid formation.* Proc Natl Acad Sci U S A, 2008. 105(13): p. 5099-104.

132. Nygren, P.A., *Alternative binding proteins: affibody binding proteins developed from a small three-helix bundle scaffold.* FEBS J, 2008. 275(11): p. 2668-76.

133. Schneeberger, A., et al., *Development of AFFITOPE vaccines for Alzheimer's disease (AD)--from concept to clinical testing.* J Nutr Health Aging, 2009. 13(3): p. 264-7.

134. Lambracht-Washington, D. and R.N. Rosenberg, *Advances in the development of vaccines for Alzheimer's disease.* Discov Med, 2013. 15(84): p. 319-26.

135. Jakob-Roetne, R. and H. Jacobsen, *Alzheimer's disease: from pathology to therapeutic approaches.* Angew Chem Int Ed Engl, 2009. 48(17): p. 3030-59.

136. Mikulca, J.A., et al., *Potential novel targets for Alzheimer pharmacotherapy: II. Update on secretase inhibitors and related approaches.* J Clin Pharm Ther, 2014. 39(1): p. 25-37.

137. ClinicalTrials.gov. *An Efficacy and Safety Trial of MK-8931 in Mild to Moderate Alzheimer's Disease (P07738) (EPOCH)*. [Web Page] 2014 September 16, 2014 [cited 2014 September 16].

138. ClinivalTrials.gov. *Safety Study of CTS21166 to Treat Alzheimer Disease*. 2014 July 7, 2008 [cited 2014 September 11].

139. Spilman, P., et al., *The multi-functional drug tropisetron binds APP and normalizes cognition in a murine Alzheimer's model.* Brain Res, 2014. 1551: p. 25-44.

140. Leissring, M.A., et al., *Enhanced proteolysis of beta-amyloid in APP transgenic mice prevents plaque formation, secondary pathology, and premature death.* Neuron, 2003. 40(6): p. 1087-93.

141. Saido, T. and M.A. Leissring, *Proteolytic degradation of amyloid beta-protein.* Cold Spring Harb Perspect Med, 2012. 2(6): p. a006379.

142. Zhu, X.C., et al., *Autophagy modulation for Alzheimer's disease therapy.* Mol Neurobiol, 2013. 48(3): p. 702-14.

143. Jiang, T., et al., *Temsirolimus promotes autophagic clearance of amyloid-beta and provides protective effects in cellular and animal models of Alzheimer's disease.* Pharmacol Res, 2014. 81: p. 54-63.

144. Kirsten, C.N. and T.H. Schrader, *Intermolecular β-Sheet Stabilization with Aminopyrazoles.* J Am Chem Soc, 1997. 119(50): p. 12061-12068.

145. Nagel-Steger, L., et al., *Modulation of aggregate size- and shape-distributions of the amyloid-beta peptide by a designed beta-sheet breaker.* Eur Biophys J, 2010. 39(3): p. 415-22.

146. Rzepecki, P., et al., *New heterocyclic beta-sheet ligands with peptidic recognition elements.* J Org Chem, 2004. 69(16): p. 5168-78.

147. Rzepecki, P., et al., *Prevention of Alzheimer's disease-associated Abeta aggregation by rationally designed nonpeptidic beta-sheet ligands.* J Biol Chem, 2004. 279(46): p. 47497-505.

148. Debnath, M.P.G.B.K.S.B.P.S. *Molecular Diagnostics: Promises and Possibilities*. 2010.

149. Belleau, B., *Rational drug design: mirage or miracle?* Can Med Assoc J, 1970. 103(8): p. 850-3.

150. Lipinski, C.A., *Lead- and drug-like compounds: the rule-of-five revolution.* Drug Discov Today Technol, 2004. 1(4): p. 337-41.

151. Lipinski, C.A., et al., *Experimental and computational approaches to estimate solubility and permeability in drug discovery and development settings.* Adv Drug Deliv Rev, 2001. 46(1-3): p. 3-26.

152. McKinlay, M.A. and M.G. Rossmann, *Rational design of antiviral agents.* Annu Rev Pharmacol Toxicol, 1989. 29: p. 111-22.

153. Tjernberg, L.O., et al., *Controlling amyloid beta-peptide fibril formation with protease-stable ligands.* J Biol Chem, 1997. 272(19): p. 12601-5.

154. Vitiello, G., et al., *The iAbeta5p beta-breaker peptide regulates the Abeta(25-35) interaction with lipid bilayers through a cholesterol-mediated mechanism.* Biochem Biophys Res Commun, 2012. 417(1): p. 88-92.

155. Bruce, N.J., et al., *Molecular dynamics simulations of Abeta fibril interactions with beta-sheet breaker peptides.* Peptides, 2010. 31(11): p. 2100-8.

156. Wiesehan, K. and D. Willbold, *Mirror-image phage display: aiming at the mirror.* Chembiochem, 2003. 4(9): p. 811-5.

157. Smith, G.P., *Filamentous fusion phage: novel expression vectors that display cloned antigens on the virion surface.* Science, 1985. 228(4705): p. 1315-7.

158. Smith, G.P. and V.A. Petrenko, *Phage Display.* Chem Rev, 1997. 97(2): p. 391-410.

159. Fukunaga, K. and M. Taki, *Practical tips for construction of custom Peptide libraries and affinity selection by using commercially available phage display cloning systems.* J Nucleic Acids, 2012. 2012: p. 295719.

160. Scott, J.K. and G.P. Smith, *Searching for peptide ligands with an epitope library.* Science, 1990. 249(4967): p. 386-90.

161. Fu, B., et al., *Identification and characterization of a novel phage display-derived peptide with affinity for human brain metastatic breast cancer.* Biotechnol Lett, 2014.

162. Larbanoix, L., et al., *Design and evaluation of a 6-mer amyloid-beta protein derived phage display library for molecular targeting of amyloid plaques in Alzheimer's disease: Comparison with two cyclic heptapeptides derived from a randomized phage display library.* Peptides, 2011. 32(6): p. 1232-43.

163. Li, L., et al., *Peptide ligands that use a novel binding site to target both TGF-beta receptors.* Mol Biosyst, 2010. 6(12): p. 2392-402.

164. Padmanaban, G., et al., *Identification of peptides that selectively bind to myoglobin by biopanning of phage displayed-peptide library.* J Biotechnol, 2014. 187C: p. 43-50.

165. Swift, J., et al., *Identification of aggregation inhibitors of the human antibody light chain repertoire by phage display.* Protein Eng Des Sel, 2014.

166. Dintzis, H.M., et al., *A comparison of the immunogenicity of a pair of enantiomeric proteins.* Proteins, 1993. 16(3): p. 306-8.

167. Schumacher, T.N., et al., *Identification of D-peptide ligands through mirror-image phage display.* Science, 1996. 271(5257): p. 1854-7.

168. Sun, N., S.A. Funke, and D. Willbold, *Mirror image phage display-- generating stable therapeutically and diagnostically active peptides with biotechnological means.* J Biotechnol, 2012. 161(2): p. 121-5.

169. Poduslo, J.F., et al., *Beta-sheet breaker peptide inhibitor of Alzheimer's amyloidogenesis with increased blood-brain barrier permeability and resistance to proteolytic degradation in plasma.* J Neurobiol, 1999. 39(3): p. 371-82.

170. Sela, M. and E. Zisman, *Different roles of D-amino acids in immune phenomena.* FASEB J, 1997. 11(6): p. 449-56.

171. Taylor, M., et al., *Development of a proteolytically stable retro-inverso peptide inhibitor of beta-amyloid oligomerization as a potential novel treatment for Alzheimer's disease.* Biochemistry, 2010. 49(15): p. 3261-72.

172. Tugyi, R., et al., *Partial D-amino acid substitution: Improved enzymatic stability and preserved Ab recognition of a MUC2 epitope peptide.* Proc Natl Acad Sci U S A, 2005. 102(2): p. 413-8.

173. Van Regenmortel, M.H. and S. Muller, *D-peptides as immunogens and diagnostic reagents.* Curr Opin Biotechnol, 1998. 9(4): p. 377-82.

174. Welch, B.D., et al., *Potent D-peptide inhibitors of HIV-1 entry.* Proc Natl Acad Sci U S A, 2007. 104(43): p. 16828-33.

175. Funke, S.A., et al., *Development of a small D-enantiomeric Alzheimer's amyloid-beta binding peptide ligand for future in vivo imaging applications.* PLoS One, 2012. 7(7): p. e41457.

176. Wiesehan, K., et al., *Selection of D-amino-acid peptides that bind to Alzheimer's disease amyloid peptide abeta1-42 by mirror image phage display.* Chembiochem, 2003. 4(8): p. 748-53.

177. Funke, S.A., et al., *Oral Treatment with the d-Enantiomeric Peptide D3 Improves the Pathology and Behavior of Alzheimer's Disease Transgenic Mice.* ACS Chemical Neuroscience, 2010. 1(9): p. 639-648.

178. Liu, H., S.A. Funke, and D. Willbold, *Transport of Alzheimer disease amyloid-beta-binding D-amino acid peptides across an in vitro blood-brain barrier model.* Rejuvenation Res, 2010. 13(2-3): p. 210-3.

179. van Groen, T., et al., *Treatment with D3 removes amyloid deposits, reduces inflammation, and improves cognition in aged AbetaPP/PS1 double transgenic mice.* J Alzheimers Dis, 2013. 34(3): p. 609-20.

180. van Groen, T., et al., *Reduction of Alzheimer's disease amyloid plaque load in transgenic mice by D3, A D-enantiomeric peptide identified by mirror image phage display.* ChemMedChem, 2008. 3(12): p. 1848-52.

181. Muller-Schiffmann, A., et al., *Combining independent drug classes into superior, synergistically acting hybrid molecules.* Angew Chem Int Ed Engl, 2010. 49(46): p. 8743-6.

182. Hoffmann, S., et al., *Competitively selected protein ligands pay their increase in specificity by a decrease in affinity.* Mol Biosyst, 2010. 6(1): p. 126-33.

183. Johansson, A.S., et al., *Physiochemical characterization of the Alzheimer's disease-related peptides A beta 1-42Arctic and A beta 1-42wt.* FEBS J, 2006. 273(12): p. 2618-30.

184. Shapiro, A.L., E. Vinuela, and J.V. Maizel, Jr., *Molecular weight estimation of polypeptide chains by electrophoresis in SDS-polyacrylamide gels.* Biochem Biophys Res Commun, 1967. 28(5): p. 815-20.

185. Weber, K. and M. Osborn, *The reliability of molecular weight determinations by dodecyl sulfate-polyacrylamide gel electrophoresis.* J Biol Chem, 1969. 244(16): p. 4406-12.

186. Schagger, H., *Tricine-SDS-PAGE.* Nat Protoc, 2006. 1(1): p. 16-22.

187. Jameson, L.P., N.W. Smith, and S.V. Dzyuba, *Dye-binding assays for evaluation of the effects of small molecule inhibitors on amyloid (abeta) self-assembly.* ACS Chem Neurosci, 2012. 3(11): p. 807-19.

188. van Groen, T., et al., *Treatment with Abeta42 binding D-amino acid peptides reduce amyloid deposition and inflammation in APP/PS1 double transgenic mice.* Adv Protein Chem Struct Biol, 2012. 88: p. 133-52.

189. van Groen, T., et al., *In vitro and in vivo staining characteristics of small, fluorescent, Abeta42-binding D-enantiomeric peptides in transgenic AD mouse models.* ChemMedChem, 2009. 4(2): p. 276-82.

190. Devlin, J.J., L.C. Panganiban, and P.E. Devlin, *Random peptide libraries: a source of specific protein binding molecules.* Science, 1990. 249(4967): p. 404-6.

191. Lam, K.S., et al., *A new type of synthetic peptide library for identifying ligand-binding activity.* Nature, 1991. 354(6348): p. 82-4.

192. Vodnik, M., et al., *Phage display: selecting straws instead of a needle from a haystack.* Molecules, 2011. 16(1): p. 790-817.

193. Borreguero, J.M., et al., *Folding events in the 21-30 region of amyloid beta-protein (Abeta) studied in silico.* Proc Natl Acad Sci U S A, 2005. 102(17): p. 6015-20.

194.   Hubin, E., et al., *Transient dynamics of Abeta contribute to toxicity in Alzheimer's disease.* Cell Mol Life Sci, 2014. 71(18): p. 3507-21.

195.   Sandberg, A., et al., *Stabilization of neurotoxic Alzheimer amyloid-beta oligomers by protein engineering.* Proc Natl Acad Sci U S A, 2010. 107(35): p. 15595-600.

196.   Krishnan, R., et al., *A bacteriophage capsid protein provides a general amyloid interaction motif (GAIM) that binds and remodels misfolded protein assemblies.* J Mol Biol, 2014. 426(13): p. 2500-19.

197.   Richman, M., et al., *In vitro and mechanistic studies of an antiamyloidogenic self-assembled cyclic D,L-alpha-peptide architecture.* J Am Chem Soc, 2013. 135(9): p. 3474-84.

198.   Chemerovski-Glikman, M., M. Richman, and S. Rahimipour, *Structure-based study of antiamyloidogenic cyclic d,l-α-peptides.* Tetrahedron, 2014. 70(42): p. 7639-7644.

199.   LeVine, H., 3rd, *Thioflavine T interaction with synthetic Alzheimer's disease beta-amyloid peptides: detection of amyloid aggregation in solution.* Protein Sci, 1993. 2(3): p. 404-10.

200.   LeVine, H., 3rd, *Quantification of beta-sheet amyloid fibril structures with thioflavin T.* Methods Enzymol, 1999. 309: p. 274-84.

201.   Bartolini, M., et al., *Kinetic characterization of amyloid-beta 1-42 aggregation with a multimethodological approach.* Anal Biochem, 2011. 414(2): p. 215-25.

202.   Cukalevski, R., et al., *Role of aromatic side chains in amyloid beta-protein aggregation.* ACS Chem Neurosci, 2012. 3(12): p. 1008-16.

203.   Veloso, A.J. and K. Kerman, *Modulation of fibril formation by a beta-sheet breaker peptide ligand: an electrochemical approach.* Bioelectrochemistry, 2012. 84: p. 49-52.

204.   Feng, Y., et al., *Resveratrol inhibits beta-amyloid oligomeric cytotoxicity but does not prevent oligomer formation.* Neurotoxicology, 2009. 30(6): p. 986-95.

205.   Jagota, S. and J. Rajadas, *Effect of phenolic compounds against Abeta aggregation and Abeta-induced toxicity in transgenic C. elegans.* Neurochem Res, 2012. 37(1): p. 40-8.

206.   Olubiyi, O.O., et al., *Amyloid aggregation inhibitory mechanism of arginine-rich D-peptides.* Curr Med Chem, 2014. 21(12): p. 1448-57.

207.   Lu, C., et al., *Design, synthesis, and evaluation of resveratrol derivatives as Ass((1)-(4)(2)) aggregation inhibitors, antioxidants, and neuroprotective agents.* Bioorg Med Chem Lett, 2012. 22(24): p. 7683-7.

208.   Sharoar, M.G., et al., *Keampferol-3-O-rhamnoside abrogates amyloid beta toxicity by modulating monomers and remodeling oligomers and fibrils to non-toxic aggregates.* J Biomed Sci, 2012. 19: p. 104.

209. Ladiwala, A.R., J.S. Dordick, and P.M. Tessier, *Aromatic small molecules remodel toxic soluble oligomers of amyloid beta through three independent pathways.* J Biol Chem, 2011. 286(5): p. 3209-18.

210. Wang, Y.P., et al., *Effect of amyloid peptides on serum withdrawal-induced cell differentiation and cell viability.* Cell Res, 2004. 14(6): p. 467-72.

211. Zettl, H., et al., *Discovery of gamma-secretase modulators with a novel activity profile by text-based virtual screening.* ACS Chem Biol, 2012. 7(9): p. 1488-95.

212. Olsauskas-Kuprys, R., A. Zlobin, and C. Osipo, *Gamma secretase inhibitors of Notch signaling.* Onco Targets Ther, 2013. 6: p. 943-55.

213. Wolfe, M.S., *gamma-Secretase inhibitors and modulators for Alzheimer's disease.* J Neurochem, 2012. 120 Suppl 1: p. 89-98.

214. Convertino, M., A. Vitalis, and A. Caflisch, *Disordered binding of small molecules to Abeta(12-28).* J Biol Chem, 2011. 286(48): p. 41578-88.

215. Esler, W.P., et al., *Point substitution in the central hydrophobic cluster of a human beta-amyloid congener disrupts peptide folding and abolishes plaque competence.* Biochemistry, 1996. 35(44): p. 13914-21.

216. Sgarbossa, A., *Natural Biomolecules and Protein Aggregation: Emerging Strategies against Amyloidogenesis.* Int J Mol Sci, 2012. 13(12): p. 17121-37.

217. Rao, P.P., T. Mohamed, and W. Osman, *Investigating the binding interactions of galantamine with beta-amyloid peptide.* Bioorg Med Chem Lett, 2013. 23(1): p. 239-43.

218. Gazit, E., *A possible role for pi-stacking in the self-assembly of amyloid fibrils.* FASEB J, 2002. 16(1): p. 77-83.

219. Hilbich, C., et al., *Substitutions of hydrophobic amino acids reduce the amyloidogenicity of Alzheimer's disease beta A4 peptides.* J Mol Biol, 1992. 228(2): p. 460-73.

220. Tjernberg, L.O., et al., *Arrest of beta-amyloid fibril formation by a pentapeptide ligand.* J Biol Chem, 1996. 271(15): p. 8545-8.

221. Porat, Y., A. Abramowitz, and E. Gazit, *Inhibition of amyloid fibril formation by polyphenols: structural similarity and aromatic interactions as a common inhibition mechanism.* Chem Biol Drug Des, 2006. 67(1): p. 27-37.

222. Rudolph, S., et al., *Competitive mirror image phage display yielded a peptide that modulates amyloid beta aggregation and decreases toxicity.* submitted, 2015.

223. Abelein, A., et al., *The hairpin conformation of the amyloid beta peptide is an important structural motif along the aggregation pathway.* J Biol Inorg Chem, 2014. 19(4-5): p. 623-34.

224.   Choonara, B.F., et al., *A review of advanced oral drug delivery technologies facilitating the protection and absorption of protein and peptide molecules.* Biotechnol Adv, 2014.

225.   Frydman-Marom, A., et al., *Structural basis for inhibiting beta-amyloid oligomerization by a non-coded beta-breaker-substituted endomorphin analogue.* ACS Chem Biol, 2011. 6(11): p. 1265-76.

226.   Patel, A., K. Cholkar, and A.K. Mitra, *Recent developments in protein and peptide parenteral delivery approaches.* Ther Deliv, 2014. 5(3): p. 337-65.

227.   Guerrero-Munoz, M.J., D.L. Castillo-Carranza, and R. Kayed, *Therapeutic approaches against common structural features of toxic oligomers shared by multiple amyloidogenic proteins.* Biochem Pharmacol, 2014. 88(4): p. 468-78.

List of Figures

List of Tables

Danksagung

Eidesstattliche Erklärung

Hiermit erkläre ich an Eides statt, dass ich die vorliegende Dissertation selbständig verfasst und keine anderen als die von mir angegebenen Quellen und Hilfsmittel verwendet und Zitate kenntlich gemacht habe.

Ferner erkläre ich, dass ich in keinem anderen Dissertationsverfahren mit oder ohne Erfolg versucht habe, diese Dissertation einzureichen.

Düsseldorf, den

_____

(Stephan Rudolph)